Present Status of the PANDA Software Trigger

K. Götzen[1], D. Kang[2], R. Kliemt[3] and F. Nerling[3]

[1] *Helmholtzzentrum für Schwerionenforschung (GSI), Darmstadt, Germany*
[2] *University Mainz (JGU), Kernphysikalisches Institut, Germany*
[3] *Helmholtz Institute Mainz (HIM) and GSI, Germany*

April 8, 2014

Abstract

This note presents the current status of the PANDA software trigger project. Apart from the present results obtained from Monte Carlo simulated events for various PANDA physics channels of interest, the task is defined and intersections to the DAQ and detector projects are pointed out.

Contents

1 Introduction and Motivation **2**

2 Definition of the Software Trigger Task **3**
2.1 Online Trigger System Overview 3
2.2 Software Trigger within PANDA Software Framework 4
2.3 Approaches by Other Experiments 5

3 Current Status of Event Reconstruction in Panda **7**

4 Physics Channels under Investigation **10**

5 Status of Present Studies and Results **11**
5.1 Event Based Efficiency and Cross-Tagging 11
5.2 Observables for Filtering Events and Optimisation of Cuts 13
5.3 Results from Toy Monte Carlo Studies 14
5.4 Results from Full Monte Carlo Studies 21
5.5 Application of Multivariate Analysis 26
5.5.1 Introduction to TMVA 26
5.5.2 Results from TMVA Application 27
5.6 Discussion of Present Results 31

6 Next and Further Steps **33**

7 Summary and Outlook **35**

8 Appendix **36**

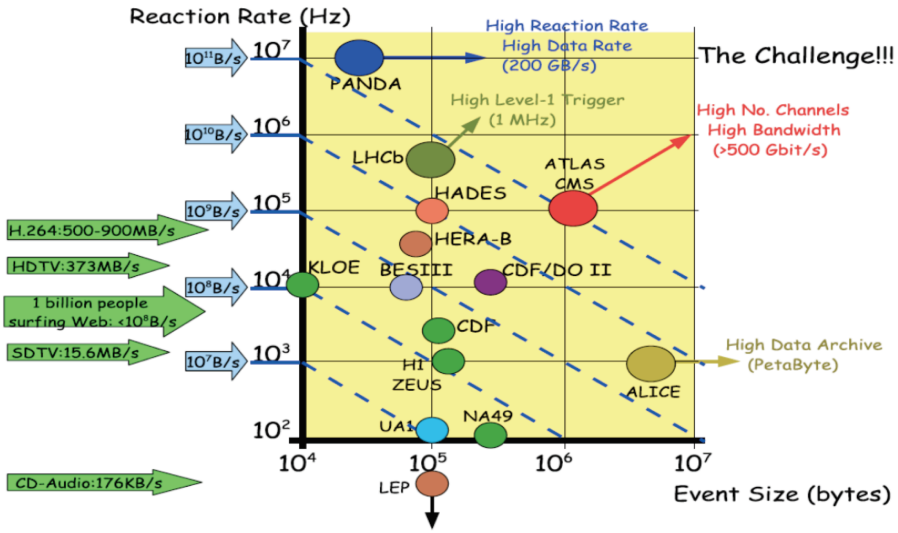

Figure 1: Event rates versus event sizes for various experiments.

1 Introduction and Motivation

The PANDA experiment will be one of the key experiments at the future Facility for Anti-proton and Ion Research (FAIR), where an anti-proton beam with momenta from 1.5 GeV/c to 15 GeV/c will impinge on a hydrogen (proton) and various nuclear targets. It aims for a broad physics program covering topics of

- hadron spectroscopy
- nucleon structure
- hadrons in nuclei, and
- hypernuclear physics.

In particular the spectroscopy of hadrons requires large statistics data to reveal important aspects of the rare charmonium and exotic candidates that have been discovered in the last decade, like the prominent $X(3872)$ and $D^*_{s0}(2317)^{\pm}$ states. The observation and discovery of new hadronic states completing the currently observed spectrum of hadrons will only be possible with a sufficient amount of high quality data.

Most of the production cross-sections for the reactions of interest in anti-proton-proton collisions are not known precisely – several ones are predicted by theory to be in the picobarn or nanobarn range. In order to produce a sufficiently large amount of these reactions for reasonable physics analysis quality, the design value for the average luminosity is projected to be $L = 2 \cdot 10^{32}\,\mathrm{cm}^{-2}\mathrm{s}^{-1}$ in the so-called high luminosity mode. Due to the rather high total cross-section of anti-proton-proton reactions of $\sigma_{\bar{p}p} \approx 60 \ldots 100\,\mathrm{mb}$, the expected average reaction rate computes to $\dot{N} = 20\,\mathrm{MHz}$ with peak values of up to $\dot{N}_{\mathrm{max}} \approx 40\,\mathrm{MHz}$. Combined with an average event size of 10-20 kB, this leads to a total raw data rate of roughly 200 GB/s as shown in Fig. 1. Assuming a duty cycle of 50 %, recording the unfiltered data stream would require a storage capacity of roughly 3000 PB per year, only a tiny fraction actually containing reactions of interest. Since providing this large amount of storage is neither efficient nor affordable, the data rate has to be reduced by approximately a factor of 1000 in order to keep the required storage capacity in the order of a few PB per year.

Due to the similarity of interesting and uninteresting reactions concerning the detector signatures, a sophisticated filtering strategy has to be developed and applied that goes far beyond conventional hardware based trigger schemes. The concept of the PANDA data acquisition (DAQ) system therefore bases on a trigger-less read-out, i.e. the detectors front-end (FE) electronics and DAQ continuously sample and buffer data without any classical gated trigger signal. This approach principally allows to pre-analyse the data in an appropriate way before deciding to keep or reject a particular part of the data. Technically, this task puts a tremendous load on the DAQ system, since the information allowing to effectively separate signal from background reactions has to be provided during data taking, and therefore requires high-level reconstruction procedures in the online environment.

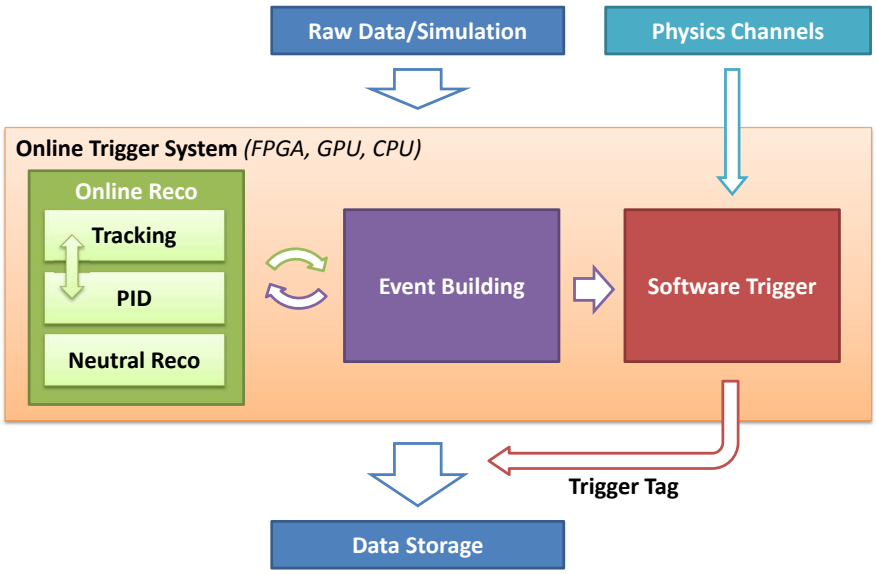

Figure 2: Schematic overview of the complete online trigger system for the PANDA experiment, consisting of various building blocks.

2 Definition of the Software Trigger Task

In order to define the actual task being addressed by the software trigger subgroup, an overview on the complete online trigger system to be realised in PANDA will be given first (Sec. 2.1). In addition to the definition of the software trigger task being subject of this report (Sec. 2.2), also a short overview of trigger system approaches by other experiments facing similar challenges as PANDA is provided (Sec. 2.3).

2.1 Online Trigger System Overview

The principal function of the online trigger system is to make the decision whether a certain fraction of the data stream should be written to the data storage or not. This has to be done online in real time with high performance. The system consists of different components as illustrated in the schematic in Fig. 2, these are

- online reconstruction
- event building and
- software trigger.

In order to cope with the challenging conditions of expected data rates (Sec. 1), several high level information derived from the reactions' data are required for appropriate signal/background separation. Therefore online reconstruction of neutral and charged particles as well as the assignment of particle identification (PID) information to the corresponding tracks has to be performed as complete as possible. This can be coupled with the event building process, probably in an iterative way, to finally provide online event candidates with reconstructed particle information to the software trigger module. This module will then calculate the input variables needed for the previously developed selection algorithms for the various trigger lines, which afterwards are executed to tag events being consistent with the signal signatures. Writing the events to the data storage will finally be triggered by a logical "OR" of the tag signals from all trigger lines currently being active. The list of physics reactions and channels to be of interest for a given runtime period has to be decided in advance, so that the selection algorithms can be prepared and installed beforehand in the software trigger module accordingly.

In order to achieve the speed being necessary to handle the complete data stream in real-time, the full system needs to be implemented on appropriate computing elements like FPGAs, GPUs or

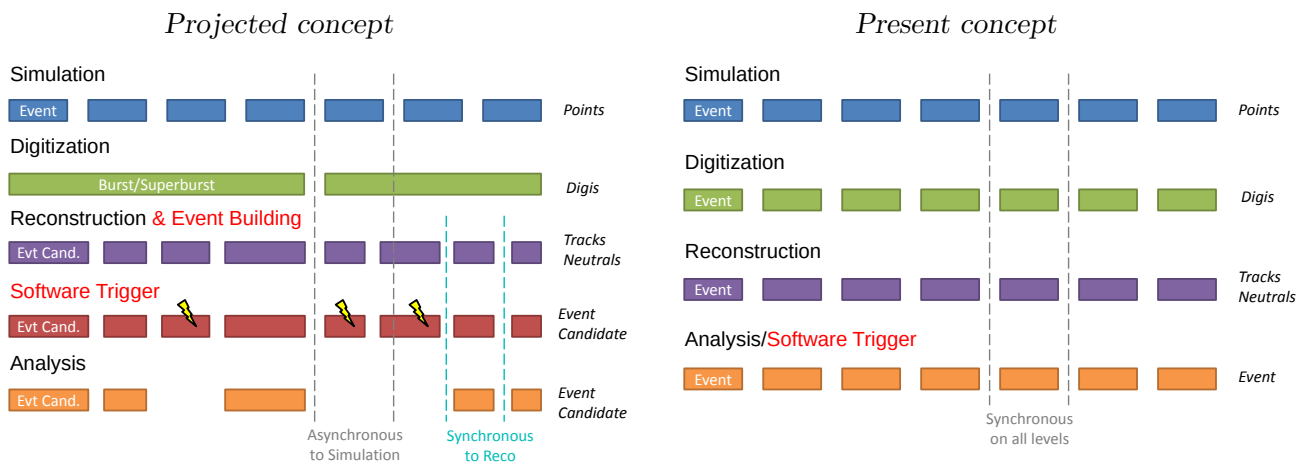

Figure 3: Projected conception of a realistic data flow and data processing using time based simulation (left). Presently realised and available concept with conventional event based simulation scheme (right).

conventional CPUs, connected with sufficient bandwidth to the DAQ system. The decision on the optimal hardware is still pending.

To which extent the DAQ system will finally be able to perform the event reconstruction in real-time, and whether selection algorithms can be developed based on low-level information has still to be investigated.

2.2 Software Trigger within PANDA Software Framework

Concerning the overview given above, the task being addressed by the software trigger subgroup is to develop and provide selection algorithms for the various physics channels of interest as input for the hardware based online trigger system programming and setup. In order to find suitable procedures, physics simulations are performed in various ways.

To reveal the principle potential, we start with simulations based on rather idealised conditions, and thus extract an upper limit of the possible performance. For getting more realistic numbers, an incremental degradation of the amount and quality of the available information can be applied until the realistic level of online reconstruction performance is achieved. The filtering process relies presently on full reconstruction of charged and neutral particles with attached PID information as well as a completed event building process. The input for the reject/retain decision is a stream of event candidates holding all reconstructed objects assigned to a single reaction. The principal strategy for each of the individual trigger lines corresponding to a certain physics channel consists of the following steps:

1. Compute *event related* observables x_i like number of charged particles, sphericity, etc. (for details, see Tab. 15).
2. Form *composite signal candidates* by appropriately combining charged/neutral reconstructed particle candidates, taking into account PID information.
3. Compute *candidate related* observables y_j like invariant mass, transverse momentum, etc. (for details, see Tab. 15).
4. Apply a rough pre-selection based on the invariant mass of the signal candidates.
5. Accept signal candidates meeting the requirements for additional observables x_i and y_j for this specific trigger algorithm; reject the rest for this trigger line.

In order to perform simulations with reliable results, the realistic data flow and processing has to be emulated by the PANDA software as good as possible. The desired scheme of processing, depicted in Fig. 3 (left), starts with generated events being simulated with an appropriate transport model in the detector environment. The Monte Carlo generated information, called *points*, is converted into a time ordered stream of data (*digis*), similar to the actual detector response in the laboratory. In PANDA that data stream probably will be segmented according to the cycling beam to either *bursts* comprising all reactions from one cycle of the anti-proton beam inside HESR, or even *superbursts*,

being the aggregation of 256 bursts. The reconstruction stage has to cope with these larger data segments comprising multiple events, which requires an event building stage in addition to split and sort the data within the stream into data packages according to the individual reactions. The reconstruction based on this stream of *digis* will be performed either by each sub-detector stand-alone, or with support from other sub-detectors. The particular challenge is to disentangle hits from sequent events from detectors with high latency such as e.g. the Straw Tube Tracker (STT), which will probably exhibit a significant overlap due to the high reaction rates being present in PANDA. *Tracks*, *neutral candidates* as well as PID information are formed employing fast online capable algorithms. After *event candidates* have been isolated and formed, the software trigger algorithms are applied to generate a trigger decision. Based on this online decision, part of the data that is not of interest is rejected, defining in the end the residual stream of event candidates stored and being available for more precise reconstruction and the physics analysis offline.

Currently this desirable approach of a realistic data simulation and reconstruction is not available yet, instead a conventional event based approach is performed presently as schematically shown in Fig. 3 (right). The current status of the PandaRoot software is described in detail in Sec. 3.

2.3 Approaches by Other Experiments

Particle physics experiments in general aim for high statistic data samples and are facing the problem of filtering the original data stream for specific signatures in order to safe storage space and computing power for offline analysis later on. This challenge appears when the cross-section related to the physics of interest is much smaller than the total cross-section of the primary reaction. There are present and past experiments facing exactly this problem. Studying approaches made by these experiments might be useful as input for the PANDA related development. It is worth to be mentioned, that as a matter of fact, there is no single experiment known that runs completely without a hardware based trigger applied for pre-filtering. The PANDA experiment will either be the first experiment running with only a software based online trigger system, or it might finally turn out that an additional hardware based trigger will be necessary for PANDA as well.

Charged Trigger of the E835 Experiment

Concerning reaction type and experimental conditions, the E835 experiment [8] at Fermilab can be considered as the most similar predecessor of PANDA. Therefore it is quite natural to take a closer look to the event filtering approach taken by that experiment. Due to the very different detector properties, in particular the lacking of magnetic field and thus momentum measurements for charged particles, the selection procedures are quite special compared to the ones being developed for PANDA. However, the triggering chain itself and the actual implementation [9] is still of interest for our current developments.

The detector consists of a charged tracking system, a threshold Cherenkov detector, an electromagnetic calorimeter, and a forward charged hodoscope, basically allowing to detect photon and electron energies as well as the direction and type of charged particles in a limited way.

E835 primarily detects charmonia through their electromagnetic final states like $\bar{p}p \to c\bar{c} \to e^+e^-(X)$. In order to detect hadronic decays of charmonia like η_c and η_c' without prominent electromagnetic decay modes, the only decay pattern possessing sufficient peculiar kinematic properties is $\bar{p}p \to c\bar{c} \to \phi\phi \to 4K^{\pm}$. The cross-section for this reaction is roughly 4 orders of magnitude lower than for $\bar{p}p \to 4$ *charged tracks*. The basic observables for discriminating signal from background are polar angles and the opening angles of the kaon pairs. The trigger is realised with programmable CAMAC modules and comprises three stages:

1. Discrimination stage: Signals from sub-detectors are discriminated and sent to the next stage.
2. Single logic stage: Units providing trigger information on track reconstruction, neutral veto, coplanarity, multiplicity and $\phi\phi$-tagging logics.
3. Final trigger stage: Processing of the single logic signals and creating trigger signals for e^+e^- and $\phi\phi$ events.

The efficiencies of the charged trigger system was about 90% for e^+e^- events and about 61-65% for $\phi\phi$ events at η_c and η_c' energies. The rate reduction factors for generic $\bar{p}p$ events assuming a total cross-section of $\sigma_{\mathrm{tot}} \approx 70$ mb and a luminosity of $L = 2.5 \cdot 10^{31}$ cm^{-2}s^{-1} compute to $f_{2e} \approx 1/8750$ and $f_{2\phi} \approx 1/116000$, respectively. The transit time through the whole trigger was about $t_{\mathrm{transit}} = 200$ ns.

Although the trigger was basically realised in hardware, it uses complex correlations to achieve a level of suppression being roughly comparable to the corresponding factor $f_{\text{sup}} \approx 1/10000$ forseen for the PANDA experiment per trigger line. It should be added, that despite the higher background suppression in the 2ϕ trigger line, for these two cases the e^+e^- trigger dominates the total final event rate due to the 13 times higher acceptance, when assuming the trigger lines run simultaneously.

High-Level Trigger of the LHCb Experiment

The LHCb experiment at CERN is the logical successor of the two B-factory experiments BaBar and Belle. The objects of investigation are predominantly B and D-like mesons. Since in pp-collisions the cross-section for the production of bottom and charm flavoured hadrons is small compared to that of light quark resonances, the purpose of the LHCb high-level trigger (HLT) is to enrich the taken data sample with bottom and charm states [6]. The detector is a one-arm spectrometer equipped with all typical components necessary for tracking, electromagnetic calorimetry and particle identifications; it is described in detail elsewhere [7].

The trigger architecture consists of two stages: the first level trigger (L0), and the High-Level Trigger (HLT).

First level trigger L0 L0 is hardware based and uses input from the calorimeter and the muon system. It is able to trigger for hadrons, photons, electrons and muons by finding coincidences between the hits in the electro-magnetic calorimeters, the hadronic calorimeters and the tracking system in a very rough way. The data stream reduction achieved by this system is approximately one order of magnitude, which decreases the initial rate of 11 MHz to 870 kHz.

High-level trigger HLT The HTL of LHCb is a program written in C++, which runs on $\approx$ 26000 compute nodes of the event filter farm (EFF) consisting of multiprocessor PCs. An event being accepted by L0 is sent to the EFF, where it is assembled by an event builder program and stored to a buffer, where it is accessed by the trigger algorithms running on the EFF cores. The time being available in the HLT for one event is limited to $\approx$ 30 ms at the given L0 rate of 870 kHz. Since this is much less time than the 2s spent for offline event reconstruction, the HLT itself is split into two stages: The HLT1 performs a much faster partial event reconstruction, which reduces the rate to 43 kHz. Events being accepted in this stage are reconstructed more complete before they are processed by the HLT2. The final event rate is about 3 kHz, i.e. the total reduction factor achieved by the trigger system is about 3700.

The HTL comprises 38 trigger lines in HLT1 stage and 131 trigger lines in HLT2. The main observables used for selection are geometrical variables like closeness to the IP and between tracks, and kinematic variables like masses, transverse momenta, energies, sums of momenta/energies and multiplicities.

Due to special geometry of the detector and the particular kinematics of the reactions of interest, the most powerful observables for initial data reduction are transvers momenta of charged and neutral candidates, leading to reasonable high efficiencies for basically all B and D channels under study for $p_t > 3$ GeV/c.

The similarity to PANDA in that respect is rather limited, since the diverse PANDA physics programme does not offer any special observable which is common for all or at least many of the channels, in particular not for varying centre-of-mass energies $\sqrt{s}$.

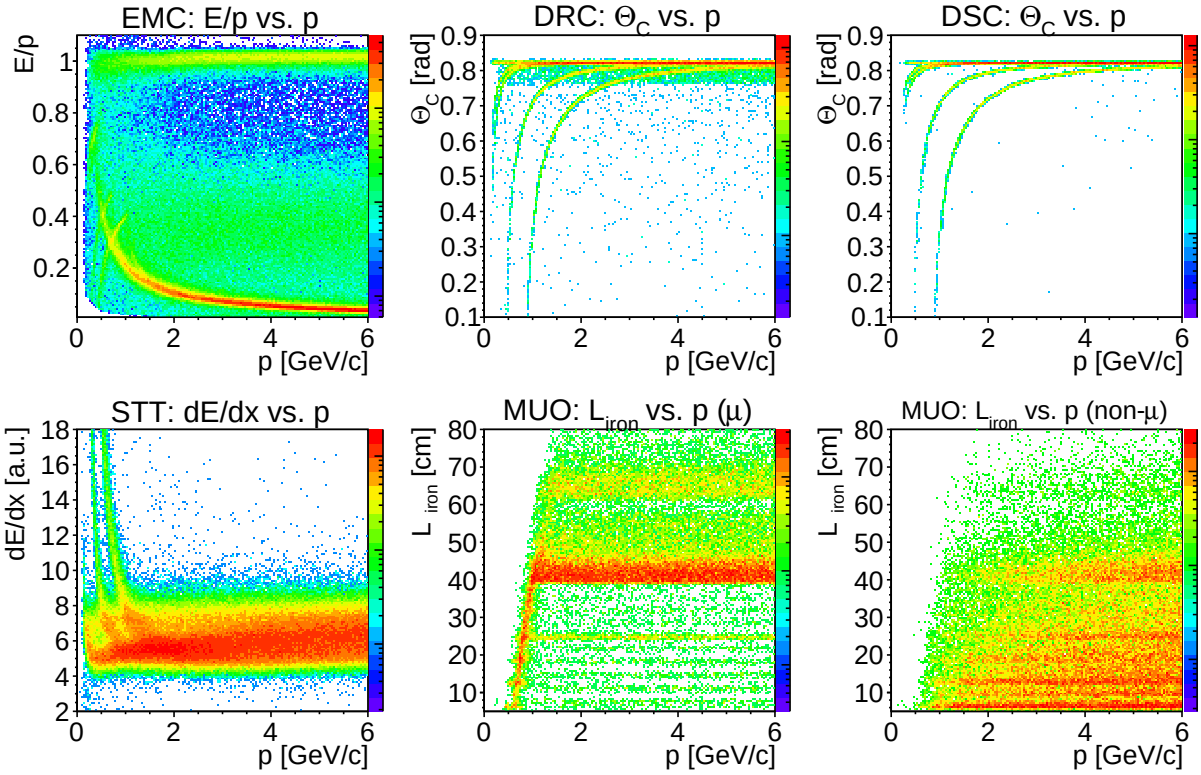

Figure 4: PID raw detector info for EMC, DIRC, DISC, STT and MUO. Distributions are superimposed for all particle species (electrons, muons, pions, kaons, protons) as a function of the particle momentum.

3 Current Status of Event Reconstruction in Panda

In the previous section, the ideal requirements for online trigger development and testing were briefly discussed, and it was pointed out that these requirements are not yet fully met at present with the official PANDA software framework PandaRoot [2].

The PandaRoot simulation/reconstruction used for the studies presented in this document were performed with the official version `release/jan14` using the recommended external packages version `apr13`. The transport model was chosen to be Geant3. All jobs were run on the Prometheus cluster at GSI [3]. In order to clarify all assumptions and at the same time compile a to-do list for future PandaRoot developments, the conditions of the present physics simulation are briefly summarised in the following.

Event building

The desirable approach for performing simulations for the PANDA experiment is given by the time-based simulation (cf. Sec. 2.2). This feature in general is in preparation for all sub-detectors, but at time of writing this report it was not available yet for the full system. Therefore all studies presented in this note are done with the conventional event-based simulation. A realistic event building was also not yet implemented, neither PandaRoot is yet suitable to perform studies for an online scenario, in which fewer or less precise information will be available.

Central tracking

The tracking in the central tracking detector STT works like in a realistic offline scenario, taking into account event mixing with a proprietary technique. No online algorithm is implemented in PandaRoot yet. Deficiencies for the reconstruction of tracks not originating from the interaction point (IP) but coming from displaced vertices are presently observed with the `release/jan14`. This has impact on the reconstruction efficiency of long living particles like e.g. Λ or K^0_S, presently hampering the performance for physics channels involving these kind of particles.

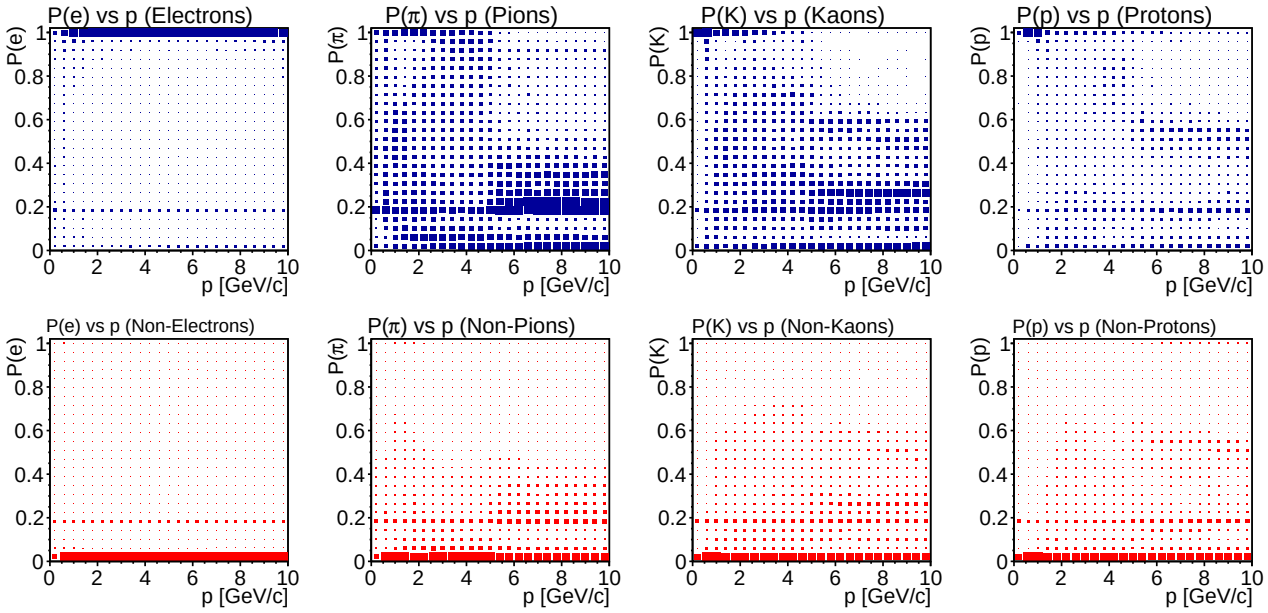

Figure 5: Graphical representation of the combined PID likelihood values (detectors: EMC, STT, DRC, DSC, MUO) for electrons, pions, kaons and protons as a function of particle momentum. The plots in the upper row show the distributions for the correct particle type, the lower ones for the incorrect type. It can clearly be seen, that for the correct type the distributions tend towards higher likelihood values, for the incorrect type they accumulate around $P = 0$. The bands at $P = 0.2$ correspond to particles, for which no PID info can be assigned. The PID preselection for the studies in this note was chosen to be $P > 0.1$ as a very loose veto against wrong particle types.

Forward tracking

The forward tracking is based on ideal pattern recognition, i.e. the hits used for a certain track fit are compiled via MC truth information. Neither a realistic online nor offline tracking is available for the time being. The efficiency for forward tracking ($\theta < 22°$) varies significantly and is in average about 50-65%.

Neutrals

The reconstruction of γ candidates based on cluster reconstruction in the electro-magnetic calorimeter is done like in a realistic offline scenario, which might be implemented online in a very similar way, but still needs to be realised and validated. A significant discrepancy in the multiplicity of reconstructed neutral objects comparing `Geant3` and `Geant4` is observed. The multiplicity of neutral candidates seems to be too large in both cases and can lead to high combinatoric counts, when reconstructing composite particles involving γ candidates, cf. [5]. Merged π^0 and other neutral particles like neutrons are not explicitly taken into account in the reconstruction process up to now.

Particle identification

Several components of the PANDA detector contribute to the PID information.

Straw Tube Tracker (STT) The specific energy loss dE/dx used for PID of low momentum particles is simulated realistically. This approach seems to be applicable in an offline as well as online implementation.

Micro Vertex Detector (MVD) The specific energy loss dE/dx is realistically simulated. The algorithms seems suitable for offline as well as online environment.

Electromagnetic calorimeter (EMC) The cluster energy combined with the momentum from tracking can be used primarily for electron identification. Due to lack of online tracking, PID using the EMC is presently considered to be of a quality as from the offline scenario for now.

Time-of-Flight (SciTil) The implementation of the barrel shaped SciTil is in preliminary shape. The time-of-flight information is simulated as if a start detector with infinite precise time resolution would exist. No time-of-flight detector is implemented for the forward region as well as the forward spectrometer behind the dipole so far.

Barrel DIRC (DRC) The barrel DIRC (Detection of Internally Reflected Cherenkov light) reconstruction is presently only available as an effective simulation of a θ_C measurement with a certain total resolution leading to a simplified likelihood calculation. The assignment of the PID info to the corresponding track object was not working efficiently in the present simulation, so that the DIRC PID was only available for a rather limited fraction of particles. No realistic reconstruction was available, neither suitable for offline nor for online analysis. The way the PID information is calculated has to be considered as idealised. The level of online achievable PID quality is not known for the time being.

Forward Disc DIRC (DSC) The disc shaped version of the forward DIRC only provides reconstruction on the same effective level as the Barrel DIRC. No realistic reconstruction was available, neither suitable for offline nor for online analysis. The PID information provided can be considered as idealised. The level of online achievable PID quality is not known until now.

Muon Detector (MUO) The PID reconstruction of the muon detector is implemented in a realistic way. It seems suitable for offline as well as online scenarios.

PID algorithms In PandaRoot, PID information are computed from likelihood values, which are provided by algorithms based on the raw PID observables of the various sub-detectors. Each sub-system individually computes for each charged candidate a vector of five probabilities for the different particle species (P_e, P_μ, P_π, P_K, P_p), which then can be combined to a global likelihood per particle species. This information is accessible through the analysis framework, where the results of the different algorithms are accessed simply by their name. The total PID information reflects the quality achievable offline. The level of online PID is not known up to now.

The raw simulated PID information for various particle types as a function of momentum are shown in Fig. 4 for the different detectors. Concluding from the discussion of the status above, the following PID detectors (with corresponding algorithm name in parenthesis) were taken into account

- STT (`PidAlgoStt`)
- EMC (`PidAlgoEmcBayes`)
- DRC (`PidAlgoDrc`)
- DSC (`PidAlgoDisc`)
- MUO (`PidAlgoMdtHardcuts`)

The distributions in Fig. 5 show the combined likelihood values from all five algorithms for electrons, pions, kaons and protons as a function of particle momentum. The distribution for muons look quite similar to the electron ones, and are therefore not shown here. The plots in the upper row show the distributions of 250k single particles of the type matching the hypothesis, the lower plots show the likelihood distribution of 1M single particles of the wrong particle species, 250k of each type. As expected the likelihoods for the correct hypothesis in the upper plots accumulate at higher likelihood values, whereas the incorrect particle types get lower likelihoods. These quantities are used to perform a PID selection in the FullMC studies with a rather loose preselection cut of $P > 0.1$, removing most of the wrong particles.

4 Physics Channels under Investigation

The PANDA experiment is designed to cover a broad physics program (Sec. 1), and a large variety of reaction types has therefore to be identified by the online trigger system for the various purposes in the final setup. Since the PANDA experiment will start running in several years from now, a complete list of reactions of interest cannot be compiled at the time of writing this document. Therefore, only the principle feasibility can be demonstrated for now on the basis of a limited subset of physics reactions. A preliminary list of about 25 channels has been defined for that purpose, including various subsequent decay modes of resonances such as D^0, D^+, η_c, etc, to be identified in order to improve the total fraction of interesting candidates. The selection has been motivated by the PANDA Physics Book [1].

For the present studies, we restrict ourselves to a subset of 10 of these channels (with the most simple and clear decay modes), still covering the main physics topics addressed by the PANDA collaboration, as listed in Tab. 1. These channels have been studied at centre-of-mass energies of $\sqrt{s} = 2.4\,\text{GeV}$, $3.77\,\text{GeV}$, $4.5\,\text{GeV}$, and $5.5\,\text{GeV}$, covering the full energy range accessible by the HESR. Corresponding datasets have been created and then processed by the trigger lines, whereas some of the reactions are kinematically not possible below a certain centre-of-mass energy, see Tab. 2.

In order to determine the performance of the single trigger lines and the full simultaneous triggering system of all 10 channels, each reaction type has an assigned trigger signature, which is designed to identify only an inclusive part of the decay pattern such as the decay $D^0 \to K^-\pi^+$ including charge conjugate (c.c.). No exclusive triggering is considered yet. Furthermore, only one dedicated signal dataset has been generated for each of the individual triggers. Future studies will also take into account reactions, which exhibit the decay pattern of interest in another context, e.g. $\bar{p}p \to D^0\bar{D}^{0*}$ to be tagged by the D^0 trigger in addition to the reaction listed in Tab. 1.

Table 1: List of 10 physics reaction channels under study (where applicable c.c. included), sorted by related physics topics. For easier reference in the text and tables, reaction types are referred to by certain codes. The corresponding trigger signatures are listed together with their abbreviating tag names.

Physics topic	Reaction channel	Code	Trigger	Tag
Electromagnetic	$p\bar{p} \to e^+e^-$	ee	$p\bar{p} \to e^+e^-$	e^+e^-
Exotics	$p\bar{p} \to \phi_{(1)}\phi_{(2)}$; $\phi_{(1)} \to$ trigger, $\phi_{(2)} \to X$	Phi	$\phi \to K^+K^-$	ϕ
Charmonium	$p\bar{p} \to \eta_c\,\pi^+\pi^-$; $\eta_c \to$ trigger	Etac	$\eta_c \to K_S K^-\pi^+$	η_c
	$p\bar{p} \to J/\psi\,\pi^+\pi^-$; $J/\psi \to$ trigger	J2e	$J/\psi \to e^+e^-$	$J/\psi(2e)$
	$p\bar{p} \to J/\psi\,\pi^+\pi^-$; $J/\psi \to$ trigger	J2mu	$J/\psi \to \mu^+\mu^-$	$J/\psi(2\mu)$
Open charm	$p\bar{p} \to D^0\overline{D^0}$; $D^0 \to$ trigger; $\overline{D^0} \to X$	D0	$D^0 \to K^-\pi^+$	D^0
	$p\bar{p} \to D^+D^-$; $D^+ \to$ trigger, $D^- \to X$	Dch	$D^+ \to K^-\pi^+\pi^+$	D^+
	$p\bar{p} \to D_s^+D_s^-$; $D_s^+ \to$ trigger, $D_s^- \to X$	Ds	$D_s^+ \to K^+K^-\pi^+$	D_s^+
Baryons	$p\bar{p} \to \Lambda\overline{\Lambda}$; $\Lambda \to$ trigger; $\overline{\Lambda} \to X$	Lam	$\Lambda \to p\pi^-$	Λ
	$p\bar{p} \to \Lambda_c\overline{\Lambda}_c$; $\Lambda_c \to$ trigger; $\overline{\Lambda}_c \to X$	Lamc	$\Lambda_c \to p\mathrm{K}^-\pi^+$	Λ_c
Background	$p\bar{p}$ generic (DPM)	DPM	–	–

Table 2: Data samples for the various reaction types for different centre-of-mass energies $\sqrt{s}$ and beam momenta $p_{\bar{p}}$. Combinations marked with "–" are kinematically not accessible and therefore not triggered at that energy. inelastic DPM events are used as generic background.

$\sqrt{s}$ [GeV]	$p_{\bar{p}}$ [GeV/c]	ee	Phi	Etac	J2e	J2mu	D0	Dch	Ds	Lam	Lamc	DPM
2.4	1.91	X	X	–	–	–	–	–	–	X	–	X
3.77	6.57	X	X	X	X	X	X	X	–	X	–	X
4.5	9.81	X	X	X	X	X	X	X	X	X	–	X
5.5	15.15	X	X	X	X	X	X	X	X	X	X	X

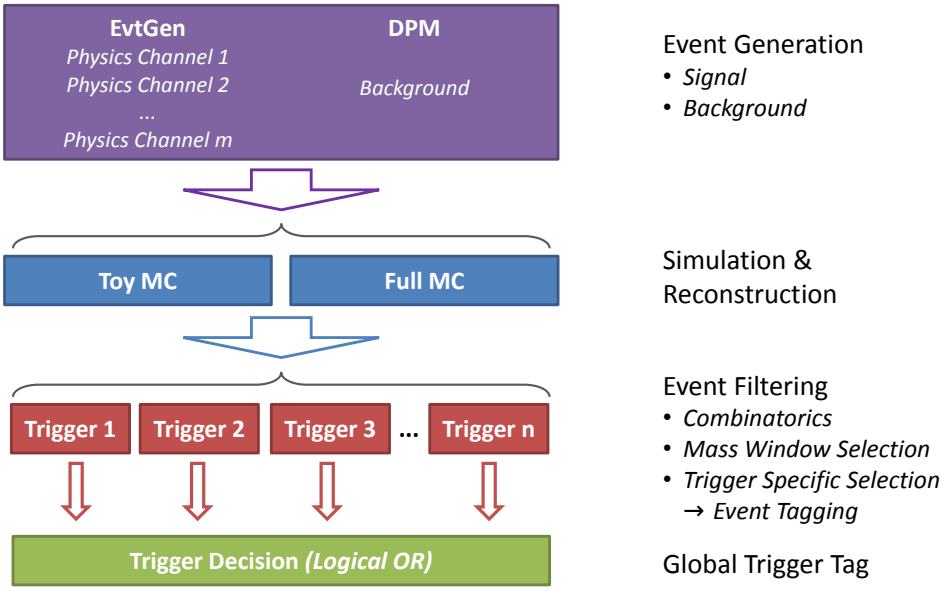

Figure 6: Scheme of the software trigger studies presented in this note.

5 Status of Present Studies and Results

In order to obtain first numbers for achievable data rate suppression using the software trigger, various possible observables have been investigated in two ways, performing simple and fast toy Monte Carlo simulation studies (ToyMC) as well as applying the full simulation in PandaRoot `release/jan14` (FullMC) with Geant3. Furthermore, instead of an optimisation of the selection criteria by hand as applied to both cases, the application of a TMVA method is evaluated in addition on the FullMC data.

A schematic overview of the software trigger studies is given in Fig. 6. Physics signal events for $m = 10$ selected channels of interest and background events have been generated using EvtGen [10] and DPMgen [11], respectively. The simulation and reconstruction of the events of the $m + 1 = 11$ different datasets is done using the ToyMC and the FullMC, respectively (in case of the ToyMC, simply energy and momentum smearing). The reconstructed events are then filtered by $n = 10$ different trigger lines (cf. Tab. 1). For each trigger line, the corresponding combinatorics is done for the given datasets (m physics channels and DPM background). Then a mass window preselection is applied, succeeded by further cuts on other trigger specific observables. Events fulfilling the criteria are tagged to be kept by the given trigger line. The final simultaneous trigger decision is a global trigger tag, consisting of a logical "OR" combination of all n trigger line tags.

The outline of this section is the following. First, the method of extracting efficiency values to characterise the performance results presented in this note are defined and the issue of cross-tagging is discussed (Sec. 5.1). Then, the observables used for filtering the events by separating signal from background are presented and the two approaches of optimisation followed presently are introduced (Sec. 5.2). The procedure of finding the observables and optimising the corresponding cuts is exemplary illustrated in detail using the ToyMC data in Sec. 5.3, where also the ToyMC results of resultant trigger efficiencies are summarised and explained using two example signal datasets and the background dataset. The FullMC case is treated in the same way, and the results are summarised and illustrated for the same three example datasets in Sec. 5.4. In Sec. 5.5, the TMVA method is introduced and applied to the FullMC data. The present results obtained for these three cases (ToyMC, FullMC, and FullMC with TMVA) are compared and discussed in Sec. 5.6.

5.1 Event Based Efficiency and Cross-Tagging

We are dealing with event related as well as candidate specific information in our trigger line algorithms, and it should be emphasised that all the efficiencies given throughout this note are determined event based – in line with the practical situation of future data taking. If any set of observables for a particular composite candidate meets all the requirements to be tagged as signal

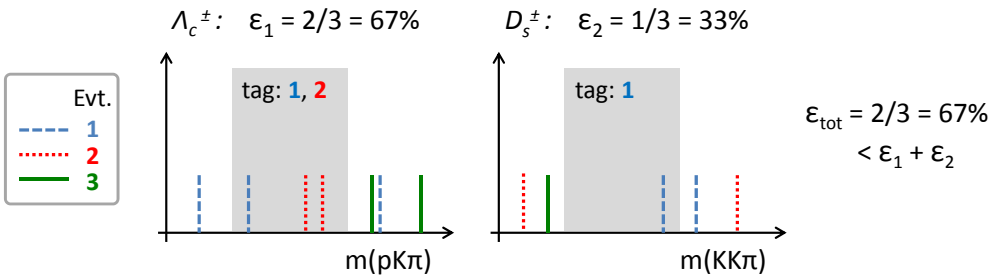

Figure 7: Schematic illustration of *event based efficiency*. The two diagrams correspond to two trigger lines (here e.g. denoted as $\Lambda_c^\pm$ and $D_s^\pm$), where the (artificial) invariant mass of trigger candidates from three events are displayed as lines of different colors/styles. The individual trigger line efficiencies are given by the fraction of events having at least one candidate tagged (lying in the grey shaded region). The total effciency is the fraction of all events being tagged by at least one trigger line.

candidate, the event containing this candidate is tagged to be accepted by a given trigger line. This is illustrated in Fig. 7, where the two diagrams correspond to two exemplary trigger lines (here $\Lambda_c^\pm$ and $D_s^\pm$). The corresponding (artificial) invariant masses of trigger candidates from three events are entered as discrete distributions of different colours/line styles. The selection region is marked as grey shaded area. The $\Lambda_c^\pm$-trigger on the left side tags $\epsilon_1 = 2/3 = 67\,\%$ of the three events (the blue dashed and red dotted one), since entries from two different events are in the selection region. The $D_s^\pm$-trigger accepts only $\epsilon_2 = 1/3 = 33\,\%$ of the events (the blue dashed one). Since in total, two of the three events contain a candidate fulfilling all criteria of at least one trigger line, the total efficiency results in $\epsilon_{\rm tot} = 2/3 = 67\%$.

It should be noted that there are four different cases leading to an event being tagged:

1. The correctly reconstructed candidate of reaction X (e.g. $D^0 \to K^-\pi^+$) for a particular trigger line supposed to tag X (let us call it T_X) leads to the tag. This case is obviously the primarily intended one.
2. A random combinatoric candidate in an event actually containing X is triggered by T_X. This is considered to be a successful tag as well. In approaches where only event related observables are considered without doing combinatorics, this case actually merges with case 1.
3. A random combinatoric candidate in an event containing another signal reaction Y causes T_X to tag the event (we call this effect *cross-tagging*). This is also considered as a successful tagging, since a signal event of dedicated interest is kept by the full trigger system consisting of multiple trigger lines operating simultaneously.
4. A random combinatoric candidate of a background event leads to a tag. This is the only unwanted case.

The event based efficiency determination and the various ways for event tagging might lead to unexpected and unintuitive effects, to be kept in mind for the understanding of the presented spectra and the resultant efficiency values.

- In general, the total efficiency is lower than the sum of all individual trigger line efficiencies, i.e. $\epsilon_{\rm tot} < \sum_i \epsilon_i$, as illustrated by the example given in Fig. 7, where $\epsilon_{\rm tot} = 67\% < 100\% = \epsilon_1 + \epsilon_2$.
- Multiple candidates formed within one single event fulfilling all selection criteria for a particular trigger do not increase the efficiency. This leads sometimes to the situation, that the integral fraction of a certain distribution does not visually match the associated efficiency value.
- The efficiency of a certain trigger line for the according signal events (T_X acting on events containing X) can be significantly higher than suggested by the efficiency based on Monte Carlo truth matched candidates.
- The total efficiency for a particular type of signal events (all T_i acting simultaneously on events containing X) can be significantly higher than the trigger line specific efficiency. This implies, that switching off e.g. trigger line T_Y in a certain trigger configuration could lead to a decreasing total efficiency for all other signal event types $X_i \neq Y$, and, at the same to a still non-vanishing efficiency for events containing Y.

5.2 Observables for Filtering Events and Optimisation of Cuts

Various observables and quantities have been investigated to obtain a highest as possible reduction factor for the event rate that will be needed to be written to the storage, while keeping as many as possible events of interest.

Initially, individual mass window cuts on the nominal masses are applied simultaneously for each trigger line. They are consistently applied in terms of $\pm 8\sigma$ mass resolution as measured after the given event reconstruction. The $\pm 8\sigma$ width for the cuts on the invariant masses is motivated by having in mind a $\pm 6\sigma$ window usually needed for a classical sideband background subtraction in later offline analysis with some additional safety buffer, not to over-cut the data.

Apart from the mass window preselection, further cuts are applied subsequently. A large set of observables has been investigated, and the complete set considered so far is listed in Tab. 15 in the Appendix (Sec. 8). The set of observables that turned out to be useful for our purpose are listed in Tab. 3. In addition to the corresponding short cut naming, a scheme used throughout this note, the individual cut variables are also briefly explained in this table. These observables are differently effective in separating signal from background for the different trigger lines, which also depends on $\sqrt{s}$. As expected, some of them turned out to be strongly correlated. Therefore, a selection of cuts out of the set of cut variables as listed in Tab. 3 are applied individually for the different trigger lines. The set and order of cuts is found by an optimisation procedure. We have applied two different approaches for optimising the cuts and to deliver numbers for background reduction and signal efficiencies. The numbers presented in this note are based on two optimisation approaches,

Table 3: List of abbreviations and short description of the various cut variables found to be effective and applied. For the definitions of the so-called event shape variables, see [12].

Short cut	Description
p	momentum p of reconstructed candidate (lab)
pt	transverse momentum p_t of reconstructed candidate
pcm	momentum p of reconstructed candidate (cms)
e	energy e of reconstructed candidate (lab)
ecm	energy e of reconstructed candidate (cms)
tht	polar angle θ of reconstructed candidate (lab)
thtcm	polar angle θ of reconstructed candidate (cms)
mmiss	missing mass of reconstructed candidate
di{p,pt,tht}	kinematic variables from i-th daughter of candidate
d$i$pidk, d$i$pidp	Kaon/Proton PID probability of i-th daughter
pmax	maximum particle momentum in event (cms)
ptmax	maximum transvers particle momentum in event
sumpc	sum of momenta of charged particles in event (cms)
sumptc	sum of transverse momenta of charged particles in event (cms)
detemcsum	sum of cluster energies in EMC
detemcmax	maximum cluster energy in EMC
lnpide	Number of loose ($P > 0.25$) electron candidates
lnpidmu	Number of loose ($P > 0.25$) muon candidates
lnpidpi	Number of loose ($P > 0.25$) pion candidates
lnpidk	Number of loose ($P > 0.25$) kaon candidates
lnpidp	Number of loose ($P > 0.25$) proton candidates
thr	Event shape: Magnitude of thrust of event (cms)
apl	Event shape: Aplanarity of event (cms)
fw1	Event shape: 1. Fox-Wolfram Moment $R_1 = H_1/H_0$ (cms)
fw2	Event shape: 2. Fox-Wolfram Moment $R_2 = H_2/H_0$ (cms)
fw3	Event shape: 3. Fox-Wolfram Moment $R_3 = H_3/H_0$ (cms)
fw4	Event shape: 4. Fox-Wolfram Moment $R_4 = H_4/H_0$ (cms)
fw5	Event shape: 5. Fox-Wolfram Moment $R_5 = H_5/H_0$ (cms)

focussing on:

a) Optimisation for high signal efficiency
The selection of observables and the corresponding cut values are optimised for high signal efficiency. A predefined relative signal efficiency of 90% (with respect to the number of signal candidates after the mass window cuts) is kept for each particular trigger line on the corresponding data set after all cuts have been applied.

b) Optimisation for high background suppression
The selection of variables and the corresponding cut values are optimised to achieve a background reduction factor of 1000. A predefined absolute background reduction factor of 1000 (being equivalent to a total background efficiency of 0.1%) at a certain energy $\sqrt{s}$ is kept after all cuts (including the mass window cuts) have been applied. In contrast to the high efficiency scenario above the reduction is related to all trigger lines at a certain $\sqrt{s}$ simultaneously, i.e. the reduction factor aimed for each of the $n(\sqrt{s})$ trigger lines was in average $1/1000 \cdot n(\sqrt{s})$.

The approach a) is motivated by keeping as much as possible of signal events and acquire the data in a most unbiased way. The approach b) on the other hand is motivated by achieving the nominal data rate level, which is mostly dominated by the huge amount of expected background events, even though a significant fraction of signal events of interest might be rejected as well.

A usual figure of merit, like the significance defined e.g. as $S/\sqrt{S+B}$, is not applied here since neither the cross-sections for the signals nor for the backgrounds are known. Any extracted performance number would depend on the corresponding signal cross-section to background cross-section ratio – such dependence is avoided by the approaches chosen and applied here.

This procedure is applied for both approaches of optimisation for both, the ToyMC (Sec. 5.3) and FullMC (Sec. 5.4) data. By the application of the TMVA method (Sec. 5.5), the optimisation is done automatically, whereas the same two approaches of optimisation (for signal efficiency and background suppression) are similarly realised, so that the three sets of resultant efficiency numbers (ToyMC, FullMC and TMVA) are directly comparable.

5.3 Results from Toy Monte Carlo Studies

For the Toy Monte Carlo (ToyMC) studies, four-vectors of particles have been taken directly from the event generator and a full geometric 4π acceptance is assumed. The following modifications have been applied to the generated particles in order to imitate appropriate reconstruction uncertainties:

- Charged particles
  - Tracking efficiency: $\epsilon_{\mathrm{trk}} = 95\,\%$.
  - Momentum resolution: $\Delta p/p = 5\,\%$
  - Angular resolution: $\Delta\theta = \Delta\phi = 1$ mrad
- PID quality for all charged particle species
  - Efficiency: $\epsilon_{\mathrm{PID}} = 95\,\%$ (correct hypothesis)
  - Mis-identification level: $\mathrm{mis}_{\mathrm{PID}} = 5\,\%$ (all incorrect hypotheses)
- Neutral particles
  - Energy resolution: $\Delta E/E = 5\,\%$
  - Angular resolution:$\Delta\theta_{\mathrm{neut}} = \Delta\phi_{\mathrm{neut}} = 3$ mrad.

Signal datasets of 50k events were generated using EvtGen for each of the 10 channels for each of the exemplary centre-of-mass $p\bar{p}$ energies $\sqrt{s} = 2.4\,\mathrm{GeV}$, $3.77\,\mathrm{GeV}$, $4.5\,\mathrm{GeV}$ and $5.5\,\mathrm{GeV}$, background datasets of 500k events were generated using DPMgen, accordingly for the same centre-of-mass $p\bar{p}$ energies (Sec. 4, Tab. 2).

Using this ToyMC, the achievable efficiencies and background reduction factors for the scenario when applying the 10 trigger lines simultaneously on all 11 reaction types (Sec. 4, Tab. 1) are studied. At the first level, the mass window preselections are applied on the nominal mass for each channel to tag events to be of interest. At a second level, further trigger specific selection cuts are applied subsequently.

The procedure and the optimisation of these further selection cuts is explained and illustrated in detail for the different levels (after mass window cuts, and after additional cuts applied) in the following, using the two signal dataset examples, namely Ds and Etac, and the dataset of DPM background events, for the centre-of-mass energy $\sqrt{s} = 5.5\,\mathrm{GeV}$. The complete result of these

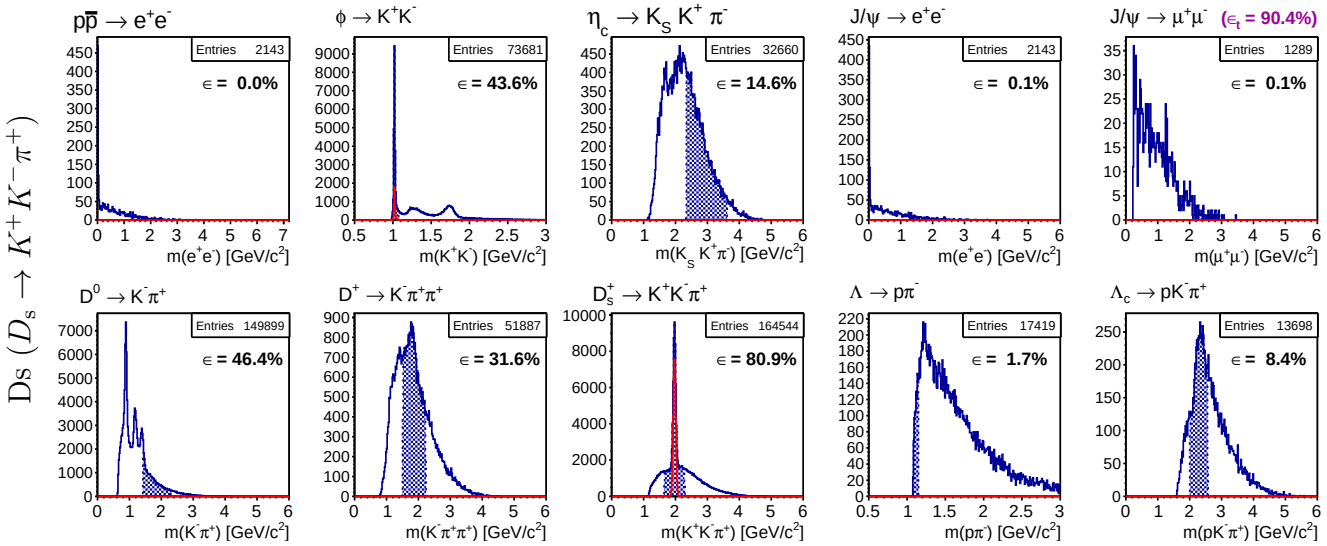

Figure 8: *ToyMC, Ds – Mass window cuts:* Illustration of the simultaneous tagging for the *Ds dataset example* at $\sqrt{s}$= 5.5 GeV. The individual signal efficiencies ϵ for the different trigger lines after the mass window cuts have been applied are given on the corresponding plots, in addition the global total efficiency ϵ_t for all 10 channels applied simultaneously for triggering are given top/right, for discussion see text.

studies for all datasets, corresponding to the 10 physics channels and the DPM background sample, is summarised in form of tables.

Signal and background efficiencies after mass window preselection

For the *Ds dataset example*, the application of the mass window preselection is illustrated in Fig. 8. A set of 10 plots is displayed showing the invariant mass spectra for the resonances involved in each of the 10 trigger lines that were reconstructed from the Ds dataset (blue histogram in each of the 10 plots, the title in each plot specifies the trigger line). In each of the 10 spectra, the blue shaded area indicates the applied mass window cut for the given trigger line, and the red histogram represents the MC truth matched candidates just for illustration. The quoted efficiencies ϵ are the fraction of the 50k input events tagged by the given trigger line for the underlaying dataset (here the Ds dataset). The total efficiency ϵ_t of the simultaneous triggering (all 10 trigger lines connected by a logical "OR"), that is the fraction of the 50k input events that have been triggered in total by at least one of the 10 trigger lines, is given at the right upper corner. For this example of the Ds dataset, one nicely sees the $D_s^{\pm}$ invariant mass peak in the plot for the $D_s^+ \to K^+K^-\pi^+$ trigger (Fig. 8). With the 8σ mass cut (blue shaded area) applied, an efficiency of detected signal events of $\epsilon = 80.9\,\%$ is achieved. Note that due to combinatorics, the 50k input events may result in a larger number of entries in the histograms, like e.g. about a factor of three larger for this example of the Ds dataset, cf. also the discussion in Sec. 5.1. The e^+e^--tag for example does not accept any event of this dataset, thus the efficiency is $\epsilon = 0.0\,\%$, whereas e.g. $\epsilon = 43.6\,\%$ of the events are accepted by the ϕ-tag, and so on. In total, the 10 trigger lines tag $\epsilon_t = 90.4\,\%$ of the events of the Ds dataset.

For the *Etac dataset example* (Fig. 9), the 8σ mass cut applied on the η_c mass for the $\eta_c \to K_S K^+\pi^-$ trigger, results in an efficiency $\epsilon = 72.5\,\%$ for the η_c-tag. Also here, the e^+e^--tag does not accept any event of this dataset ($\epsilon = 0.0\,\%$), and e.g. $\epsilon = 0.3\,\%$ of the events are accepted by the ϕ-tag, and so on. The total efficiency of the 10 simultaneous trigger lines for the Etac dataset results in $\epsilon_t = 89.1\,\%$.

In case of the *DPM background dataset example* (Fig. 10), applying the 8σ mass window preselection for all 10 trigger lines result in a total efficiency of $\epsilon_t = 21.9\,\%$ (and e.g. $\epsilon = 2.8\,\%$ for the D_s^+-tag, $\epsilon = 3.4\,\%$ for the η_c-tag, $\epsilon = 0.0\,\%$ for the e^+e^--tag, and $\epsilon = 0.8\,\%$ for the ϕ-tag). It should be emphasised again, that the total efficiency in general is not the sum of the individual efficiencies, since individual events (signal or background) might be triggered by multiple trigger lines at the same time.

The total efficiencies of the 10 simultaneous trigger lines for these three example datasets of

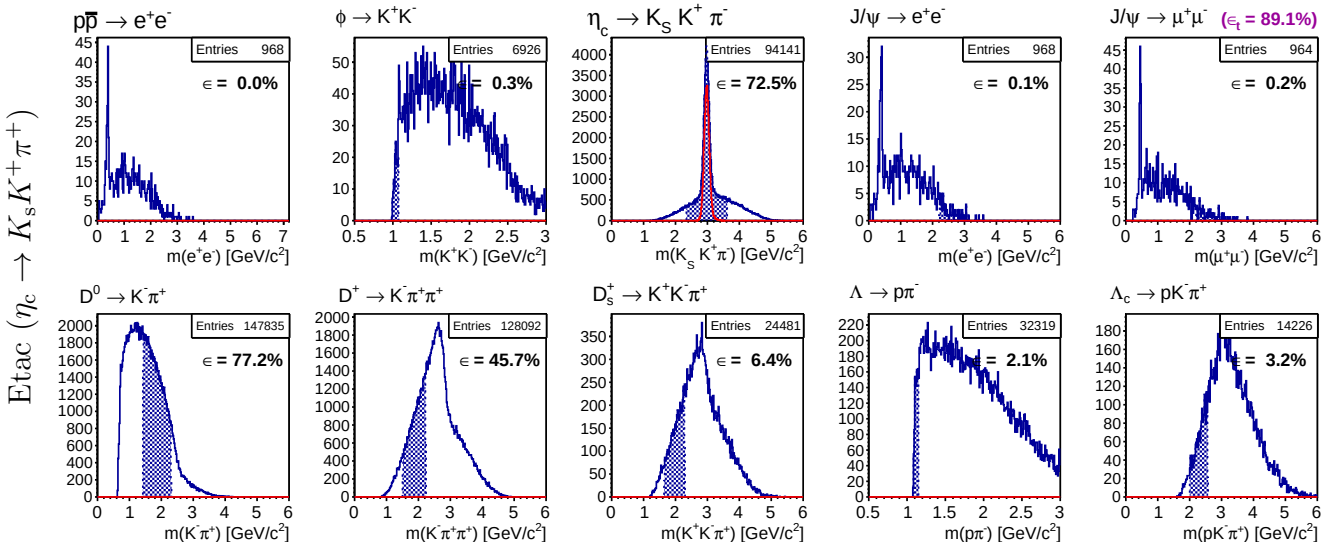

Figure 9: *ToyMC, Etac – Mass window cuts:* Illustration of simultaneous tagging for the *Etac dataset example* at $\sqrt{s}$= 5.5 GeV. The individual signal efficiencies ϵ for the different trigger lines after the mass window cuts have been applied are given on the corresponding plots, in addition the global efficiency $\epsilon_{\rm tot}$ for all 10 channels applied simultaneously for triggering are given top/right, for discussion see text.

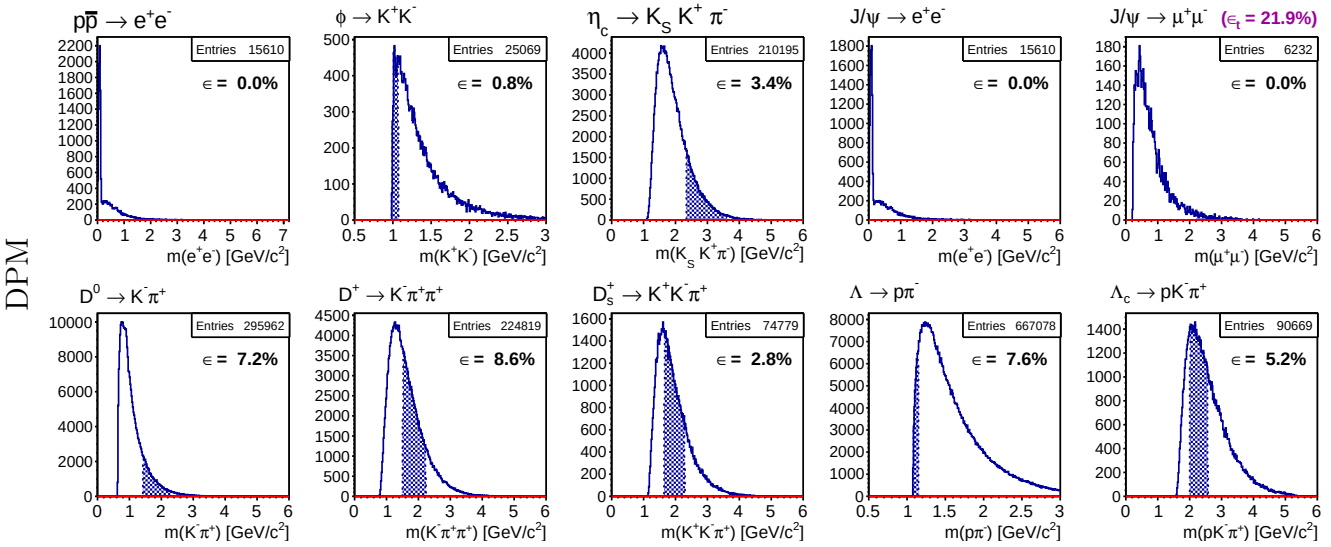

Figure 10: *ToyMC, DPM – Mass window cuts:* Illustration of simultaneous tagging for the *DPM background dataset example* at $\sqrt{s}$= 5.5 GeV. The individual signal efficiencies ϵ for the different trigger lines after the mass window cuts have been applied are given on the corresponding plots, in addition the global efficiency $\epsilon_{\rm tot}$ for all 10 channels applied simultaneously for triggering are given top/right, for discussion see text.

Table 4: *ToyMC – Mass window cuts:* Summary of the total simultaneous trigger efficiencies ϵ_t [%] for the different datasets, after mass window cuts applied.

$\sqrt{s}$ (GeV)	ee	Phi	Etac	J2e	J2mu	D0	Dch	Ds	Lam	Lamc	DPM
2.4	79.41	88.32	-	-	-	-	-	-	91.12	-	3.46
3.77	80.28	91.16	87.41	79.88	81.49	85.16	81.87	-	91.12	-	11.70
4.5	80.43	92.08	89.24	80.55	82.01	87.36	85.55	89.13	90.87	-	15.27
5.5	80.88	91.81	89.14	80.84	82.78	87.04	85.54	90.38	91.05	89.06	21.93

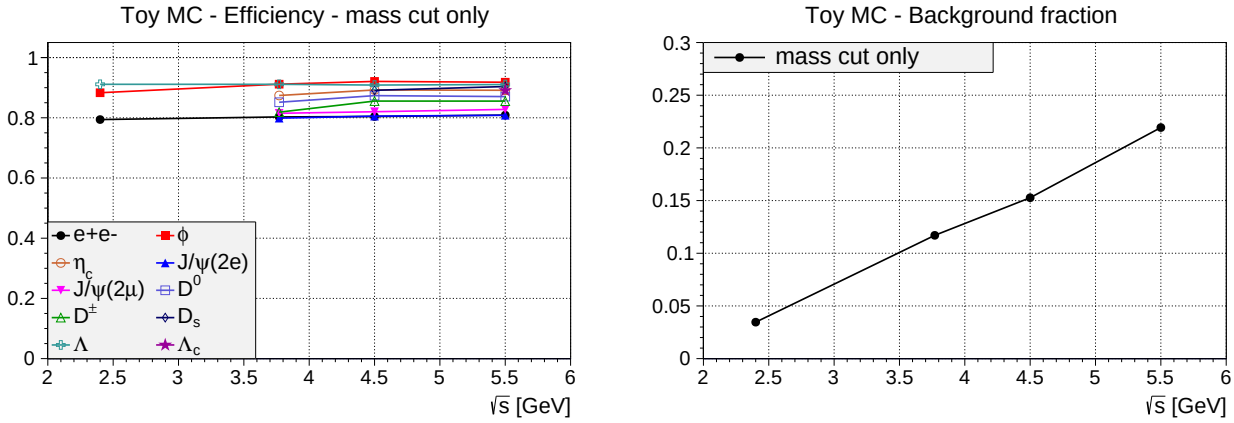

Figure 11: *ToyMC:* Summary of total simultaneous signal (left) and background (right) efficiencies, after mass window cuts applied.

$\epsilon_t = 90.4\,\%$ (Ds dataset), $\epsilon_t = 89.1\,\%$ (Etac dataset) and $\epsilon_t = 21.9\,\%$ (DPM dataset), respectively, at $\sqrt{s} = 5.5\,\text{GeV}$ can also be read from Tab. 4. In this table, the total efficiencies of the 10 simultaneous trigger lines ϵ_t are summarised for all 10 datasets produced at the four different energies. The full information on the results for each individual trigger line and dataset is given as well, these individual efficiencies are summarised for completeness in Tab. 16 in the Appendix (Sec. 8). All the results of signal and background efficiencies obtained after the mass window cuts applied (Tab. 4) are in addition graphically compiled in Fig. 11. While the achieved signal efficiencies of each dataset stay rather constant versus $\sqrt{s}$, the fraction of background events accepted by the trigger lines is constantly increasing with increasing $\sqrt{s}$.

To summarise, using mass window cuts only, signal efficiencies are kept to be larger than about 80 %, however, the achievable background suppression is in the order of a factor of 1/20 - 1/5 depending on $\sqrt{s}$, which is far away from the needed suppression factor of order 1/1000.

Optimisation of further cuts

A list of those cuts that turned out to significantly further reduce the event rates by decreasing DPM background efficiencies, while keeping the signal efficiencies reasonably high, are summarised in Tab. 3. In order to optimise these selection cuts for the two approaches of signal efficiency and background suppression, the various selection cuts have been studied concerning their effectivity[1].

To identify the observables with the maximal discrimination potential, a ranking has been performed in two different ways for the two approaches of optimisation for signal efficiency and for background suppression. For the former approach, a fixed signal efficiency was required and the observables were sorted by the achievable suppression fraction for background. For the latter approach, a certain suppression fraction was required and the ordering was performed with respect to the achievable signal efficiency. This is illustrated in Fig. 12 for the $D^{\pm}$ selection observables at $\sqrt{s} = 5.5$ GeV/c. In the top row, the plots show the four best selection cuts on observables that all keep the event based efficiency of the signal (blue distributions) on the level of $\epsilon = 98\%$. They are sorted (from left to right) by the suppression fraction of background events (red distributions) as noted in the plot titles, varying in this example between 93.4 % and 29.2 %. The bottom row shows the four best cuts to retain high signal efficiency values between 79.3 % and 30.3 %, while reducing the background events by $f_{\text{sup}} = 98\,\%$. These ranking plots were iteratively inspected for each new cut. After the application of a certain criterion, the ranking was repeated to identify the next best observable, until the current optimisation goal (either high efficiency or high background suppression) was reached for a particular trigger line acting on the corresponding signal and DPM background events. This process has not been performed fully automatically to keep better control over the selection process. Typically three to five cuts are significantly important for a given trigger line and dataset, and have been applied for the two approaches as summarised in Tab. 17 and Tab. 18, respectively, in the Appendix.

For the example of the $D^+ \to K^-\pi^+\pi^+$ trigger on the Dch and DPM datasets at $\sqrt{s} = 5.5\,\text{GeV}$, the observables of the momentum of the reconstructed D^+ candidate in the centre-of-mass frame

[1]It should be mentioned, that due to the special way PID is emulated for ToyMC by defining a certain efficiency and mis-identification without probability distributions for the various species, a possible PID tightening (observables in the table: d*i*pidk, d*i*pidp, lnpide, lnpidmu, lnpidpi, lnpidk, lnpidp) could not be applied during the optimisation.

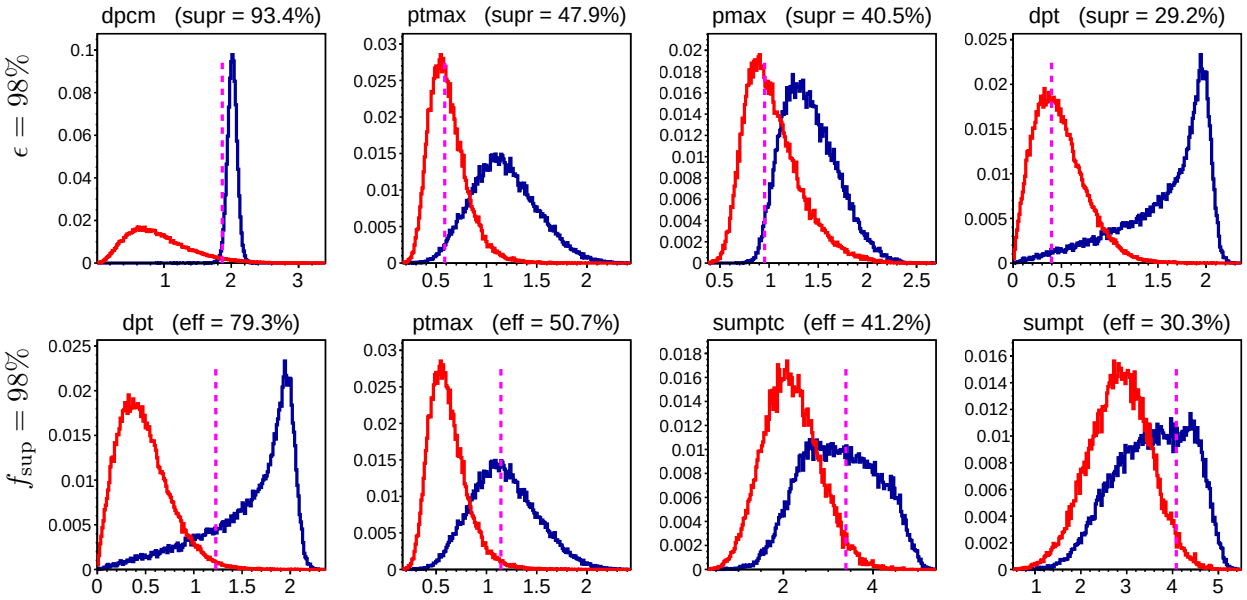

Figure 12: *ToyMC:* Illustration of observable ranking for $D^{\pm}$ at $\sqrt{s} = 5.5\,\text{GeV}$. *Top:* Ranking with respect to background suppression for fixed signal efficiency of $\epsilon = 98\%$. *Bottom:* Ranking with respect to signal efficiency for fixed suppression fraction of $f_{\rm sup} = 98\%$. For the ranking procedure, a MC-truth match has been applied for the signal distributions, not being the case for those in Fig. 13 used for efficiency determination.

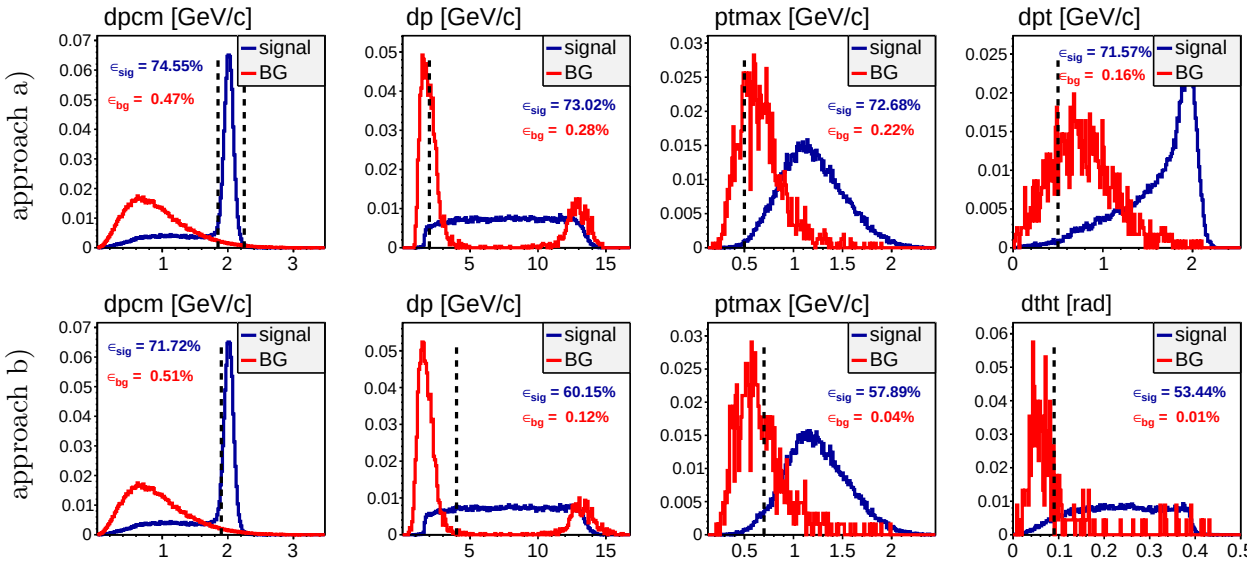

Figure 13: *ToyMC:* Illustration of the cut optimisation for the $D^{\pm}$ example at $\sqrt{s} = 5.5\,\text{GeV}$. *Top:* Optimisation for signal efficiency. *Bottom:* Optimisation for background suppression.

p^*_D (dpcm), the momentum of the D^+ candidate in the laboratory frame p_D (dp) and the maximum transverse particle momentum in the event $p_{t,max}$ (ptmax) in the laboratory frame (Tab. 3), are found to be most relevant and have been applied. In this particular example, we find these three cuts on the same observables for both approaches, which is not the case in general. Further, the transverse momentum of the reconstructed D^+ candidate $p_{t,D}$ (dpt), in case of optimisation for signal efficiency, and the polar angle of the reconstructed D^+ candidate θ_D (dtht), in case of optimisation for background suppression, are relevant and applied, respectively. The optimisation of these cuts is demonstrated in Fig. 13 for both approaches in Fig. 13 (top) and Fig. 13 (bottom), respectively.

To optimise for signal efficiency, the cuts on these variables are chosen such that more than about 90 % of the signal events that passed the mass window preselection are kept. The cuts |dpcm - 2.05| < 0.2, dp > 2, dpt > 0.5 and ptmax > 0.5 are consecutively applied as illustrated from left to right in Fig. 13 (top). The fraction of kept signal events (blue curve) is consecutively reduced from $\epsilon = 79.37\,\%$, that is obtained just after the mass window preselection (see Tab. 16, Dch-mode - line, $D^\pm$ - column, at $\sqrt{s} = 5.5\,\mathrm{GeV}$) to $\epsilon_{\mathrm{sig}} = 74.55\,\%$ (|dpcm-2.05|<0.2), then to $\epsilon_{\mathrm{sig}} = 73.02\,\%$ (dp > 2), then to $\epsilon_{\mathrm{sig}} = 72.68\,\%$ (ptmax > 0.5), and finally to $\epsilon_{\mathrm{sig}} = 71.57\,\%$ (dpt > 0.5). This final value of $\epsilon_{\mathrm{sig}} = 71.57\,\%$ corresponds to about 90 % of the signal efficiency as obtained before these further cuts. For this approach, the fraction of kept background events (red curve) is in this example reduced from $\epsilon = 8.58\,\%$ (see Tab. 16, last line, $D^\pm$–column) to finally $\epsilon_{\mathrm{bg}} = 0.16\,\%$ (Tab. 19, last line, $D^\pm$–column).

In case of the optimisation for background suppression, the cuts dpcm > 1.9, dp > 4, ptmax < 0.7 and dtht > 0.09 are consecutively applied as illustrated in Fig. 13 (bottom). The fraction of kept background events (red curve) is consecutively reduced from $\epsilon = 8.58\,\%$ to $\epsilon_{\mathrm{bg}} = 0.51\,\%$ (dpcm > 1.9), then $\epsilon_{\mathrm{bg}} = 0.12\,\%$ (dp > 4), then to $\epsilon_{\mathrm{bg}} = 0.04\,\%$ (ptmax < 0.7), and finally to $\epsilon_{\mathrm{bg}} = 0.01\,\%$ (dtht > 0.09). This final value of $\epsilon_{\mathrm{bg}} = 0.01\,\%$ is a background suppression factor of about 1/10000, required for each of the 10 individual channels to achieve in total a suppression of 1/1000. The fraction of kept signal events (blue curve) is for this approach, however, drastically reduced from $\epsilon = 79.37\,\%$ (see Tab. 16) to finally $\epsilon_{\mathrm{bg}} = 53.44\,\%$ (Tab. 20, last line, $D^\pm$–column).

To summarise the example discussed here in detail, a background suppression factor of about 1/10 can be achieved while keeping a signal efficiency of about 70 %, whereas a suppression factor of about 1/10000 is reachable on the cost of loosing about 50 % of signal events. Forcing such a rigorous suppression results in cutting significantly into signal regions, compare e.g. the applied cuts on the dp and ptmax variables in both approaches for this example (Fig. 13, second and third plots from left, top/bottom), an effect that is even more problematic in case of the FullMC case, where signal distributions are usually broader.

A complete summary of the individually for each trigger line and corresponding dataset identified, optimised and applied cuts, is given for both approaches in Tab. 17 and Tab. 18, respectively, in the Appendix (Sec. 8).

Signal and background efficiencies after application of all cuts

Similarly as for the mass window preselection (Figs. 8 - 10), the results after all cuts are illustrated for each of the three dataset examples (Ds, Etac, DPM, at 5.5 GeV) by the corresponding set of 10 plots for each trigger line in the Appendix (Sec. 8). There, the same set of 10 plots for each trigger are given for the approach of optimisation for signal efficiency (Fig. 24) as well as for the approach of optimisation for background suppression (Fig. 25), respectively.

For these three dataset examples at $\sqrt{s} = 5.5\,\mathrm{GeV}$ (Fig. 24), the total simultaneous trigger efficiencies obtained in case of cut optimisation for signal efficiency are $\epsilon_{\mathrm{t}} = 74.2\,\%$ (*Ds dataset example*), $\epsilon_{\mathrm{t}} = 70.0\,\%$ (*Etac dataset example*) and $\epsilon_{\mathrm{t}} = 1.0\,\%$ (DPM dataset), respectively. And in case of cut optimisation for background suppression (Fig. 25), the total simultaneous trigger efficiencies obtained are $\epsilon_{\mathrm{t}} = 57.8\,\%$ (Ds dataset), $\epsilon_{\mathrm{t}} = 57.0\,\%$ (Etac dataset) and — "by definition" — $\epsilon_{\mathrm{t}} = 0.1\,\%$ (DPM dataset), respectively. Again, the efficiency values are summarised for all datasets at all four $p\bar{p}$ centre-of-mass energies under study in Tab. 5 and Tab. 6. In addition to the absolute efficiency numbers, the values relative to the ones obtained by application of the mass window cuts (cf. Tab. 4) are given in italics.

The results of signal and background efficiencies obtained after the simultaneous triggering for the two approaches of optimisation (Tab. 5 and Tab. 6) are in addition graphically compiled in Fig. 14 and Fig. 15, and the complete set of resulting efficiencies for each individual trigger line on each dataset is summarised for completeness in Tab. 19 and Tab. 20, in the Appendix (Sec. 8).

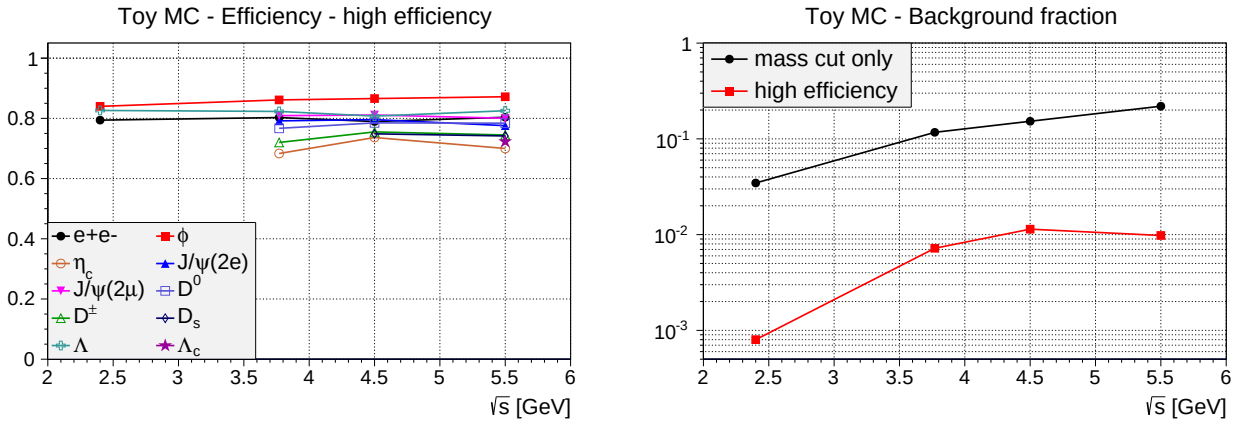

Figure 14: *ToyMC:* Summary of signal and background efficiencies after all cuts, mass window cuts and further cuts optimised for signal efficiency.

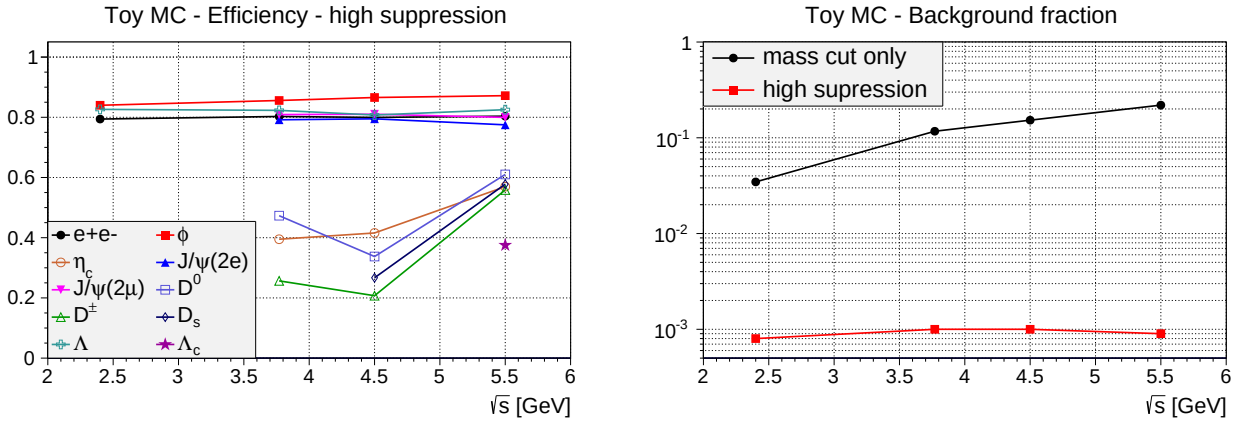

Figure 15: *ToyMC:* Summary of signal and background efficiencies after all cuts, mass window cuts and further cuts optimised for background suppression.

Table 5: *ToyMC – High efficiency selection:* Summary of the total simultaneous trigger efficiencies ϵ_t [%] for the different datasets — after all cuts applied, optimised for signal efficiencies. Numbers in italics are relative to Tab. 4.

$\sqrt{s}$ (GeV)	ee	Phi	Etac	J2e	J2mu	D0	Dch	Ds	Lam	Lamc	DPM
2.4	79.41	83.99	–	–	–	–	–	–	82.63	–	0.08
	100.00	*95.10*	–	–	–	–	–	–	*90.68*	–	*2.31*
3.77	80.27	86.13	68.33	79.17	80.90	76.69	72.00	–	82.30	–	0.72
	99.99	*94.48*	*78.17*	*99.11*	*99.28*	*90.05*	*87.94*	–	*90.32*	–	*6.15*
4.5	79.95	86.58	73.64	79.59	81.12	78.50	75.50	74.86	80.75	–	1.14
	99.40	*94.03*	*82.52*	*98.81*	*98.91*	*89.86*	*88.25*	*83.99*	*88.86*	–	*7.47*
5.5	80.37	87.18	70.01	77.58	80.03	78.40	74.48	74.16	82.53	72.29	0.98
	99.37	*94.96*	*78.54*	*95.97*	*96.68*	*90.07*	*87.07*	*82.05*	*90.64*	*81.17*	*4.47*

While in the case of signal efficiency optimised cuts an significantly improved background suppression (about a factor 1/10 - 1/15) can be achieved as compared to the mass window preselection only, the signal efficiencies are basically kept (losses up to about 10%). "Forcing" however the background to be suppressed by a factor 1/1000 the signal efficiencies are significantly reduced, especially for the Ds, D0, Dch, Etac and Lamc datasets they drop well below 50-60 %.

To summarise the ToyMC studies, using additional observables optimised for the individual triggers and datasets, a data reduction in form of background suppression of order 1/100 - 1/1000 can be achieved depending on $\sqrt{s}$, while keeping signal efficiencies above 70 %. The reach of a background suppression factor of 1/1000 over the full $\sqrt{s}$ range, results in signal efficiencies of 10 - 80 % as well as heavily cutting into signals of interest. Covering more physics channels by adding more corresponding trigger lines of interest will, of course, further limit the reachable compromise of a highest as possible background suppression level while keeping as much as possible the signal efficiencies.

5.4 Results from Full Monte Carlo Studies

For the studies using the full Geant3 simulation in PandaRoot `release/jan14` (FullMC), the generated events have been passed through the PandaRoot detector simulation and reconstruction. Here, a minimum momentum of 100 MeV for charged tracks and a minimum EMC cluster energy of 100 MeV for photons are required. For all particle types, a rather loose PID cut of a minimum PID probability of 10 % has been applied, see Sec. 3 for more details.

Signal datasets of 500k events were generated using EvtGen for each of the 10 channels and for each of the exemplary centre-of-mass $p\bar{p}$ energies $\sqrt{s}$ = 2.4 GeV, 3.77 GeV, 4.5 GeV and 5.5 GeV, according to Tab. 2. Background datasets of 1M events were generated using DPMgen, accordingly for the same centre-of-mass $p\bar{p}$ energies.

Similarly to the ToyMC case (Sec. 5.3), the achievable signal efficiencies and background reduction factors for the scenario of using the 10 physics channels (Sec.4, Tab. 1) and simultaneous trigger lines are studied here for the FullMC case. At the first level, the same mass window preselection cuts of 8σ mass resolution are applied on the nominal mass for each channel to tag events to be of interest. This is done for all trigger lines. At a second level, the selection by cuts on the further observables (Tab. 3) optimised as explained and illustrated in detail for the ToyMC case are trigger line specifically applied subsequently.

Again, the complete results are presented in tables, whereas those for the two signal dataset examples of Ds and Etac as well as the DPM background dataset at $\sqrt{s}$ = 5.5 GeV are discussed in detail and illustrated showing the same set of plots as were shown for ToyMC.

Signal and background efficiencies after mass window preselection

For each of the three dataset examples (Ds, Etac, DPM), the application of mass window cuts is illustrated in Fig. 16. A set of 10 plots is displayed for each dataset example, showing the invariant mass spectra (blue histogram in each of the 10 plots, for each plot the title specifies the trigger line) of the involved resonances for each of the 10 trigger lines reconstructed from the Ds (Fig. 16,

Table 6: *ToyMC – High suppression selection:* Summary of the total simultaneous trigger efficiencies ϵ_t [%] for the different datasets – after all cuts applied, optimised to achieve a 1/1000 DPM reduction. Numbers in italics are relative to Tab. 4.

$\sqrt{s}$ (GeV)	ee	Phi	Etac	J2e	J2mu	D0	Dch	Ds	Lam	Lamc	DPM
2.4	79.41	83.99	–	–	–	–	–	–	82.63	–	0.08
	100.00	*95.10*	–	–	–	–	–	–	*90.68*	–	*2.31*
3.77	80.27	85.58	39.49	79.17	80.90	47.31	25.66	–	82.30	–	0.10
	99.99	*93.88*	*45.18*	*99.11*	*99.28*	*55.55*	*31.34*	–	*90.32*	–	*0.85*
4.5	79.95	86.57	41.57	79.49	81.02	33.75	20.73	26.69	80.75	–	0.10
	99.40	*94.02*	*46.58*	*98.68*	*98.79*	*38.63*	*24.23*	*29.95*	*88.86*	–	*0.65*
5.5	80.37	87.18	56.96	77.49	79.96	61.01	55.85	57.79	82.53	37.52	0.09
	99.37	*94.96*	*63.90*	*95.86*	*96.59*	*70.09*	*65.29*	*63.94*	*90.64*	*42.13*	*0.41*

top), Etac (Fig. 16, centre) and the DPM (Fig. 16, bottom) datasets. Due to the much higher combinatorics compared to the ToyMC case, only the mass range of interest was considered and is displayed here. In each of the invariant mass spectra, the shaded area indicates the accepted mass window region for the given trigger line, and the red histograms represent the MC truth matched candidates. The quoted trigger line efficiencies ϵ on each plot are the fraction of the 500k input events tagged by the given trigger line for the underlying dataset (e.g. the Ds dataset, Fig. 16, top). The total efficiency ϵ_t of the simultaneous trigger formed by all 10 trigger lines connected by a logical "OR", is given at the right upper corner. It is the fraction of the 500k input events that have been triggered in total by at least one of the 10 trigger lines.

For the *Ds dataset example* (Fig.16, top), one sees the D_s invariant mass peak in the plot for the $D_s^+ \to K^+K^-\pi^+$ trigger on a (combinatorial) background that is significantly higher as compared to the ToyMC case (cf. Fig. 8). The reasons are basically secondary particle production (and accordingly more combinatorics) and more realistic detector performances. With the 8σ mass cut applied, an efficiency for detection of signal events of $\epsilon = 36.9\,\%$ is achieved for this trigger line (on this corresponding signal dataset). This value compares to $\epsilon = 80.9\,\%$ achieved in the ToyMC case (Fig. 8). For the e^+e^- tag, the efficiency on this dataset example is $\epsilon = 0.1\,\%$, whereas e.g. $\epsilon = 19.9\,\%$ of the events are accepted by the ϕ-tag, and so on. In total, the trigger in form of the simultaneous 10 trigger lines accept $\epsilon_t = 58.3\,\%$ of the events of the Ds-dataset, which compares to $\epsilon_t = 90.4\,\%$ in case of ToyMC. The examples of the Etac and the DPM datasets are illustrated for FullMC in Fig.16 (centre) and Fig.16 (bottom), respectively.

The total efficiencies of the 10 simultaneous trigger lines for these three example datasets at $\sqrt{s} = 5.5\,\text{GeV}$ are $\epsilon_t = 58.3\,\%$ (Ds dataset), $\epsilon_t = 58.2\,\%$ (Etac dataset) and $\epsilon_t = 45.1\,\%$ (DPM dataset). In Tab. 7, the total efficiencies of the 10 simultaneous trigger lines ϵ_t are summarised for all 10 datasets and at all four $p\bar{p}$ centre-of-mass energies under study. The full information of the resultant efficiencies for each individual trigger line and for all datasets is summarised for completeness in Tab. 21 in the Appendix (Sec. 8).

Figure 17 shows the results of signal and background efficiencies obtained after the mass window preselection (Tab. 7) for all data sets graphically compiled versus $\sqrt{s}$. The qualitative results of the dependencies of the signal and background efficiencies are consistent with the results from the ToyMC studies. While the achieved signal efficiency of each trigger line stay rather constant as a function of $\sqrt{s}$, the fraction of background events accepted by the trigger lines is constantly increasing with increasing $\sqrt{s}$.

To summarise, after the mass window preselection in the FullMC studies, signal efficiencies are kept to be larger than at least 20 %, while the achievable background suppression is in the order of a factor of 1/20 - 1/2.5 depending on $\sqrt{s}$, which is still far away from the desired suppression factor of order 1/1000.

Optimisation of further cuts

In order to further reduce the (background) data rate, additional selection cuts are applied on various further observables (Tab. 3). For the FullMC studies, the best suited set of variables is found and optimised individually for each trigger line by the same procedure as it was done and explained in detail for the ToyMC case (Sec. 5.3). And again these further cuts are optimised for the two approaches of signal efficiency and background suppression, respectively.

A summary of the optimised and applied cuts, as well as the resulting signal and background efficiencies, is given for both approaches in Tab. 22 and Tab. 23, respectively (Appendix, Sec. 8).

Table 7: *FullMC – Mass window preselection:* Summary of the total simultaneous trigger efficiencies ϵ_t [%] for the different datasets, after mass window cuts applied.

$\sqrt{s}$ (GeV)	ee	Phi	Etac	J2e	J2mu	D0	Dch	Ds	Lam	Lamc	DPM
2.4	50.61	35.62	-	-	-	-	-	-	19.79	-	4.40
3.77	43.32	43.75	42.91	43.52	56.45	49.55	40.73	-	21.10	-	20.32
4.5	45.40	43.43	52.60	42.91	55.07	54.99	50.73	53.34	21.58	-	31.30
5.5	36.34	41.47	58.20	47.41	58.11	57.51	55.18	58.31	23.00	61.01	45.10

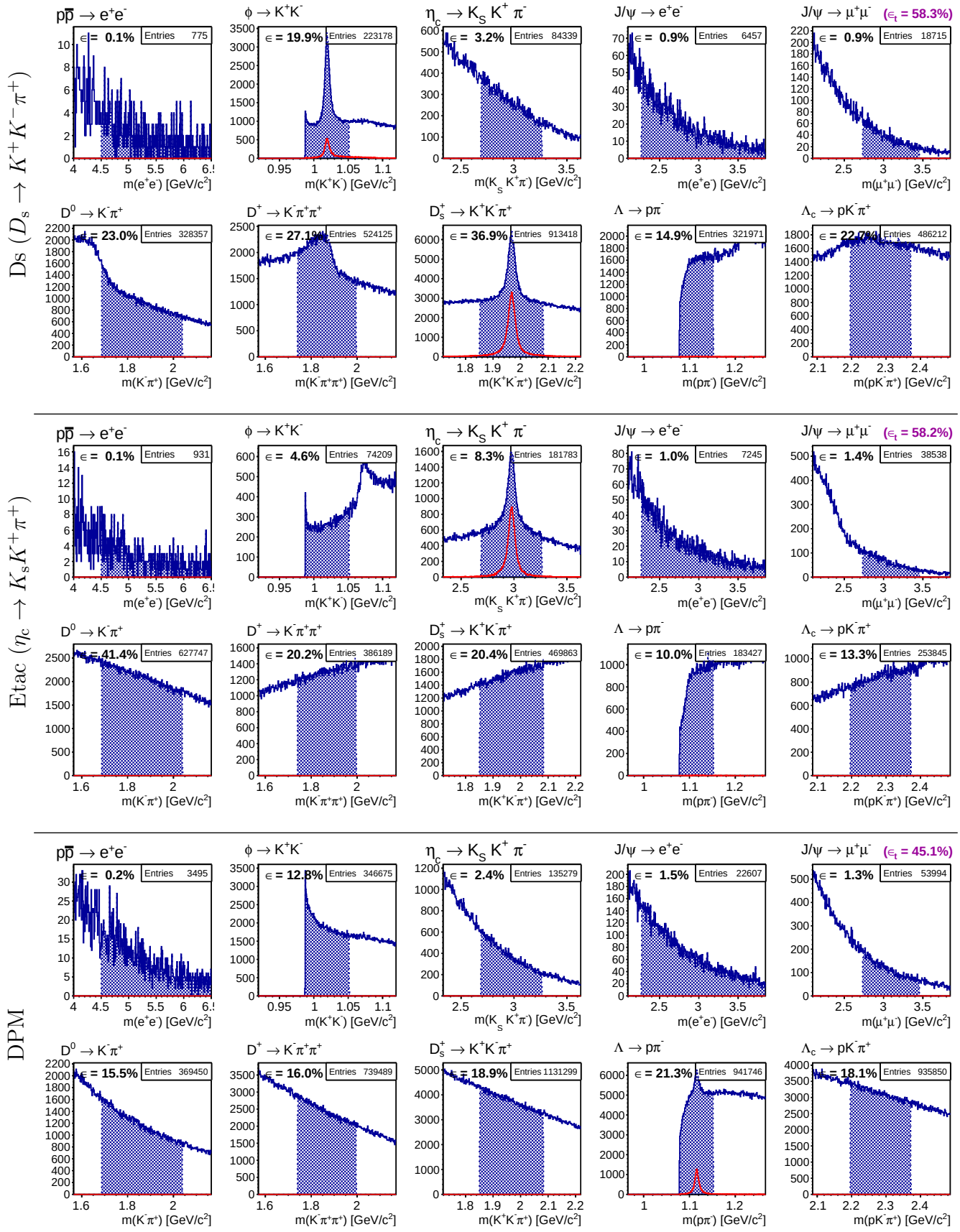

Figure 16: *FullMC – Mass window preselection:* Illustration of simultaneous tagging for the two signal *dataset examples Ds (top)* and *Etac (centre)*, and the *DPM background dataset (bottom)* at $\sqrt{s}$= 5.5 GeV. The individual signal efficiencies ϵ for the different trigger lines are given on the corresponding plots, in addition the global efficiency ϵ_t for all channels applied simultaneously for triggering are given top/right for each set of 10 plots, for discussion see text.

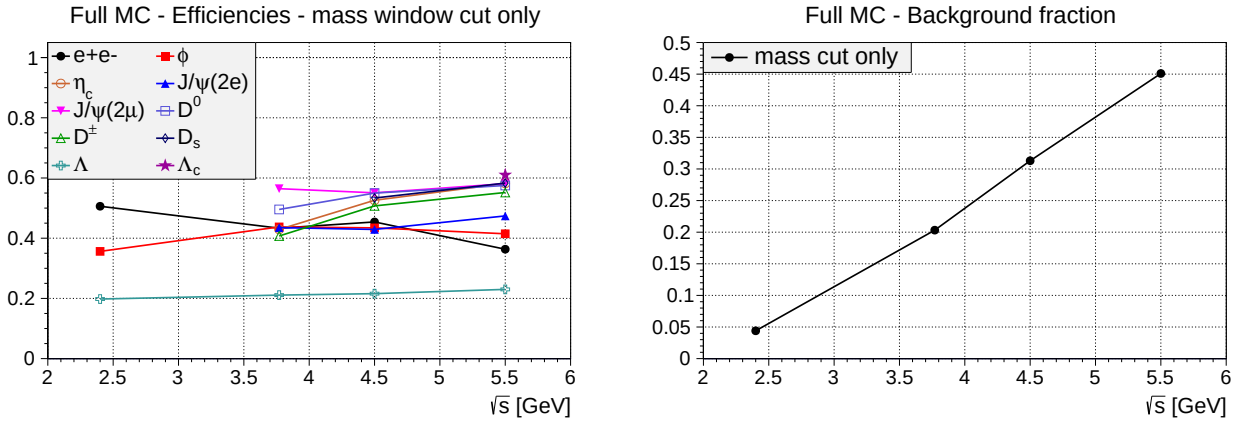

Figure 17: *FullMC:* Summary of signal (left) and background (right) efficiencies, after mass window cuts applied.

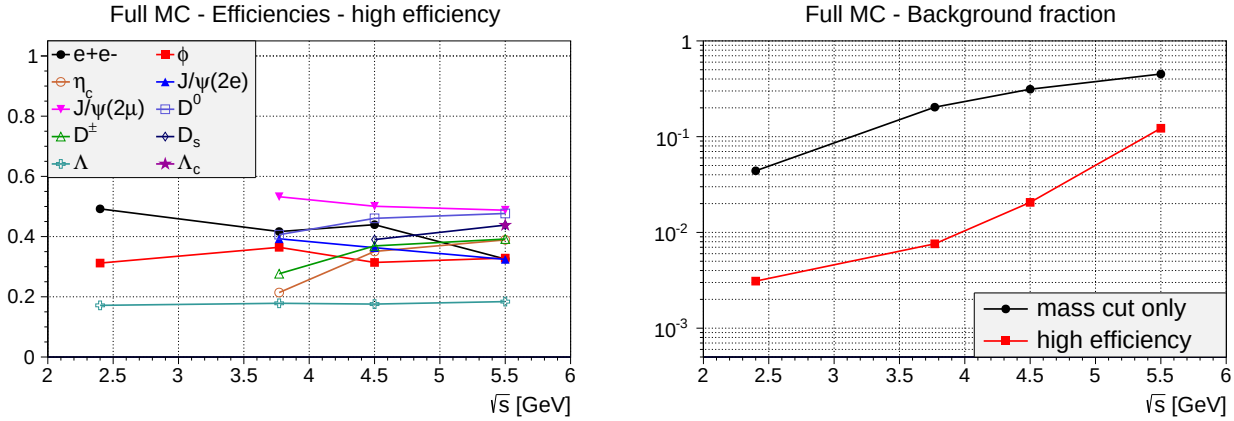

Figure 18: *FullMC:* Summary of signal and background efficiencies after all cuts, mass window cuts and further cuts optimised for signal efficiency.

Signal and background efficiencies after application of all cuts

Similarly as for the mass window cuts (Fig. 16), the results after all cuts applied are illustrated for each of the three dataset examples (Ds, Etac, DPM, at 5.5 GeV) by the corresponding set of 10 invariant mass spectra for each trigger line in the Appendix (Sec. 8). They are provided for both approaches, optimisation for signal efficiency (Fig. 26) as well as optimisation for background suppression (Fig. 27).

For our three dataset examples, the total simultaneous trigger efficiencies obtained in the case of cut optimisation for signal efficiency are $\epsilon_t = 43.8\,\%$ (Ds dataset), $\epsilon_t = 38.9\,\%$ (Etac dataset) and $\epsilon_t = 12.2\,\%$ (DPM dataset), respectively (Fig. 26). And in the case of cut optimisation for background suppression, the total simultaneous trigger efficiencies obtained are $\epsilon_t = 14.5\,\%$ (Ds

Table 8: *FullMC – High efficiency selection:* Summary of the total simultaneous trigger efficiencies ϵ_t [%] for the different datasets after all cuts applied, mass window cuts and further cuts optimised for signal efficiency. Numbers in italics are relative to Tab. 7.

$\sqrt{s}$ (GeV)	ee	Phi	Etac	J2e	J2mu	D0	Dch	Ds	Lam	Lamc	DPM
2.4	49.21	31.20	-	-	-	-	-	-	17.16	-	0.31
	97.23	*87.59*	–	–	–	–	–	–	*86.71*	–	*7.05*
3.77	41.67	36.44	21.41	39.27	53.24	40.64	27.66	-	17.84	-	0.76
	96.19	*83.29*	*49.90*	*90.23*	*94.31*	*82.02*	*67.91*	–	*84.55*	–	*3.74*
4.5	43.95	31.41	35.07	36.31	50.07	46.06	36.90	39.00	17.58	-	2.06
	96.81	*72.32*	*66.67*	*84.62*	*90.92*	*83.76*	*72.74*	*73.12*	*81.46*	–	*6.58*
5.5	32.54	32.85	38.91	32.43	48.76	47.68	39.18	43.81	18.40	43.79	12.24
	89.54	*79.21*	*66.86*	*68.40*	*83.91*	*82.91*	*71.00*	*75.13*	*80.00*	*71.78*	*27.14*

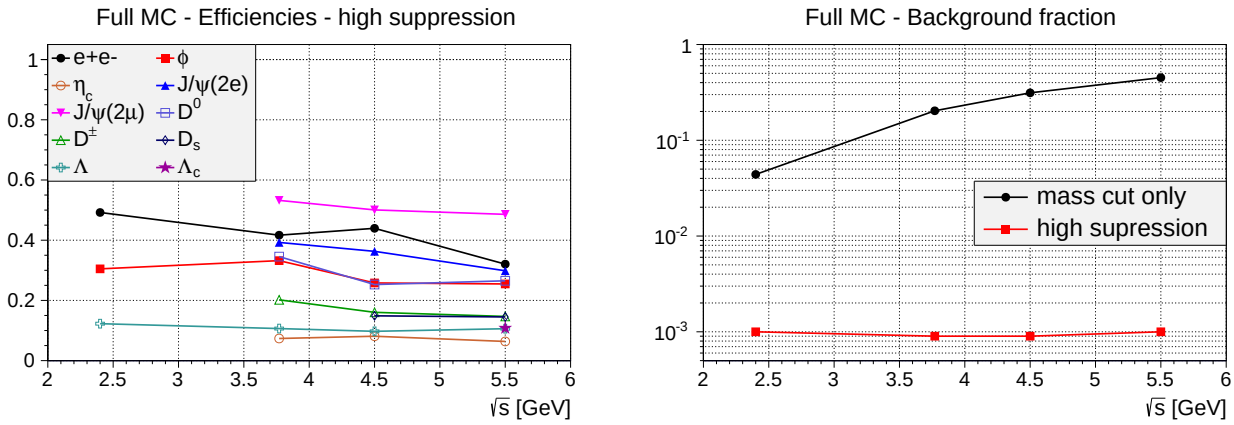

Figure 19: FullMC: Summary of signal and background efficiencies after all cuts, mass window cuts and further cuts optimised for background suppression.

dataset), $\epsilon_t = 6.4\,\%$ (Etac dataset) and – "by definition" – $\epsilon_t = 0.1\,\%$ (DPM dataset), respectively (Fig. 27). The efficiency values for all datasets at all four $p\bar{p}$ centre-of-mass energies under study are summarised in Tab. 8 and Tab. 9, where in addition to the absolute efficiency numbers, the values relative to the ones obtained after the mass window preselection (cf. Tab. 7) are given in italics. The signal and background efficiencies versus $\sqrt{s}$ obtained for both approaches of optimisation (Tab. 8 and Tab. 9) are graphically compiled in Fig. 18 and Fig. 19. The full information on these results of each individual trigger line for each dataset is summarised in Tab. 24 and Tab. 25 in the Appendix (Sec. 8). While in the case of signal efficiency optimised cuts, a significantly improved background suppression (gain factors roughly between 4 and 25) can be achieved, the signal efficiencies are basically kept (losses of up to about 10 %). "Forcing" however the background to be suppressed by a factor 1/1000 the signal efficiencies are significantly reduced. In line with the predictions by the ToyMC especially affected are the Ds, D0, Dch, Etac and Lamc datasets, for which the signal efficiencies drop below about 10 - 20 %.

To summarise, using additional observables optimised for the individual trigger lines and datasets, a data reduction in form of background suppression in the order 1/10 - 1/300 can be achieved depending on $\sqrt{s}$, while keeping signal efficiencies in the range of about 20-50 %. The requirement of a background suppression factor of 1/1000 over the full $\sqrt{s}$ range, results in signal efficiencies of about 10-50 % as well as heavily cutting into signals of interest. For the Lamc dataset, the signal efficiency is for example cut down from about 60 % to merely 10 %. Similarly in the case of the Etac dataset, the signal efficiency drops even more dramatically from initially 60% to only 6% for the highest energy. In this case one should note, however, that the initial efficiency value after mass window preselection is dominated by cross-tagging from e.g. the open charm channels (cf. Tab. 21), whereas the η_c trigger line drops merely by a factor of two (and not ten). Adding more trigger lines of interest, will of course further limit the reachable compromise of a highest as possible background suppression level, while keeping the signal efficiencies as high as possible.

Table 9: *FullMC – High suppression selection:* Summary of the total simultaneous trigger efficiencies ϵ_t [%] for the different datasets after all cuts applied, mass window cuts and further cuts optimised to achieve 1/1000 DPM reduction. Numbers in italics are relative to Tab. 7.

$\sqrt{s}$ (GeV)	ee	Phi	Etac	J2e	J2mu	D0	Dch	Ds	Lam	Lamc	DPM
2.4	49.21	30.48	-	-	-	-	-	-	12.27	-	0.10
	97.23	*85.57*	–	–	–	–	–	–	*62.00*	–	*2.27*
3.77	41.67	33.21	7.35	39.26	53.23	34.55	20.19	-	10.65	-	0.09
	96.19	*75.91*	*17.13*	*90.21*	*94.30*	*69.73*	*49.57*	–	*50.47*	–	*0.44*
4.5	43.95	25.80	8.10	36.30	50.06	25.27	16.04	14.88	9.73	-	0.09
	96.81	*59.41*	*15.40*	*84.60*	*90.90*	*45.95*	*31.62*	*27.90*	*45.09*	–	*0.29*
5.5	32.05	25.47	6.37	29.85	48.59	26.51	14.68	14.51	10.60	10.81	0.10
	88.19	*61.42*	*10.95*	*62.96*	*83.62*	*46.10*	*26.60*	*24.88*	*46.09*	*17.72*	*0.22*

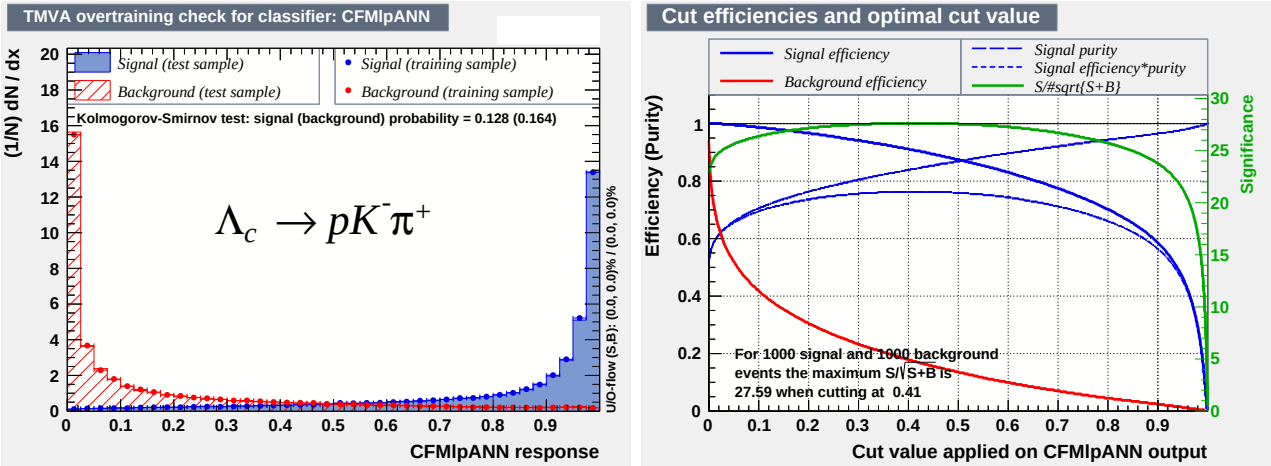

Figure 20: Working principle of the TMVA method – TMVA response output for the Clermont-Ferrand (CFMlpANN) classifier for background and signal sample (left). Distributions of efficiency, purity, and significance can help to find an optimal cut value.

5.5 Application of Multivariate Analysis

As it was discussed in detail all results presented up to now have been achieved by a manual cut and count technique, where numerous observables have been individually inspected and chosen to be used for further selection. Since the task is a typical classification problem in a multi-dimensional parameter space, the application of a multivariate analysis (MVA) method is obvious. These kind of algorithms allow to achieve reasonable classification performance even for strongly correlated variable sets. Therefore it is in particular interesting to compare the performances of such techniques to those obtained with the manual approach. For this purpose the TMVA package [13] distributed together with the ROOT analysis framework is used.

5.5.1 Introduction to TMVA

The TMVA package is a toolkit for multivariate analysis offering a large number of different techniques for classification problems on high-dimensional datasets. Although being developed within the high energy physics community, it can be applied in a very general and versatile way.

The application of TMVA for a particular problem requires two stages. In the training phase, distinct training datasets of all classes (typically signal and background, but also more categories are possible) of data intended to be separated are needed. These are used to adapt the algorithm specific weights and/or structures to distinguish between the different data types usually provided as one or more floating point output values. During this stage, the current performance of the algorithm is determined by applying it to a statistical independent test datasample to avoid so-called *over-training* effects. The training limit is typically reached, when the performance on the test dataset does not improve anymore. The training phase usually is a quite time-consuming process. When the training is finished, the configuration of the MVA algorithm is stored for further application.

In the application phase, the configuration found in the training phase is used to classify unknown samples. This stage, of course depending on the actual type of algorithm, typically should be applicable in an online scenario due to the deterministic computability.

Classification of signal and background

An exemplary discriminator distribution is shown in Fig. 20 (left) as obtained after training on the Lamc signal and a DPM background datasets applying a neural network classifier (CFMlpANN). The red hatched distribution represents the network output for background samples (DPM), whereas the blue shaded histogram corresponds to the signals. For the actual classification process, a certain threshold on the output is set, rejecting candidates below and accepting the ones above this values.

The outcome of the application of different classifiers for the example of the $\bar{p}p \to J/\psi(\to \ell^+\ell^-)\,\pi^+\pi^-$ events are shown in Fig. 28 in the Appendix (Sec. 8). One clearly sees that the twelve

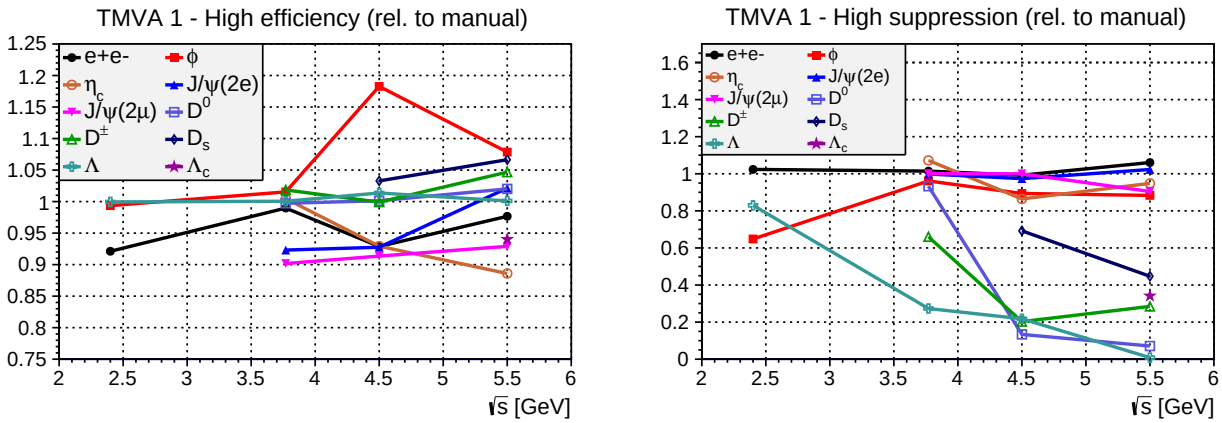

Figure 21: *TMVA Approach 1*: CFMlpANN based on trigger line specific variables from manual optimisation (FullMC) — Summary of efficiencies relative to those achieved with manual optimisation for high signal efficiency (left) and high background suppression (right).

different classifiers applied show quite different separation qualities for the J/ψ selection in this data. Accordingly, we chose the Clermont-Ferrand Multilayer Perception classifier (CFMlpANN) classifier (lower right diagram) that delivers the best separation of signal from background.

The resulting relations between background suppression versus signal efficiency can nicely be displayed using the so-called relative operating characteristic (ROC) curve. A ROC curve describes the performance of a binary classifier by plotting the background suppression versus the signal efficiency. The ROC curves obtained for our data example of $\bar{p}p \to J/\psi(\to \ell^+\ell^-)\,\pi^+\pi^-$ (at E = 5.5 GeV) for the various linear and non-linear classifiers is given in Fig. 29 in the Appendix (Sec. 8). The minimum distance of the individual curves to the point (1,1) in the diagram is a measure for the separation power; the closer a curve passes, the better the separation.

There are certain possibilities to evaluate the performance of a particular threshold value, as being illustrated in Fig. 20 (right). Given the signal $S(x)$ (solid blue curve) and background fraction $B(x)$ (solid red curve) as function of the network output x, the purity of the signal can be computed as $P(x) = S(x)/[S(x) + B(x)]$ (dashed blue curve). The product of the purity and efficiency $P(x) \cdot S(x)/S_0$ (dotted blue curve), with S_0 being the initial number of signals, is a commonly used measure for the quality, as it exhibits a maximum, here located at around $x \approx 0.41$. An alternative representation is the so-called *significance* $S(x)/\sqrt{S(x) + B(x)}$ with exactly the same optimum classification threshold as the former quantity, since it only differs by the normalisation factor $1/S_0$ when squared.

However, as previously discussed in Sec. 5.2, both measures are not well suitable for our purpose, since they depend on the absolute relationship between signal and background. In order to compare the results achieved by application of MVA techniques with those of the manual optimisation applied in Sec. 5.4, the selection thresholds are chosen such that the two optimisation approaches (for signal efficiency and for background suppression) are realised here as well using the TMVA method.

5.5.2 Results from TMVA Application

The results from application of the TMVA method on the FullMC data are obtained using the CFMlpANN classifier, providing one of the best signal from background separations for our purpose. As input, the already identified set of useful variables (Tab. 3, Sec. 5.2) serves as a basis, whereas two different ways of using them are described in the following.

Approach 1: CFMlpANN classifier based on trigger line specific variables

To ensure an one-to-one comparison to the results obtained using the TMVA method and the results obtained from the FullMC data with manual selection cut optimisation (Sec. 5.4), exactly the same observables that were found and applied per trigger line manually for each optimisation approach (Tab. 22 and Tab. 23, Sec. 8) are taken as input variables. These input variables are used for the training phase and classification for the different trigger lines as specified in Tab. 26 (Appendix, Sec. 8).

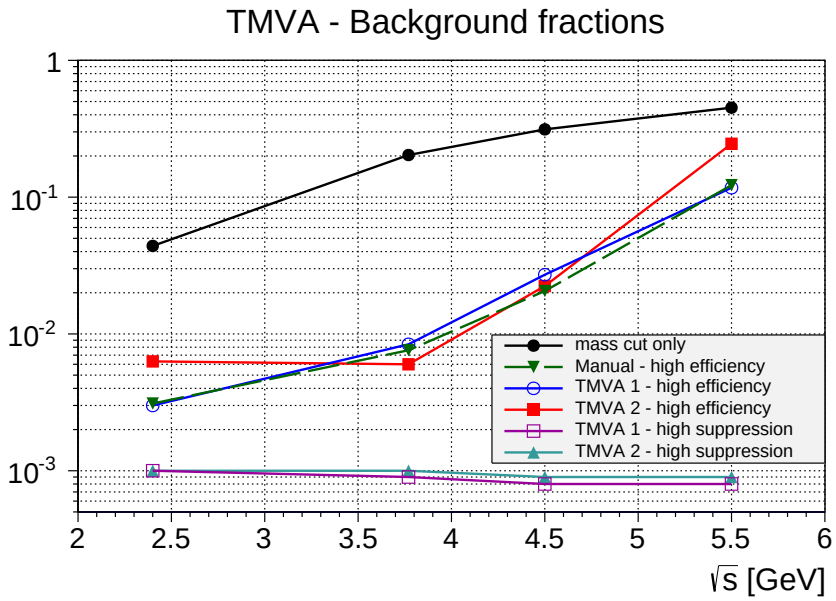

Figure 22: *Background efficiencies obtained with TMVA Approach 1 & 2 compared to manual optimisation of selection cuts*: CFMlpANN based on trigger line specific variables from manual optimisation (FullMC) for both approaches 1 & 2 — Summary of background suppression factors for both TMVA approaches 1 & 2 compared to manual optimisation.

Table 10: *TMVA Approach 1 (FullMC, High Efficiency Selection)*: CFMlpANN based on trigger line specific variables from manual optimisation — Summary of the total simultaneous trigger efficiencies ϵ_t [%] for the different data sets, after mass window cuts and CFMlpANN high efficiency selection applied. Numbers in italics are relative to Tab. 7

$\sqrt{s}$ (GeV)	ee	Phi	Etac	J2e	J2mu	D0	Dch	Ds	Lam	Lamc	DPM
2.4	45.33	31.00	–	–	–	–	–	–	17.15	–	0.30
	89.58	*87.05*	–	–	–	–	–	–	*86.66*	–	*6.79*
3.77	41.24	37.00	21.51	36.25	48.01	40.53	28.17	–	17.85	–	0.84
	95.21	*84.57*	*50.13*	*83.30*	*85.06*	*81.81*	*69.15*	–	*84.60*	–	*4.15*
4.5	40.82	37.15	32.59	33.68	45.74	46.12	36.87	40.28	17.82	–	2.71
	89.91	*85.53*	*61.96*	*78.48*	*83.06*	*83.88*	*72.68*	*75.51*	*82.56*	–	*8.65*
5.5	31.78	35.43	34.47	33.12	45.30	48.64	41.01	46.72	18.42	41.17	11.72
	87.46	*85.44*	*59.23*	*69.87*	*77.95*	*84.57*	*74.32*	*80.12*	*80.10*	*67.48*	*25.99*

Table 11: *TMVA Approach 1 (FullMC, High Suppression Selection)*: CFMlpANN based on trigger line specific variables from manual optimisation — Summary of the total simultaneous trigger efficiencies ϵ_t [%] for the different data sets, after mass window cuts and CFMlpANN high suppression selection applied. Numbers in italics are relative to Tab. 7

$\sqrt{s}$ (GeV)	ee	Phi	Etac	J2e	J2mu	D0	Dch	Ds	Lam	Lamc	DPM
2.4	50.37	19.76	–	–	–	–	–	–	10.18	–	0.10
	99.52	*55.49*	–	–	–	–	–	–	*51.45*	–	*2.18*
3.77	42.27	31.92	7.88	39.21	53.26	32.23	13.33	–	2.91	–	0.09
	97.58	*72.97*	*18.36*	*90.11*	*94.36*	*65.05*	*32.71*	–	*13.77*	–	*0.45*
4.5	43.61	23.06	7.00	35.35	50.05	3.38	3.25	10.30	2.12	–	0.08
	96.06	*53.09*	*13.30*	*82.37*	*90.87*	*6.15*	*6.41*	*19.30*	*9.84*	–	*0.26*
5.5	33.99	22.50	6.04	30.54	43.95	1.88	4.18	6.49	0.09	3.69	0.08
	93.54	*54.27*	*10.38*	*64.42*	*75.64*	*3.28*	*7.58*	*11.12*	*0.38*	*6.04*	*0.18*

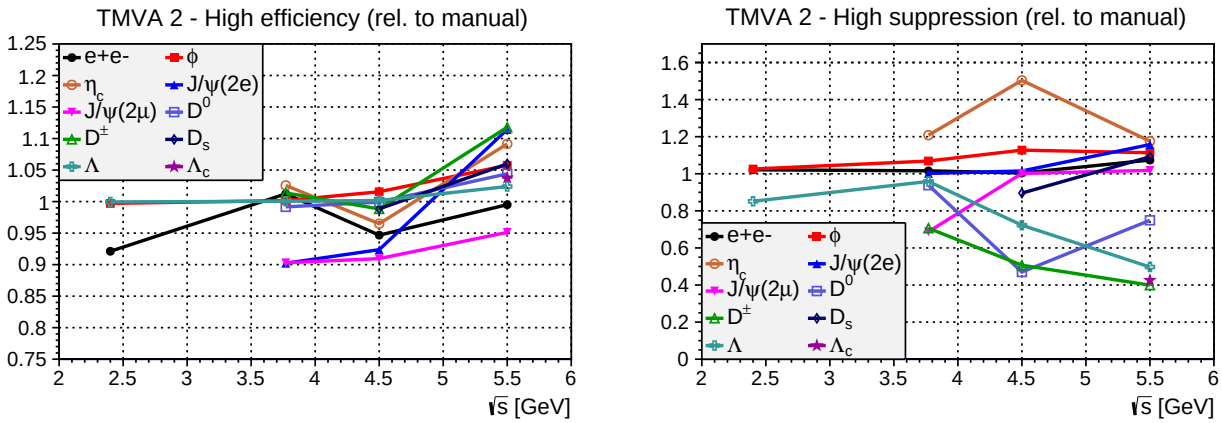

Figure 23: *TMVA Approach 2*: CFMlpANN based on all variables from manual optimisation (FullMC) — Summary of efficiencies relative to those achieved with manual optimisation for high signal efficiency (left) and high background suppression (right).

For both approaches of optimisation, the resultant signal efficiencies are summarised in Fig. 21 and the background reduction factors in Fig. 22. The absolute efficiency and background reduction numbers are summarised in Tab. 10 and Tab. 11, where the numbers are given in addition relative to the ones obtained after mass window preselection (Tab. 7). The obtained signal efficiencies in Fig. 21 are presented relative to the ones obtained by the manual optimisation (Sec. 5.4). The resulting background suppression factors are summarised in Fig. 22 (open circles and open squares for TMVA approach 1).

In the case of the optimisation for high signal efficiency (Fig. 21, left), the TMVA method leads to significantly higher signal efficiencies for the ϕ and for the D_s-tags on the corresponding signal datasets (improved by up to about 17 % and up to about 7 %, respectively, depending on $\sqrt{s}$), while the DPM background suppression is about the same over the whole range of $\sqrt{s}$ (Fig. 22, open blue circles and full green triangles). For the other 8 trigger lines and datasets, the signal efficiencies obtained using the TMVA method are slightly worse (up to about 10 %) than the ones obtained by the manual optimisation of the selection cuts.

When optimising for background suppression, the reduction factor of DPM events is by definition practically the same, namely 1/1000 (Fig. 22, purple squares). The resultant signal efficiencies from the TMVA method application are in this approach (of same observables per trigger line) similar or worse. Especially in case of the Dch, Lam, Lamc, D0 and Ds dataset, the obtained signal efficiencies for higher $\sqrt{s}$ are significantly lower. In case of the Lamc and the Dch data at $\sqrt{s} = 5.5$ GeV for instance, the obtained signal efficiencies are about a factor of three worse as compared to the manual optimisation of selection cuts. The efficiency achieved by this TMVA approach on the Lam dataset is extremely low. It amounts merely 1 % absolutely (4 % relative to the efficiency after the mass preselection), see Tab. 11, which was 11 % (46 %) for the manual optimisation of selection cuts (Tab. 9, Sec. 5.4).

Approach 2: CFMlpANN classifier based on the full set of useful variables

To ensure still compatibility, while giving more freedom to the TMVA classification concerning the set of variables, in this second approach, the complete set of observables as manually applied (Tab. 22 and Tab. 23, Sec. 8) are used as input variables, while allowing all of them for all trigger lines, i.e. all the input variables as listed in Tab. 3 are used for the training phase and classification.

This set is applied during the training phase performed on the 10 physics data and the DPM background data sets. The resultant signal efficiencies are summarised for both approaches of optimisation in Fig. 23 and the background reduction factors in Fig. 22. The absolute efficiency and background reduction numbers are also summarised in Tab. 12 and Tab. 13, where the numbers are given in addition relative to the ones obtained after mass window preselection. Again, the obtained signal efficiencies compiled in Fig. 23 are presented relative to the ones obtained by the manual optimisation (Sec. 5.4). For the optimisation for high signal efficiency (Fig. 23, left), the TMVA method leads to significantly higher signal efficiencies for mostly all trigger lines, except for the ee and the J2mu datasets at 5.5 GeV, where the gain is up to 10 %. At lower energies, similar or worse performance (by about up to 10 %) are obtained, while the DPM background suppression is

about the same over the whole range of $\sqrt{s}$ (full red squares in Fig. 22) as for the case of manual optimisation of the selection cuts. For the optimisation for background suppression, the resultant signal efficiencies from the TMVA method application are in this approach (of same observables independent of trigger lines) better for the Etac dataset (about 20-40 %), similar in case of the ee and the Phi and J2e datasets, and worse for the other three datasets (by up to 40 %). Especially in case of the Dch, Lam, Lamc, and D0 datasets, the obtained signal efficiencies are significantly lower, depending on $\sqrt{s}$, by up to 40 %.

Systematic checks of the TMVA classifier applied

As a systematic check, another well known non-linear classification method, the Boosted Decision Tree (BDT) has been applied as well. Here, also several algorithms for boosted classifiers exist. We applied a version of an adaptive boost tree, namely BDTD with variable transformation. To reduce the correlation among the variables for the boosted algorithms, all input variables are transformed into more appropriate forms in advance. This preprocessing transformations may lead to better performance for the BDT method and to reduce the training time. A decorrelation via the square-root of the covariance matrix has been applied to all input variables. The observed difference in the resultant estimation of efficiency and background efficiencies obtained with BDTD versus CFMlpANN is merely on the level of a few %. Further studies with different numbers of input variables (from 2 up to 50), different size of training data samples (both, signal and background), and using events including elastic background events have also been carried out to test the systematic behaviour of the TMVA application. The various tests performed so far do not show any significant change in the performances.

Table 12: *TMVA Approach 2 (FullMC, High Efficiency Selection)*: CFMlpANN based on all variables from manual optimisation — Summary of the total simultaneous trigger efficiencies ϵ_t [%] for the different data sets, after mass window cuts and CFMlpANN high efficiency selection applied. Numbers in italics are relative to Tab. 7

$\sqrt{s}$ (GeV)	ee	Phi	Etac	J2e	J2mu	D0	Dch	Ds	Lam	Lamc	DPM
2.4	45.33	31.11	–	–	–	–	–	–	17.15	–	0.63
	89.56	*87.36*	–	–	–	–	–	–	*86.66*	–	*14.24*
3.77	42.18	36.50	21.96	35.43	48.07	40.30	28.04	–	17.85	–	0.60
	97.37	*83.43*	*51.17*	*81.41*	*85.15*	*81.35*	*68.84*	–	*84.60*	–	*2.93*
4.5	41.61	31.90	33.84	33.54	45.54	46.02	36.47	38.55	17.61	–	2.24
	91.66	*73.45*	*64.33*	*78.15*	*82.68*	*83.69*	*71.90*	*72.26*	*81.60*	–	*7.16*
5.5	32.38	34.74	42.47	36.14	46.38	49.78	43.80	46.43	18.84	45.44	24.55
	89.11	*83.77*	*72.97*	*76.23*	*79.82*	*86.55*	*79.37*	*79.62*	*81.94*	*74.49*	*54.43*

Table 13: *TMVA Approach 2 (FullMC, High Suppression Selection)*: CFMlpANN based on all variables from manual optimisation — Summary of the total simultaneous trigger efficiencies ϵ_t [%] for the different data sets, after mass window cuts and CFMlpANN high suppression selection applied. Numbers in italics are relative to Tab. 7

$\sqrt{s}$ (GeV)	ee	Phi	Etac	J2e	J2mu	D0	Dch	Ds	Lam	Lamc	DPM
2.4	50.27	31.26	–	–	–	–	–	–	10.45	–	0.10
	99.32	*87.76*	–	–	–	–	–	–	*52.80*	–	*2.18*
3.77	42.33	35.49	8.88	39.34	36.60	32.42	14.26	–	10.21	–	0.10
	97.72	*81.12*	*20.70*	*90.39*	*64.83*	*65.44*	*35.00*	–	*48.41*	–	*0.48*
4.5	44.12	29.09	12.18	36.85	50.16	11.88	8.13	13.33	7.03	–	0.09
	97.19	*66.98*	*23.16*	*85.86*	*91.07*	*21.60*	*16.02*	*24.99*	*32.59*	–	*0.28*
5.5	34.42	28.36	7.49	34.55	49.47	19.86	5.86	15.84	5.27	4.60	0.09
	94.72	*68.39*	*12.87*	*72.87*	*85.13*	*34.53*	*10.62*	*27.16*	*22.91*	*7.54*	*0.19*

5.6 Discussion of Present Results

The primary goal of the studies carried out and presented in this note is the demonstration of the achievable reduction of background reactions, while keeping the signal efficiencies at a reasonably high level. The results obtained from ToyMC (Sec. 5.3) and FullMC (Sec. 5.4) are qualitatively similar, whereas quantitatively they turn out to be significantly different. Furthermore, a TMVA method has been applied on the FullMC data as a more automatic approach of optimising the selection cuts.

The following general observations are made:

- The background level increases almost linearly with increasing centre-of-mass energy $\sqrt{s}$, when trying to keep the signal efficiencies roughly constant, see Figs. 11, 17, and 22.
- The selection observables and cut values are different for different channels, and depend also on the centre-of-mass energy $\sqrt{s}$. Even the set of observables used for separation can change, as it can be observed in Tabs. 17, 18, 22 and 23. As a result, a selection procedure has to be developed for each new trigger line for every single energy it should be applied for.
- When forcing the background reduction to 1/1000, this comes along with severe loss of signal efficiency in some cases (see Tab. 9). This holds in particular for the results of the FullMC case, where resolutions are worse and the corresponding distributions are broader.
- Since the system is based on simultaneous tagging for many channels, the background level increases with increasing number of signal channels. In order to keep the reduction constant, signal efficiency has to be sacrificed at the same time.
- Signal channels with open charm decays, charmed baryon decays or non-leptonic charmonium are more difficult to separate from background reactions than others, see e.g. Tab. 9 and Fig. 19, respectively. This seems to be related to the higher number of final state particles and/or pions in the final state, but needs further investigation. In the FullMC there might be in addition a relationship to the suboptimal working PID due to the lack of the DIRC signal for many tracks with higher momenta, and the current tracking efficiency, being lower than assumed for the ToyMC case. A significant amount of especially pion and kaon tracks is presently cut out by the in principal rather loose cut of $P > 0.1$, see Fig. 5.
- For the FullMC study Tab. 22 and 23 suggest that PID information at least in terms of event based multiplicities play an important role to suppress the background for many reactions. In some cases, like the leptonic channels, it was almost sufficient to use only PID in this way.
- For the TMVA studies based on the same input variables, the results as compared to the manual optimisation are kind of two-fold. For the high efficiency approach, a similar background suppression (Fig. 22) is achieved, while the total signal efficiencies are comparable (within 10%). In case of optimisation for high background suppression, no clear tendency for the resultant signal efficiencies is observed. For some signal datasets, the achieved total trigger efficiencies are significantly lower, in some cases even below 20 % relative to the ones obtained by manual optimisation (Fig. 21, right). On the other hand, for one single dataset (Etac), the total efficiencies improve by up to 50 % (Fig. 23, right).

The current performance in terms of numbers is summarised in Tab. 14. For the ToyMC studies representing the suppression potential in an idealised way, the initial signal efficiencies after combinatorics and a simple $\pm 8\sigma$ mass window requirement are almost all in the order of 80% with moderate background suppression up to a factor 1/30. In the high efficiency optimisation scenario, at least a suppression about two orders of magnitude seems achievable. When forcing the suppression to factor 1/1000, the D modes, the η_c and Λ_c have a clear drop in effiency, which stays at least above 30-40%.

In the FullMC case, the situation looks worse, in line with the initial efficiency values being mostly about 50% lower (and presumably more realistic) than in the ToyMC case. This could be related to the observation, that the charged tracking efficiency is not isotropic and in average lower than assumed in ToyMC. In addition, a loose PID preselection was performed to reduce combinatorics right from the beginning, being hardly comparable to the PID emulation applied in the ToyMC. The case of the Lam dataset with an obtained total efficiency of 20% is not taken to be serious here, as the current PandaROOT release turned out to have a reduced reconstruction efficiency for particles originating from displaced vertices. For some of the channels like $J/\psi \to \mu^+\mu^-$ or $\bar{p}p \to e^+e^-$, the efficiency stays quite constant on that level even for a more strict selection, but e.g. for $\eta_c \to K_S K^\pm \pi^\mp$ and $\Lambda_c \to pK^-\pi^+$, the efficiencies decrease dramatically in the high

background suppression mode to approximately 6% and 9%, respectively. The reasons is, that for the datasets like Etac and Lamc, many events are accepted by the other trigger lines in addition (cross-tagging), as it can clearly be seen from Tab. 21. In the last to next line for the Lamc dataset, the total efficiency for all trigger lines running simultaneously is $\epsilon_t = 61.01$ %, whereas the Λ_c trigger only accepts $\epsilon = 37.25\%$. This effect of cross-tagging is strongly reduced in the strict selection scenario, as it can be seen in Tab. 25. There the maximum additional contribution is merely $\epsilon = 0.27\%$ coming from the η_c trigger line, which does not significantly enhance the efficiency for events from the Lamc dataset.

The TMVA method application leads to partly comparable results, and partly performs significantly worse. However, before a final conclusion on the principal application for our purpose can be drawn, further dedicated studies concerning the choice of input variables, tuning of the configuration and the selection of the classifier are necessary. Even though an automatic approach for defining selection algorithms for such a complex task is desirable, a rash application is not reasonable.

One caveat has to be re-emphasised. All numbers presented in this document only represent the current status of the design and development process, and thus might not be optimal in an absolute meaning. In particular they are based on an environment that does not yet fully meet the requirements being mandatory to extract reliable numbers. As it has been discussed in detail (Sec. 3), the issues pointed out have to be addressed soon.

Table 14: Summary of trigger performance for ToyMC and FullMC for the full energy range after the mass window preselection cuts (pre), optimisation for high efficiency (eff), and optimisation for high background suppression (sup). The results from TMVA application (approach 1 and 2) on the FullMC data are given as well. The ranges of total simultaneous trigger efficiencies ϵ_t [%] are covering the datasets for all energies. Numbers are extracted from Tabs. 4 - 13. The numbers for DPM suppression are given as inverse reduction factors.

Dataset	ee	Phi	Etac	J2e	J2mu	D0	Dch	Ds	Lam	Lamc	DPM (red.)
ToyMC/pre	79-81	88-92	87-89	80	81-83	85-87	82-86	89-90	91	89	5-29
ToyMC/eff	79-80	84-87	68-74	78-80	80-81	77-79	72-76	74-75	81-83	72	88-1250
ToyMC/sup	79-80	84-87	39-57	77-79	80-81	34-61	21-56	27-58	81-83	38	≈ 1000
FullMC/pre	36-51	36-44	43-58	43-47	55-58	50-58	41-55	53-58	20-23	61	2-23
FullMC/eff	33-49	31-36	21-39	32-39	49-53	41-48	28-39	39-44	17-18	44	8-323
FullMC/sup	32-49	25-33	6-8	30-39	49-53	25-35	15-20	15	10-12	11	≈ 1000
TMVA1/eff	32-45	31-37	22-34	33-36	45-48	41-49	28-41	40-47	17-18	41	9-333
TMVA1/sup	34-50	20-32	6-8	31-39	44-53	2-32	3-13	6-10	0-10	4	≈ 1000
TMVA2/eff	32-45	31-37	22-42	34-36	46-48	40-50	28-44	39-46	17-19	45	4-159
TMVA2/sup	34-50	29-35	7-12	35-39	36-50	12-32	6-14	13-16	5-10	5	≈ 1000

6 Next and Further Steps

The results presented in this document are not be considered final. They rather give kind of an upper limit (ToyMC) and first numbers achieved using the present status of PandaRoot (FullMC), based on a particular selection of physics channels and reflecting limitations by assumed and presently achieved detector performances. Further aspects not yet tackled at all have to be studied. In order to provide more realistic performance numbers of developed and proposed algorithms to be implemented on the FPGA/GPU level, the PANDA simulation and reconstruction has to advance. Especially to derive reasonable predictions for the final performance of the Online Trigger System, efforts have to be made from various groups.

Software Trigger related

- **Distortion of phase space**
  Apart from providing selection performance in terms of background suppression and signal efficiency for the channels to be tagged, it has to be studied whether the further physics analyses after the trigger level are harmed by possible distortions of the kinematic distributions, especially in cases where signal efficiencies are already relatively low. Since the algorithms perform cuts on kinematic variables, this might affect results from e.g. partial-wave analysis relying on well behaving, flat acceptance and backgrounds.
- **Speed optimisation**
  Not only the efficiency and suppression levels play an important role, also time issues are crucial. Since some trigger lines partially make use of the same observables for selection (e.g. event shape variables), it should be investigated, how the necessary computing cycles could be minimised. Cascading of the different trigger lines might be useful as well, like e.g. starting with the fastest algorithms, or by those with the highest probability of acceptance.
- **Physics topics**
  The physics topics *Hypernuclei* and *Hadrons in nuclei* have to be taken into account explicitly. Specific trigger signatures have to be identified to tag corresponding reactions. These studies can be carried out only with the corresponding dedicated detector setup, being quite different from the standard one and being not yet available.

Physics and Priority related

- **Trigger lines**
  The final (or at least a more complete) list of physics channels has to be defined in order to start developing and testing algorithms for the corresponding set of trigger lines. This is also important to consider implementation of the routines on specific trigger compute nodes and make realistic tests, cf. DAQ related issues below.
- **Simultaneous tagging**
  It has to be discussed and clarified, whether all possible trigger lines covering all physics channels of interest should run always simultaneously, or how possible trigger configurations might look like for beam times with different purpose.
- **Generic background**
  An alternative generator for generic background is urgently needed in order to check the robustness of the trigger algorithms.

Computing (PandaRoot) related

- **Time-based simulation**
  Most important for concluding about feasibility issues of the trigger system is the complete implementation of the time-based simulation. This goes along with a realistic event building allowing to estimate impact on efficiencies and event mixing.
- **Online reconstruction**
  For the time being PandaRoot provides merely the reconstruction routines being designed for offline application. This has to be complemented by algorithms explicitly suitable for online implementation in terms of timing and complexity in order to determine the impact of less accuracy of reconstructed observables.

DAQ related

- **Data flow**
  The concept of data handling in the interplay of hardware and computing has to be developed and tested. One approach could be related to the 0MQ concept already being discussed for that purpose [14].
- **Trigger implementation**
  The implementation of algorithms provided in this document on various compute elements qualified for data real time processing can be started. This is in particular essential for the identification of the technique(s) most suitable for PANDA.

7 Summary and Outlook

The current status of the software trigger project has been presented. The studies are based on two kinds of Monte Carlo simulation data input, namely from simple ToyMC and the complete PandaRoot based FullMC chain. Two different optimisation approaches have been studied, namely achieving high data reduction while keeping a predefined *High signal efficiency* on the one hand, and achieving a predefined *High background suppression* (and thus high data reduction) while keeping high signal efficiencies on the other hand. A TMVA method for automatic optimisation has in addition been applied on the FullMC data to compare the results to those obtained by manual optimisation. Based on these studies considering presently a set of ten physics channels at four different centre-of-mass energies, first numbers for an achievable performance of the PANDA Online Trigger System have been provided.

A large set of observables related to event shapes as well as to composite candidates has been explored, based on which tagging algorithms have been developed for all the cases. These dataset and trigger specific tagging algorithms have been applied to simultaneously search the event stream for signal decay signatures. Events with at least one positive tag from one out of the set of ten trigger lines under investigation are triggered to be accepted. The specific selection algorithms are explained and provided in detail for all studied trigger lines and centre-of-mass energies, and thus serve as input to the implementation efforts for the compute elements dedicated for real time data processing, like FPGA, GPU or conventional CPU systems.

The resultant performances for the simplified ToyMC case are, as expected, collectively better than for the more realistic FullMC data, whereas qualitatively, the results are in overall agreement. Using TMVA for optimisation leads to similar or worse results, except for a few examples, for which an improved performance is achieved at higher centre-of-mass energies. However, in order to ensure comparability this first comparison might be a little biased in favour of the manual optimisation – surely more dedicated studies are needed to make best use of the TMVA method, nevertheless such application needs to be taken with care and thorough tuning.

The achieved quantitative performances have been presented and summarised in terms of efficiency for signals and suppression for background. In the high signal efficiency approach, reduction factors between 1/10 and 1/300 can be achieved, while retaining 20% – 50% of signal events, strongly depending on the centre-of-mass energy and the number of active trigger lines. Requiring a high background suppression results in significant loss of signal efficiency for part of the investigated channels. In case of a forced data suppression factor of 1/1000, as projected to be needed as computing requirement for PANDA due to limited data storage space, the efficiency numbers for the more realistic FullMC studies varies between approximately 6% and 50%, strongly depending on the type of reaction. To which extent (significantly) reduced signal efficiencies might affect the stored data (artificial peaking backgrounds, flatness of acceptance) in view of offline physics data analysis later on, has still to be investigated.

In order to achieve more final results, apart from software trigger related issues, many other aspects concerning physics channels, the software environment, and the data acquisition system have to be addressed, which make the studies more comparable to the real data environment.

8 Appendix

The document at hand describes in detail the approach of the online software trigger studies. The key results are presented and discussed. In order to complete the picture as well as to provide the in-depth view for the readers of various physics interest, all individual results and more detailed information are compiled in this Appendix.

Appendix – Observables and optimisation of cuts

The full list of observables that have been considered and investigated in order to present the first performance estimation for the software trigger are listed in Tab. 15. Out of this full list, a subset (Tab. 3, Sec. 5.2) has been found to be relevant and applied for the results in Secs. 5.3 - 5.5.

Table 15: List of abbreviations of all cut variables under consideration. For the definitions of the so-called event shape variables, see [12].

Short cut	Description
e, px, py, pz	components of 4-vector for composite/daughters (lab)
ecm, pxcm, pycm, pzcm	components of 4-vector for composite/daughters (cms)
p	momentum p of reconstructed candidate/daughters (lab, cms)
pcm	momentum p of reconstructed candidate (cms)
pt	transvers momentum p_t of reconstructed candidate/daughters
tht, phi	angles of candidate/daughters (lab)
thtcm, phicm	angles of candidate/daughters (lab, cms)
pide, pidmu, pidpi, pidk, pidp	PID probabilities of daughters
oang, decang	opening/decay angle of 2-body candidates
pocvx, pocvy, pocvz, pocqa	Vertex quality of POCA finder for charged daughters
various	if daughter is π^0, detailed information about itself and the two photons
various	if daughter is K^0_S, detailed information about itself and the two pions
npart	multiplicity of all particles in event
nneut	multiplicity of neutral particles in event
nchrg	multiplicity of charged particles in event
npide	multiplicity of electrons
lnpide	multiplicity of electrons with loose PID ($P > 0.25$)
l1npide	multiplicity of electrons with loose PID ($P > 0.25$) and $p > 1$ GeV/c
tnpide	multiplicity of electrons with tight PID ($P > 0.5$)
t1npide	multiplicity of electrons with tight PID ($P > 0.5$) and $p > 1$ GeV/c
vtnpide	multiplicity of electrons with very tight PID ($P > 0.9$)
...	*last 6 variables also for muons, pions, kaons, protons*
np05, ..., np50	multiplicity of particles with $p > [0.5, 1.0, 2.0, 3.0, 4.0, 5.0]$ GeV/c (cms)
np05l, ..., np50l	multiplicity of particles with $p > [0.5, 1.0, 2.0, 3.0, 4.0, 5.0]$ GeV/c (lab)
npt05, ..., npt30	multiplicity of particles with $p_t > [0.5, 1.0, 1.5, 2.0, 2.5, 3.0]$ GeV/c
nne003l, ..., nne05l	multiplicity of neutral part. with $E > [0.03, 0.05, 0.1, 0.5]$ GeV (lab)
ncp005, ..., ncp10	multiplicity of charged part. with $p > [0.03, 0.05, 0.1, 0.5]$ GeV/c (cms)
ncp005l, ..., ncp10l	multiplicity of charged part. with $p > [0.03, 0.05, 0.1, 0.5]$ GeV/c (lab)
pmax	maximum particle momentum in event (cms)
pmaxl	maximum particle momentum in event (lab)
ptmax	maximum transvers particle momentum in event
pmin	minimum particle momentum in event (cms)
pminl	minimum particle momentum in event (lab)
ptmin	minimum transvers particle momentum in event
prapmax	maximum pseudorapidity of a particle in event

Continuation of Tab. 15: List of abbreviations of all cut variables under consideration. For the definitions of the so-called event shape variables, see [12].

Short cut	Description
sumpc	sum of momenta of charged particles in event (cms)
sumpcl	sum of momenta of charged particles in event (lab)
sumen	sum of energies of neutral particles in event (cms)
sumenl	sum of energies of neutral particles in event (lab)
sumpt	sum of transverse momenta of all particles in event (cms)
sumptl	sum of transverse momenta of all particles in event (lab)
sumptc	sum of transverse momenta of charged particles in event (cms)
sumptcl	sum of transverse momenta of charged particles in event (lab)
sumetn	sum of transverse energies of neutral particles in event (cms)
sumetnl	sum of transverse energies of neutral particles in event (lab)
sumpt05, sumpt10	sum of transverse momenta of all particles with $p_t > [0.5, 1.0]$ GeV/c
sumpc05, sumpc10	sum of momenta of charged particles with $p > [0.5, 1.0]$ GeV/c (cms)
sumpc05l, sumpc10l	sum of momenta of charged particles with $p > [0.5, 1.0]$ GeV/c (lab)
sumen05, sumen10	sum of energies of neutral particles with $E > [0.5, 1.0]$ GeV (cms)
sumen05l, sumen10l	sum of energies of neutral particles with $E > [0.5, 1.0]$ GeV (lab)
thr	Event shape: Magnitude of thrust (cms)
sph	Event shape: Sphericity (cms)
cir	Event shape: Circularity (cms)
apl	Event shape: Aplanarity (cms)
pla	Event shape: Planarity (cms)
fw1	Event shape: 1. Fox-Wolfram Moment $R_1 = H_1/H_0$ (cms)
fw2	Event shape: 2. Fox-Wolfram Moment $R_2 = H_2/H_0$ (cms)
fw3	Event shape: 3. Fox-Wolfram Moment $R_3 = H_3/H_0$ (cms)
fw4	Event shape: 4. Fox-Wolfram Moment $R_4 = H_4/H_0$ (cms)
fw5	Event shape: 5. Fox-Wolfram Moment $R_5 = H_5/H_0$ (cms)

Appendix – ToyMC

In addition to the total efficiencies ϵ_t obtained after simultaneously applying the 10 different trigger lines (Sec. 5.3), the complete information of obtained efficiencies for each trigger line and dataset is provided as well. For the case after the mass window preselection, these numbers are summarised in Tab. 16. The further individual, trigger specific selection cuts that have been applied, are summarised for both approaches of optimisation, for signal efficiency in Tab. 17 and for background suppression in Tab. 18. The resulting mass spectra after all the further cuts are shown for the two signal dataset examples (Etac and Ds) and the DPM background dataset, both at 5.5 GeV, for both optimisation approaches in Fig. 24 and Fig. 25, respectively. Also for the case of all selection cuts have been applied for both approaches of optimisation, the complete results in terms of the resultant individual efficiencies for each trigger line and dataset are summarised in Tab. 19 and Tab. 20.

Table 16: *ToyMC – Mass window preselection:* Complete summary of obtained tag fractions [%] obtained with the different triggers for the different data sets (modes) and the total simultaneous trigger efficiencies ϵ_{tot} [%].

mode	$\sqrt{s}$	e^+e^-	ϕ	η_c	J/ψ (1)	J/ψ (2)	D^0	$D^\pm$	D_s	Λ	Λ_c	ϵ_{tot}
ee	2.4	79.41	0.00	–	–	–	–	–	–	0.00	–	79.41
Phi	2.4	0.00	88.20	–	–	–	–	–	–	0.80	–	88.32
Lam	2.4	0.00	0.23	–	–	–	–	–	–	91.11	–	91.12
DPM	2.4	0.01	0.30	–	–	–	–	–	–	3.17	–	3.46
ee	3.77	79.21	0.00	0.00	76.39	0.19	0.01	0.00	–	0.00	–	80.28
Phi	3.77	0.00	88.04	1.54	0.00	0.00	31.76	1.67	–	0.46	–	91.16
Etac	3.77	0.00	0.62	75.13	0.01	0.02	67.84	66.12	–	4.21	–	87.41
J2e	3.77	76.35	0.06	0.01	79.15	0.21	1.87	0.26	–	1.82	–	79.88
J2mu	3.77	0.22	0.07	0.01	0.22	80.87	1.97	0.31	–	1.79	–	81.49
D0	3.77	0.00	3.87	19.56	0.00	0.00	83.71	30.20	–	1.84	–	85.16
Dch	3.77	0.00	7.30	8.88	0.00	0.00	22.08	79.37	–	2.37	–	81.87
Lam	3.77	0.01	0.06	0.20	0.12	0.09	0.12	0.24	–	91.11	–	91.12
DPM	3.77	0.00	0.39	1.15	0.00	0.01	3.44	4.67	–	5.35	–	11.70
ee	4.5	78.91	0.00	0.00	5.65	0.01	0.00	0.00	0.00	0.00	–	80.43
Phi	4.5	0.00	87.91	1.66	0.04	0.03	35.51	1.08	17.27	0.33	–	92.08
Etac	4.5	0.00	0.45	75.19	0.03	0.03	74.72	59.10	8.10	2.70	–	89.24
J2e	4.5	13.62	0.01	0.00	79.49	0.28	5.47	0.06	0.09	0.38	–	80.55
J2mu	4.5	0.03	0.01	0.00	0.28	80.99	5.65	0.09	0.06	0.37	–	82.01
D0	4.5	0.00	2.63	19.73	0.03	0.02	84.98	20.52	17.95	1.51	–	87.36
Dch	4.5	0.00	3.49	20.16	0.01	0.02	30.40	80.31	29.38	2.02	–	85.55
Ds	4.5	0.00	44.43	8.33	0.00	0.00	29.77	31.18	81.92	2.50	–	89.13
Lam	4.5	0.06	0.02	0.02	0.14	0.14	0.19	0.13	0.17	90.86	–	90.87
DPM	4.5	0.00	0.54	1.99	0.01	0.01	4.86	6.14	1.79	6.56	–	15.27
ee	5.5	78.88	0.00	0.00	2.18	0.01	0.00	0.00	0.00	0.00	0.00	80.88
Phi	5.5	0.00	88.10	0.44	0.20	0.24	25.84	0.65	11.68	0.33	0.57	91.81
Etac	5.5	0.00	0.32	72.47	0.15	0.16	77.15	45.75	6.37	2.06	3.22	89.14
J2e	5.5	0.07	0.01	0.00	79.22	0.37	7.88	0.03	0.03	0.11	0.01	80.84
J2mu	5.5	0.00	0.01	0.00	0.39	81.33	8.11	0.02	0.02	0.13	0.02	82.78
D0	5.5	0.00	1.62	14.99	0.15	0.15	85.33	13.08	10.72	1.21	1.74	87.04
Dch	5.5	0.00	2.33	23.11	0.16	0.17	37.03	79.37	22.72	1.64	7.37	85.54
Ds	5.5	0.00	43.55	14.56	0.10	0.08	46.43	31.62	80.94	1.75	8.40	90.38
Lam	5.5	0.10	0.00	0.00	0.06	0.05	0.67	0.09	0.07	91.03	1.71	91.05
Lamc	5.5	0.00	2.16	5.50	0.01	0.02	10.46	29.41	15.81	37.26	79.99	89.06
DPM	5.5	0.00	0.77	3.40	0.03	0.03	7.17	8.58	2.83	7.60	5.17	21.93

Table 17: *ToyMC – High efficiency selection:* Summary of the selected, optimised and applied further cuts for each trigger and the corresponding data set. The cut values and the resulting signal and background efficiencies are listed for each trigger (Efficiencies are given in %)

$\sqrt{s}$	Trigger	Selection	ϵ_{sig}	ϵ_{bg}
2.4	$p\bar{p} \to e^+e^-$	-	79.4	0.009
2.4	$\phi(K^+K^-)$	pmax<0.6 & phipcm>0.55 & phipcm<0.7	84.0	0.041
2.4	$\Lambda(p\pi^-)$	abs(lampcm-0.44)<0.04 & fw1>0.1 & fw2>0.1	82.6	0.028
3.77	$p\bar{p} \to e^+e^-$	-	79.2	0.001
3.77	$\phi(K^+K^-)$	thr>0.87 & phipcm>1.35 & phip>0.8	85.3	0.009
3.77	$\eta_c(K_SK^-\pi^+)$	etace>4.95 & sumpc>2.9 & etacpcm<0.75 & sumptc>1.63	67.6	0.217
3.77	$J/\psi(e^+e^-)$	-	79.1	0.004
3.77	$J/\psi(\mu^+\mu^-)$	-	80.9	0.008
3.77	$D^0(K^-\pi^+)$	abs(d0pcm-0.285)<0.085 & d0e>3.2 & ptmax>0.415	75.4	0.203
3.77	$D^+(K^-\pi^+\pi^+)$	abs(dpcm-0.2425)<0.0625 & dp>2.65 & ptmax>0.3 & de>3.25	71.2	0.312
3.77	$\Lambda(p\pi^-)$	fw2>0.66 & fw5>0.21 & lampcm>1.4 & fw1<0.75	82.3	0.017
4.5	$p\bar{p} \to e^+e^-$	-	78.9	0.001
4.5	$\phi(K^+K^-)$	thr>0.93 & phipcm>1.8	86.6	0.006
4.5	$\eta_c(K_SK^-\pi^+)$	sumptc>2.06 & ptmax>0.64 & sumpc>3.45 & pmax>0.8 & etace>5	67.7	0.205
4.5	$J/\psi(e^+e^-)$	sumpc>3	79.4	0.009
4.5	$J/\psi(\mu^+\mu^-)$	sumpc>3	80.9	0.008
4.5	$D^0(K^-\pi^+)$	abs(d0pcm-1.27)<0.13 & ptmax>0.64 & d0e>2.7	76.5	0.235
4.5	$D^+(K^-\pi^+\pi^+)$	abs(dpcm-1.255)<0.105 & de>2.6 & ptmax>0.48 & dtht<0.33	72.4	0.483
4.5	$D_s^+(K^+K^-\pi^+)$	abs(dspcm-1.095)<0.096 & dse>2.9 & ptmax>0.39 & dstht<0.28	73.7	0.311
4.5	$\Lambda(p\pi^-)$	lampcm>1.7 & fw2>0.75 & lamtht>0.09 & fw4>0.5 & pmax>1.4	80.7	0.013
5.5	$p\bar{p} \to e^+e^-$	-	78.9	0.000
5.5	$\phi(K^+K^-)$	thr>0.955 & phipcm>2	87.1	0.001
5.5	$\eta_c(K_SK^-\pi^+)$	ptmax>0.75 & pmax>1.1 & sumptc>2.8 & sumpc>4	65.6	0.115
5.5	$J/\psi(e^+e^-)$	sumptc>2.1 & pmax>1.5	77.2	0.010
5.5	$J/\psi(\mu^+\mu^-)$	sumptc>2.1 & pmax>1.5	79.7	0.010
5.5	$D^0(K^-\pi^+)$	d0pcm>1.84 & sumpt>2.1 & d0e>2.1 & ptmax>0.8 & d0tht<0.45	77.1	0.074
5.5	$D^+(K^-\pi^+\pi^+)$	abs(dpcm-2.05)<0.2 & dp>2 & dpt>0.5 & ptmax>0.5	71.6	0.165
5.5	$D_s^+(K^+K^-\pi^+)$	abs(dspcm-1.96)<0.24 & ptmax>0.55 & dse>3	73.0	0.151
5.5	$\Lambda(p\pi^-)$	fw2>0.87 & sumptc>0.9 & lampcm>2.2 & fw1>-0.1	82.5	0.004
5.5	$\Lambda_c(pK^-\pi^+)$	abs(lamcpcm-1.54)<0.16 & fw1>-0.05 & lamcp>3.3 & sumptc>1.3	72.1	0.493

Table 18: *ToyMC – High suppression selection:* Summary of the selected, optimised and applied further cuts for each trigger and the corresponding data set. The cut values and the resulting signal and background efficiencies are listed for each trigger (Efficiencies are given in %)

$\sqrt{s}$	Trigger	Selection	ϵ_{sig}	ϵ_{bg}
2.4	$p\bar{p} \to e^+e^-$	-	79.4	0.009
2.4	$\phi(K^+K^-)$	pmax<0.6 & phipcm>0.55 & phipcm<0.7	84.0	0.041
2.4	$\Lambda(p\pi^-)$	abs(lampcm-0.44)<0.04 & fw1>0.1 & fw2>0.1	82.6	0.028
3.77	$p\bar{p} \to e^+e^-$	-	79.2	0.001
3.77	$\phi(K^+K^-)$	thr>0.87 & phipcm>1.35 & phip>0.8	85.3	0.009
3.77	$\eta_c(K_SK^-\pi^+)$	sumpc>3.3 & ptmax>0.83 & etace>5.5	38.9	0.021
3.77	$J/\psi(e^+e^-)$	-	79.1	0.004
3.77	$J/\psi(\mu^+\mu^-)$	-	80.9	0.008
3.77	$D^0(K^-\pi^+)$	abs(d0pcm-0.275)<0.045 & d0e>3.1 & ptmax>0.68 & pmax>0.85	46.5	0.018
3.77	$D^+(K^-\pi^+\pi^+)$	abs(dpcm-0.23)<0.03 & de>3.3 & ptmax>0.58 & pmax<0.8	24.5	0.020
3.77	$\Lambda(p\pi^-)$	fw2>0.66 & fw5>0.21 & lampcm>1.4 & fw1<0.75	82.3	0.017
4.5	$p\bar{p} \to e^+e^-$	-	78.9	0.001
4.5	$\phi(K^+K^-)$	thr>0.93 & phipcm>1.8	86.6	0.006
4.5	$\eta_c(K_SK^-\pi^+)$	sumptc>3 & ptmax >0.7 & sumpc>4.1 & ptmax>0.85	38.6	0.014
4.5	$J/\psi(e^+e^-)$	sumpc>3	79.4	0.009
4.5	$J/\psi(\mu^+\mu^-)$	sumpc>3	80.9	0.008
4.5	$D^0(K^-\pi^+)$	abs(d0pcm-1.28)<0.09 & ptmax>1 & sumpt>3 & d0tht<0.31	30.9	0.014
4.5	$D^+(K^-\pi^+\pi^+)$	abs(dpcm-1.25)<0.05 & ptmax>0.87 & abs(dp-5)<2 & dpt>1.1	17.4	0.015
4.5	$D_s^+(K^+K^-\pi^+)$	abs(dspcm-1.1)<0.07 & ptmax>0.85 & dspt>0.8 & dstht<0.27	26.3	0.019
4.5	$\Lambda(p\pi^-)$	lampcm>1.7 & fw2>0.75 & lamtht>0.09 & fw4>0.5 & pmax>1.4	80.7	0.013
5.5	$p\bar{p} \to e^+e^-$	-	78.9	0.000
5.5	$\phi(K^+K^-)$	thr>0.955 & phipcm>2	87.1	0.001
5.5	$\eta_c(K_SK^-\pi^+)$	ptmax>1 & sumptc>2.6 & sumpc>4.9	52.4	0.011
5.5	$J/\psi(e^+e^-)$	sumptc>2.1 & pmax>1.5	77.2	0.010
5.5	$J/\psi(\mu^+\mu^-)$	sumptc>2.1 & pmax>1.5	79.7	0.010
5.5	$D^0(K^-\pi^+)$	d0pcm>1.8 & sumpt>2.7 & ptmax>0.8 & d0pt>1.3 & d0tht<0.41	59.7	0.012
5.5	$D^+(K^-\pi^+\pi^+)$	dpcm>1.9 & dp>4 & ptmax>0.7 & dtht>0.09	53.4	0.013
5.5	$D_s^+(K^+K^-\pi^+)$	dspcm>1.8 & ptmax>0.8 & dsp>3 & dspt>1 & dspcm<2.1	57.2	0.015
5.5	$\Lambda(p\pi^-)$	fw2>0.87 & sumptc>0.9 & lampcm>2.2 & fw1>-0.1	82.5	0.004
5.5	$\Lambda_c(pK^-\pi^+)$	lamcpcm>1.43 & lamcpcm<1.65 & fw1>0 & lamcpt>1.27	37.4	0.019

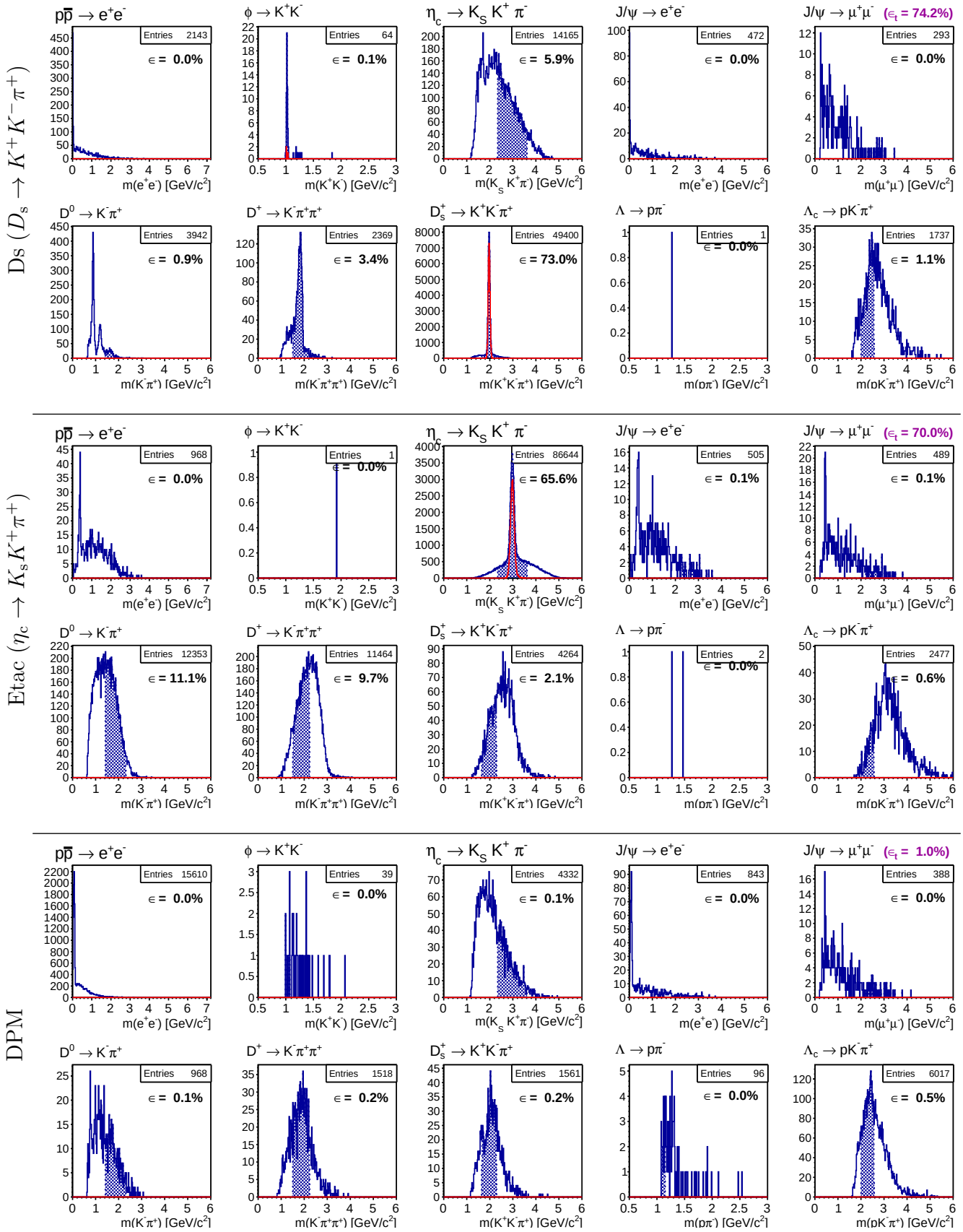

Figure 24: *ToyMC – High efficiency selection:* Simultaneous tagging for the two signal *dataset examples Ds (top)* and *Etac (centre)*, and the *DPM background dataset (bottom)* at $\sqrt{s}$= 5.5 GeV. The individual signal efficiencies ϵ for the different trigger lines are given on the corresponding plots, in addition the global efficiency ϵ_t for all channels applied simultaneously for triggering are given top/right for each set of 10 plots.

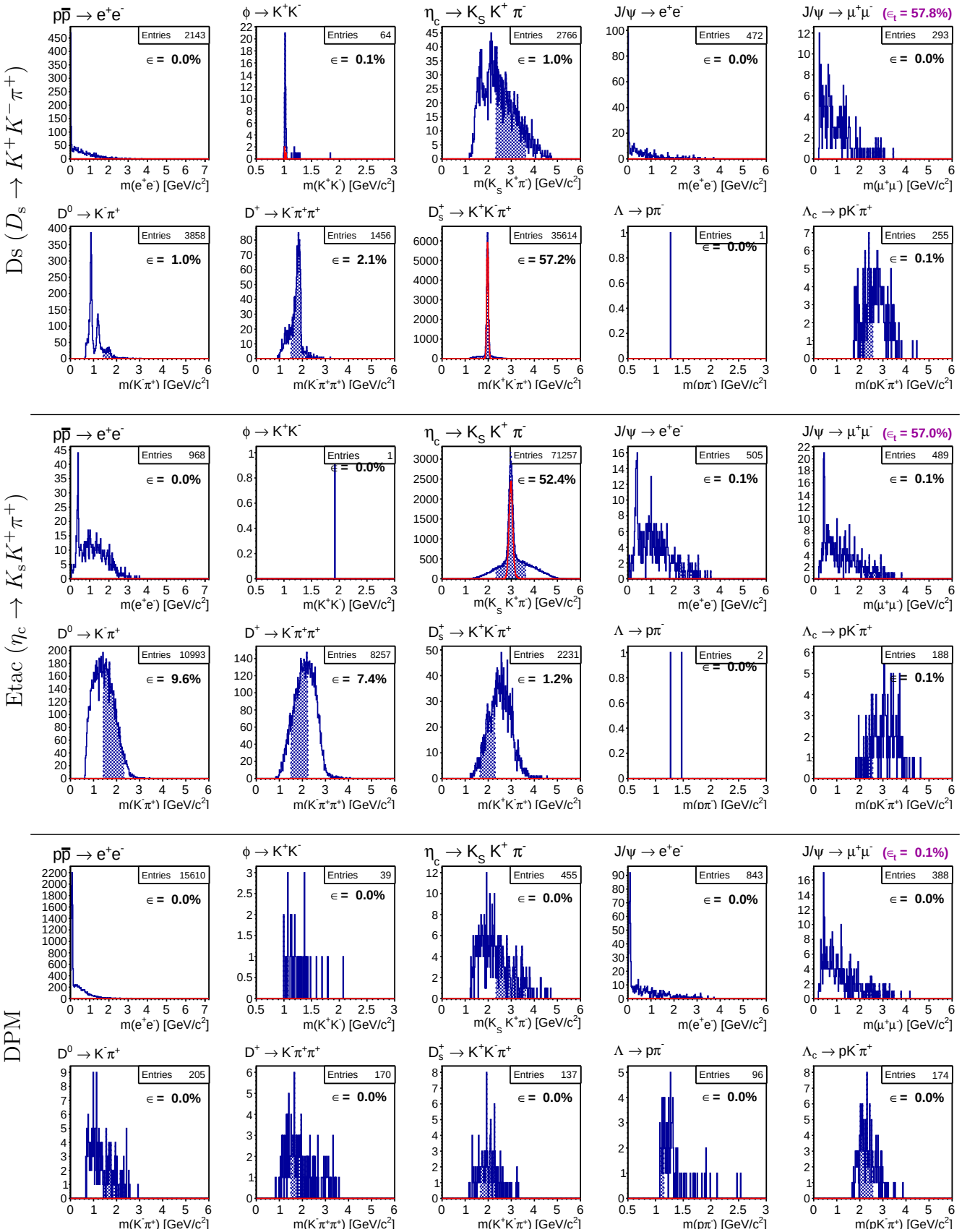

Figure 25: *ToyMC – High suppression selection:* Simultaneous tagging for the two signal *dataset examples Ds (top)* and *Etac (centre)*, and the *DPM background dataset (bottom)* at $\sqrt{s}$= 5.5 GeV. The individual signal efficiencies ϵ for the different trigger lines are given on the corresponding plots, in addition the global efficiency ϵ_t for all channels applied simultaneously for triggering are given top/right for each set of 10 plots.

Table 19: *ToyMC – High efficiency selection:* Complete summary of obtained tag fractions [%] obtained with the different triggers for the different data sets (modes) and the total simultaneous trigger efficiencies ϵ_{tot} [%].

mode	$\sqrt{s}$	e^+e^-	ϕ	η_c	J/ψ (1)	J/ψ (2)	D^0	$D^\pm$	D_s	Λ	Λ_c	ϵ_{tot}
ee	2.4	79.41	0.00	–	–	–	–	–	–	0.00	–	79.41
Phi	2.4	0.00	83.99	–	–	–	–	–	–	0.03	–	83.99
Lam	2.4	0.00	0.02	–	–	–	–	–	–	82.63	–	82.63
DPM	2.4	0.01	0.04	–	–	–	–	–	–	0.03	–	0.08
ee	3.77	79.21	0.00	0.00	76.39	0.19	0.00	0.00	–	0.00	–	80.27
Phi	3.77	0.00	85.33	0.07	0.00	0.00	9.61	0.04	–	0.04	–	86.13
Etac	3.77	0.00	0.04	67.61	0.01	0.02	3.06	0.93	–	0.01	–	68.33
J2e	3.77	76.35	0.00	0.01	79.15	0.21	0.00	0.00	–	0.01	–	79.17
J2mu	3.77	0.22	0.00	0.00	0.22	80.87	0.00	0.00	–	0.00	–	80.90
D0	3.77	0.00	1.22	6.45	0.00	0.00	75.39	7.95	–	0.00	–	76.69
Dch	3.77	0.00	0.06	2.43	0.00	0.00	5.75	71.17	–	0.00	–	72.00
Lam	3.77	0.01	0.01	0.13	0.12	0.09	0.00	0.00	–	82.29	–	82.30
DPM	3.77	0.00	0.01	0.22	0.00	0.01	0.20	0.31	–	0.02	–	0.72
ee	4.5	78.91	0.00	0.00	5.17	0.01	0.00	0.00	0.00	0.00	–	79.95
Phi	4.5	0.00	86.56	0.03	0.03	0.03	0.01	0.02	0.00	0.01	–	86.58
Etac	4.5	0.00	0.00	67.69	0.03	0.03	19.60	15.36	1.94	0.00	–	73.64
J2e	4.5	13.62	0.00	0.00	79.42	0.28	0.69	0.00	0.00	0.03	–	79.59
J2mu	4.5	0.03	0.00	0.00	0.28	80.95	0.76	0.00	0.00	0.02	–	81.12
D0	4.5	0.00	0.00	10.20	0.03	0.02	76.51	10.10	4.85	0.00	–	78.50
Dch	4.5	0.00	0.00	10.43	0.01	0.02	8.25	72.43	10.02	0.00	–	75.50
Ds	4.5	0.00	0.00	2.97	0.00	0.00	2.77	3.51	73.68	0.00	–	74.86
Lam	4.5	0.06	0.00	0.00	0.14	0.14	0.00	0.00	0.00	80.74	–	80.75
DPM	4.5	0.00	0.01	0.21	0.01	0.01	0.23	0.48	0.31	0.01	–	1.14
ee	5.5	78.88	0.00	0.00	1.64	0.00	0.00	0.00	0.00	0.00	0.00	80.37
Phi	5.5	0.00	87.12	0.00	0.09	0.10	0.04	0.25	1.62	0.02	0.00	87.18
Etac	5.5	0.00	0.00	65.58	0.09	0.12	11.09	9.73	2.11	0.00	0.59	70.01
J2e	5.5	0.07	0.00	0.00	77.24	0.36	1.75	0.00	0.00	0.00	0.00	77.58
J2mu	5.5	0.00	0.00	0.00	0.38	79.73	1.90	0.00	0.00	0.00	0.00	80.03
D0	5.5	0.00	0.00	9.15	0.13	0.13	77.10	6.23	2.28	0.00	0.16	78.40
Dch	5.5	0.00	0.00	13.13	0.09	0.08	6.78	71.57	8.47	0.00	0.66	74.48
Ds	5.5	0.00	0.11	5.88	0.05	0.04	0.95	3.38	73.04	0.00	1.09	74.16
Lam	5.5	0.10	0.00	0.00	0.05	0.04	0.07	0.04	0.02	82.51	0.00	82.53
Lamc	5.5	0.00	0.00	0.86	0.00	0.00	0.01	0.07	0.57	0.00	72.12	72.29
DPM	5.5	0.00	0.00	0.12	0.01	0.01	0.07	0.16	0.15	0.00	0.49	0.98

Table 20: *ToyMC – High suppression selection:* Complete summary of obtained tag fractions [%] obtained with the different triggers for the different data sets (modes) and the total simultaneous trigger efficiencies ϵ_{tot} [%].

mode	$\sqrt{s}$	e^+e^-	ϕ	η_c	J/ψ (1)	J/ψ (2)	D^0	$D^\pm$	D_s	Λ	Λ_c	ϵ_{tot}
ee	2.4	79.41	0.00	–	–	–	–	–	–	0.00	–	79.41
Phi	2.4	0.00	83.99	–	–	–	–	–	–	0.03	–	83.99
Lam	2.4	0.00	0.02	–	–	–	–	–	–	82.63	–	82.63
DPM	2.4	0.01	0.04	–	–	–	–	–	–	0.03	–	0.08
ee	3.77	79.21	0.00	0.00	76.39	0.19	0.00	0.00	–	0.00	–	80.27
Phi	3.77	0.00	85.33	0.01	0.00	0.00	4.00	0.00	–	0.04	–	85.58
Etac	3.77	0.00	0.04	38.89	0.01	0.02	1.10	0.04	–	0.01	–	39.49
J2e	3.77	76.35	0.00	0.01	79.15	0.21	0.00	0.00	–	0.01	–	79.17
J2mu	3.77	0.22	0.00	0.00	0.22	80.87	0.00	0.00	–	0.00	–	80.90
D0	3.77	0.00	1.22	0.81	0.00	0.00	46.53	0.04	–	0.00	–	47.31
Dch	3.77	0.00	0.06	0.10	0.00	0.00	1.01	24.50	–	0.00	–	25.66
Lam	3.77	0.01	0.01	0.00	0.12	0.09	0.00	0.00	–	82.29	–	82.30
DPM	3.77	0.00	0.01	0.02	0.00	0.01	0.02	0.02	–	0.02	–	0.10
ee	4.5	78.91	0.00	0.00	5.17	0.01	0.00	0.00	0.00	0.00	–	79.95
Phi	4.5	0.00	86.56	0.00	0.03	0.03	0.00	0.00	0.00	0.01	–	86.57
Etac	4.5	0.00	0.00	38.60	0.03	0.03	6.58	3.45	0.77	0.00	–	41.57
J2e	4.5	13.62	0.00	0.00	79.42	0.28	0.31	0.00	0.00	0.03	–	79.49
J2mu	4.5	0.03	0.00	0.00	0.28	80.95	0.32	0.00	0.00	0.02	–	81.02
D0	4.5	0.00	0.00	2.03	0.03	0.02	30.89	2.52	2.32	0.00	–	33.75
Dch	4.5	0.00	0.00	1.55	0.01	0.02	1.46	17.37	3.26	0.00	–	20.73
Ds	4.5	0.00	0.00	0.11	0.00	0.00	0.47	0.56	26.34	0.00	–	26.69
Lam	4.5	0.06	0.00	0.00	0.14	0.14	0.00	0.00	0.00	80.74	–	80.75
DPM	4.5	0.00	0.01	0.01	0.01	0.01	0.01	0.02	0.02	0.01	–	0.10
ee	5.5	78.88	0.00	0.00	1.64	0.00	0.00	0.00	0.00	0.00	0.00	80.37
Phi	5.5	0.00	87.12	0.00	0.09	0.10	0.04	0.48	0.30	0.02	0.00	87.18
Etac	5.5	0.00	0.00	52.37	0.09	0.12	9.63	7.41	1.20	0.00	0.06	56.96
J2e	5.5	0.07	0.00	0.00	77.24	0.36	1.30	0.02	0.00	0.00	0.00	77.49
J2mu	5.5	0.00	0.00	0.00	0.38	79.73	1.41	0.02	0.00	0.00	0.00	79.96
D0	5.5	0.00	0.00	3.50	0.13	0.13	59.65	4.59	1.31	0.00	0.02	61.01
Dch	5.5	0.00	0.00	4.33	0.09	0.08	5.87	53.44	5.69	0.00	0.08	55.85
Ds	5.5	0.00	0.11	0.99	0.05	0.04	0.99	2.12	57.20	0.00	0.15	57.79
Lam	5.5	0.10	0.00	0.00	0.05	0.04	0.06	0.07	0.01	82.51	0.00	82.53
Lamc	5.5	0.00	0.00	0.00	0.00	0.00	0.02	0.02	0.11	0.00	37.43	37.52
DPM	5.5	0.00	0.00	0.01	0.01	0.01	0.01	0.01	0.01	0.00	0.02	0.09

Appendix – FullMC

The same additional material of figures and tables as discussed for the ToyMC case are compiled in this section for the FullMC case:

- Tag fractions, preselection (Tab. 21, high eff. (Tab. 24) and high suppr. selection (Tab. 25))
- Selection details, high eff. (Tab. 22) and high suppr. (Tab. 23)
- Example triggerline plots – high eff. (Fig. 26), high suppr. (Fig. 27)

Table 21: *FullMC – Mass window preselection:* Complete summary of obtained tag fractions (FullMC) obtained with the trigger lines of the different data (set) modes (Efficiencies are given in %.).

mode	$\sqrt{s}$	e^+e^-	ϕ	η_c	J/ψ (1)	J/ψ (2)	D^0	$D^\pm$	D_s	Λ	Λ_c	ϵ_{tot}
ee	2.4	50.37	0.18	–	–	–	–	–	–	0.20	–	50.61
Phi	2.4	0.13	34.39	–	–	–	–	–	–	2.60	–	35.62
Lam	2.4	0.07	3.42	–	–	–	–	–	–	19.05	–	19.79
DPM	2.4	0.14	2.35	–	–	–	–	–	–	3.23	–	4.40
ee	3.77	37.45	0.61	0.00	41.53	0.09	0.30	0.07	–	0.81	–	43.32
Phi	3.77	0.09	32.03	0.79	0.16	0.13	17.90	5.87	–	4.35	–	43.75
Etac	3.77	0.08	5.11	7.56	0.13	0.21	20.91	20.80	–	9.95	–	42.91
J2e	3.77	27.56	1.92	0.06	39.34	0.08	1.44	0.72	–	3.69	–	43.52
J2mu	3.77	0.16	1.15	0.05	0.19	53.33	2.67	1.51	–	2.96	–	56.45
D0	3.77	0.06	5.13	1.18	0.12	0.15	39.63	11.17	–	7.62	–	49.55
Dch	3.77	0.06	8.27	0.53	0.11	0.14	4.26	30.35	–	9.26	–	40.73
Lam	3.77	0.08	1.10	0.09	0.15	0.08	1.25	0.72	–	19.83	–	21.10
DPM	3.77	0.13	5.93	0.35	0.23	0.20	4.93	5.64	–	10.07	–	20.32
ee	4.5	34.14	0.99	0.01	15.35	0.07	0.48	0.16	0.32	1.31	–	45.40
Phi	4.5	0.11	29.05	1.22	0.40	0.29	18.70	4.40	6.53	5.30	–	43.43
Etac	4.5	0.09	4.69	8.19	0.32	0.33	30.89	23.05	22.72	9.09	–	52.60
J2e	4.5	0.23	1.66	0.09	37.00	0.18	4.44	1.64	2.32	2.93	–	42.91
J2mu	4.5	0.04	0.87	0.04	0.33	50.28	7.72	1.62	1.61	1.67	–	55.07
D0	4.5	0.06	5.74	2.66	0.24	0.28	44.63	11.11	13.34	8.44	–	54.99
Dch	4.5	0.06	7.37	2.37	0.24	0.22	14.51	33.13	31.24	10.73	–	50.73
Ds	4.5	0.07	20.09	1.56	0.23	0.22	12.45	24.46	36.54	14.15	–	53.34
Lam	4.5	0.11	1.00	0.06	0.52	0.48	2.10	0.84	1.25	19.51	–	21.58
DPM	4.5	0.15	8.79	0.84	0.55	0.51	9.09	9.37	10.93	14.95	–	31.30
ee	5.5	26.82	1.52	0.03	7.76	0.08	0.78	0.34	0.62	2.07	0.56	36.34
Phi	5.5	0.15	28.18	0.72	1.33	1.34	12.26	4.15	6.12	6.37	4.54	41.47
Etac	5.5	0.11	4.58	8.32	0.98	1.45	41.37	20.19	20.40	9.95	13.32	58.20
J2e	5.5	0.13	1.87	0.16	35.67	0.88	14.69	2.04	2.41	3.07	1.71	47.41
J2mu	5.5	0.06	0.98	0.05	1.56	49.78	16.28	1.41	1.47	1.47	0.99	58.11
D0	5.5	0.08	6.33	2.51	0.83	1.27	46.67	10.46	12.67	9.60	9.05	57.51
Dch	5.5	0.09	7.29	3.74	0.89	0.93	23.85	33.02	31.40	11.99	20.26	55.18
Ds	5.5	0.08	19.91	3.16	0.86	0.85	23.00	27.06	36.85	14.87	22.74	58.31
Lam	5.5	0.16	1.11	0.09	0.94	0.55	3.63	1.09	1.57	19.69	1.39	23.00
Lamc	5.5	0.10	14.78	2.67	0.86	0.52	16.77	25.51	34.09	26.79	37.25	61.01
DPM	5.5	0.20	12.83	2.38	1.51	1.31	15.49	16.02	18.93	21.25	18.11	45.10

Table 22: *FullMC – High efficiency selection:* Summary of the selected, optimised and applied further cuts for each trigger and the corresponding data set. The cut values and the resulting signal and background efficiencies are listed for each trigger (Efficiencies are given in %)

$\sqrt{s}$	Trigger	Selection	ϵ_{sig}	ϵ_{bg}
2.4	$p\bar{p} \to e^+e^-$	detemcsum>0.46	49.2	0.003
2.4	$\phi(K^+K^-)$	lnpidk>1 & phipcm<0.75 & phipcm>0.4	31.1	0.018
2.4	$\Lambda(p\pi^-)$	lnpidp>0 & mmiss>1 & lampcm>0.31 & lamd0pcm<0.52	17.2	0.293
3.77	$p\bar{p} \to e^+e^-$	lnpide>1	37.4	0.009
3.77	$\phi(K^+K^-)$	lnpidk>1 & phipcm>1.2 & thr>0.8	29.0	0.009
3.77	$\eta_c(K_SK^-\pi^+)$	lnpidk>0	7.0	0.017
3.77	$J/\psi(e^+e^-)$	lnpide>1 & jpsipcm<1.1	39.1	0.002
3.77	$J/\psi(\mu^+\mu^-)$	lnpidmu>1 & jpsipcm<1.1	53.2	0.000
3.77	$D^0(K^-\pi^+)$	lnpidk>0 & d0pcm<0.39 & d0d0pt>0.25	35.7	0.018
3.77	$D^+(K^-\pi^+\pi^+)$	lnpidk>0	26.9	0.282
3.77	$\Lambda(p\pi^-)$	lnpidp>0 & lampcm>1.3 & lamp>0.7 & mmiss<1.52	17.8	0.447
4.5	$p\bar{p} \to e^+e^-$	lnpide>1 & eepcm<2	34.1	0.001
4.5	$\phi(K^+K^-)$	lnpidk>1 & phipcm>1.5 & thr>0.79	26.2	0.010
4.5	$\eta_c(K_SK^-\pi^+)$	lnpidpi>2 & sumptcl>1.8 & etacpcm<1.4 & mmiss<1.7 & etacd1p>0.25	7.4	0.288
4.5	$J/\psi(e^+e^-)$	lnpide>1 & detemcmax>2.5 & jpsipcm<1.7	36.3	0.004
4.5	$J/\psi(\mu^+\mu^-)$	lnpidmu>1 & jpsipcm<1.6	50.1	0.002
4.5	$D^0(K^-\pi^+)$	lnpidk>0 & d0pcm<1.6 & d0pcm>0.8 & d0d1p<6	40.2	0.218
4.5	$D^+(K^-\pi^+\pi^+)$	lnpidk>0	29.4	0.747
4.5	$D_s^+(K^+K^-\pi^+)$	lnpidk>0 & dspcm>0.55 & dsp<8 & dsthtcm>0.5	32.9	0.745
4.5	$\Lambda(p\pi^-)$	lnpidp>0 & mmiss<2.1 & lamp>1.1 & apl<0.028	17.6	0.605
5.5	$p\bar{p} \to e^+e^-$	lnpide>1 & eepcm<2	26.8	0.001
5.5	$\phi(K^+K^-)$	lnpidk>1 & phipcm>1.8 & phipt>0.5	25.4	0.009
5.5	$\eta_c(K_SK^-\pi^+)$	etacpcm<2 & etacd1p>0.38 & etacecm>2.8 & lnpide<1	7.5	1.001
5.5	$J/\psi(e^+e^-)$	lnpide>1 & jpsipcm<1.86 & detemcmax>3.5	32.1	0.019
5.5	$J/\psi(\mu^+\mu^-)$	lnpidmu>1 & jpsipcm<2	48.6	0.004
5.5	$D^0(K^-\pi^+)$	lnpidk>0 & d0pcm<2.3 & d0pcm>0.95	42.1	0.821
5.5	$D^+(K^-\pi^+\pi^+)$	lnpidk>0	29.3	2.026
5.5	$D_s^+(K^+K^-\pi^+)$	lnpidk>0 & dspcm>0.6 & dsthtcm>0.5	33.4	2.099
5.5	$\Lambda(p\pi^-)$	thr>0.87 & lampcm>1 & mmiss<2.4	17.7	0.719
5.5	$\Lambda_c(pK^-\pi^+)$	lnpidp>0 & lamcp>2.7	33.6	8.600

Table 23: *FullMC – High suppression selection:* Summary of the selected, optimised and applied further cuts for each trigger and the corresponding data set. The cut values and the resulting signal and background efficiencies are listed for each trigger (Efficiencies are given in %)

$\sqrt{s}$	Trigger	Selection	ϵ_{sig}	ϵ_{bg}
2.4	$p\bar{p} \to e^+e^-$	detemcsum>0.46	49.2	0.003
2.4	$\phi(K^+K^-)$	lnpidk>1 & phipcm<0.75 & phipcm>0.5	30.5	0.014
2.4	$\Lambda(p\pi^-)$	lnpidp>0 & lnpidpi>0 & abs(lampcm-0.435)<0.035 & lamp>0.4	12.3	0.080
3.77	$p\bar{p} \to e^+e^-$	lnpide>1	37.4	0.009
3.77	$\phi(K^+K^-)$	lnpidk>1 & phipcm>1.2 & thr>0.8	29.0	0.009
3.77	$\eta_c(K_SK^-\pi^+)$	lnpidk>0 & lnpidpi>2 & etacpcm<1	6.7	0.007
3.77	$J/\psi(e^+e^-)$	lnpide>1 & jpsipcm<1.1	39.1	0.002
3.77	$J/\psi(\mu^+\mu^-)$	lnpidmu>1 & jpsipcm<1.1	53.2	0.000
3.77	$D^0(K^-\pi^+)$	lnpidk>0 & d0pcm<0.35 & d0d0pt>0.34	33.7	0.010
3.77	$D^+(K^-\pi^+\pi^+)$	lnpidk>0 & dpmpcm<0.3	19.4	0.023
3.77	$\Lambda(p\pi^-)$	lnpidp>0 & abs(lampcm-2.105)<0.695 & thr>0.9 & lampt>0.8	10.6	0.036
4.5	$p\bar{p} \to e^+e^-$	lnpide>1 & eepcm<2	34.1	0.001
4.5	$\phi(K^+K^-)$	lnpidk>1 & phipcm>1.55 & thr>0.85	25.3	0.005
4.5	$\eta_c(K_SK^-\pi^+)$	lnpidk>0 & lnpidpi>2 & etacd1pt>0.4 & etacd0pt>0.4 & etacpcm<1.4	4.9	0.013
4.5	$J/\psi(e^+e^-)$	lnpide>1 & detemcmax>2.5 & jpsipcm<1.7	36.3	0.004
4.5	$J/\psi(\mu^+\mu^-)$	lnpidmu>1 & jpsipcm<1.6	50.1	0.002
4.5	$D^0(K^-\pi^+)$	lnpidk>0 & abs(d0pcm-1.25)<0.07 & d0p<6.5 & d0d0pidk>0.21	23.7	0.008
4.5	$D^+(K^-\pi^+\pi^+)$	lnpidk>0 & abs(dpmpcm-1.25)<0.05 & mmiss<1.96 & dpmp<6.5	14.0	0.019
4.5	$D_s^+(K^+K^-\pi^+)$	lnpidk>1 & abs(dspcm-1.095)<0.055 & dspt>0.6	13.4	0.022
4.5	$\Lambda(p\pi^-)$	lnpidp & lampcm>1.7 & thr>0.94 & mmiss<1.35 & sumpt>1.8	9.7	0.021
5.5	$p\bar{p} \to e^+e^-$	lnpide>1 & eepcm<2	26.8	0.001
5.5	$\phi(K^+K^-)$	lnpidk>1 & phipcm>1.9 & phipt>0.55	25.0	0.006
5.5	$\eta_c(K_SK^-\pi^+)$	lnpidk>0 & lnpidpi>2 & ptmax>1.1 & npart<15 & mmiss>0	4.2	0.013
5.5	$J/\psi(e^+e^-)$	lnpide>1 & jpsipcm<2 & detemcmax>3.5 & jpsid1tht>0.1	29.8	0.007
5.5	$J/\psi(\mu^+\mu^-)$	lnpidmu>1 & jpsipcm<2	48.6	0.004
5.5	$D^0(K^-\pi^+)$	lnpidk>0 & d0pcm>1.95 & d0pcm<2.1 & d0tht>0.12 & d0p>3	25.4	0.011
5.5	$D^+(K^-\pi^+\pi^+)$	lnpidk>0 & abs(dpmpcm-2)<0.1 & dpmpt>1 & dpmd0pt>0.35	12.8	0.020
5.5	$D_s^+(K^+K^-\pi^+)$	lnpidk>1 & abs(dspcm-1.925)<0.075 & dspt>1.0	11.8	0.011
5.5	$\Lambda(p\pi^-)$	abs(lampcm-2.4)<0.2 & apl<0.01 & mmiss<1.2 & lamp>3 & fw1<0.8	10.6	0.011
5.5	$\Lambda_c(pK^-\pi^+)$	lnpidp>0 & lnpidk>0 & abs(lamcpcm-1.53)<0.04 & lamcp>4 & lamcpt>1	10.3	0.015

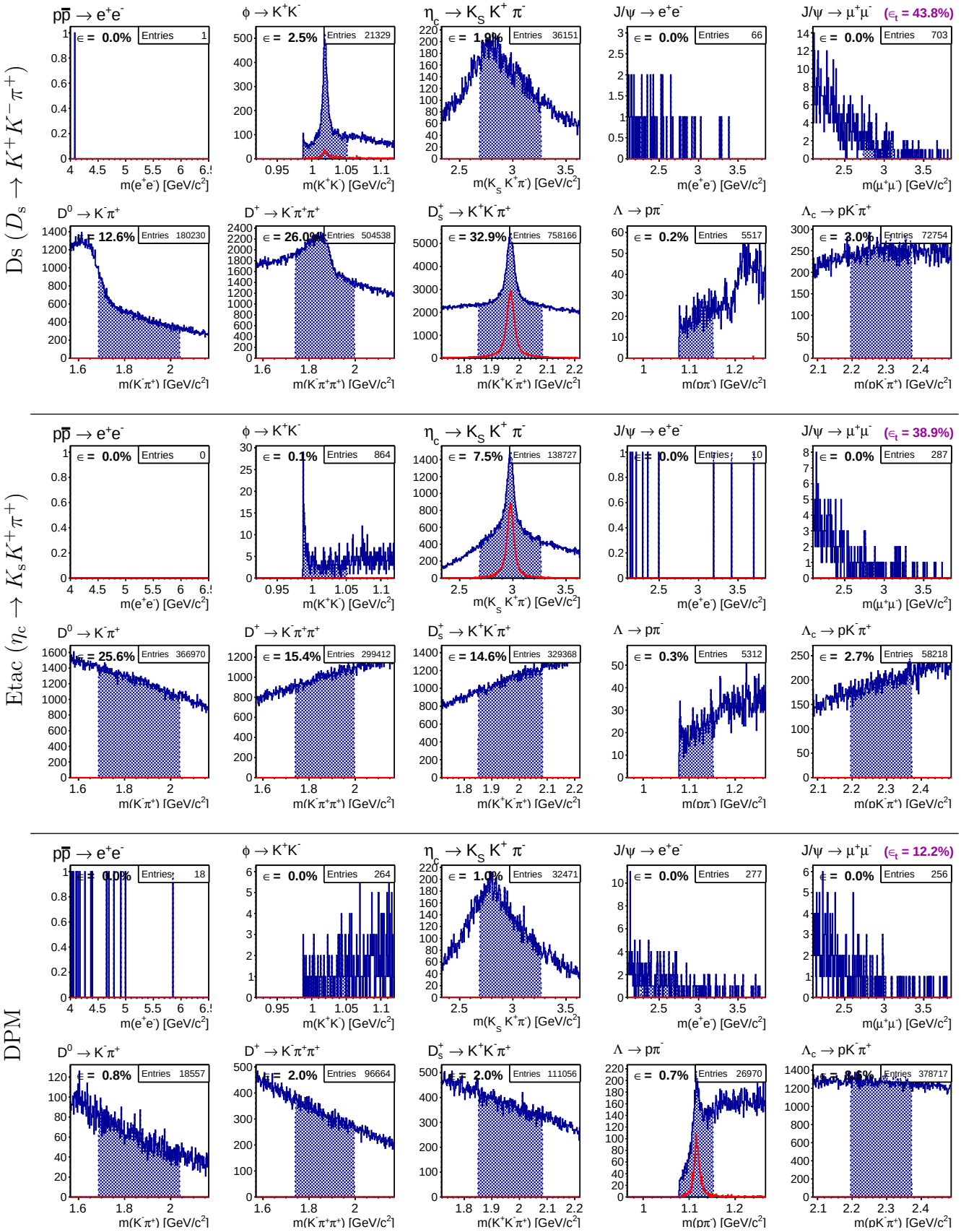

Figure 26: *FullMC – High efficiency selection:* Illustration of simultaneous tagging for the two signal *dataset examples Ds (top)* and *Etac (centre)*, and the *DPM background dataset (bottom)* at $\sqrt{s}$= 5.5 GeV. The individual signal efficiencies ϵ for the different trigger lines are given on the corresponding plots, in addition the global efficiency ϵ_t for all channels applied simultaneously for triggering are given top/right for each set of 10 plots.

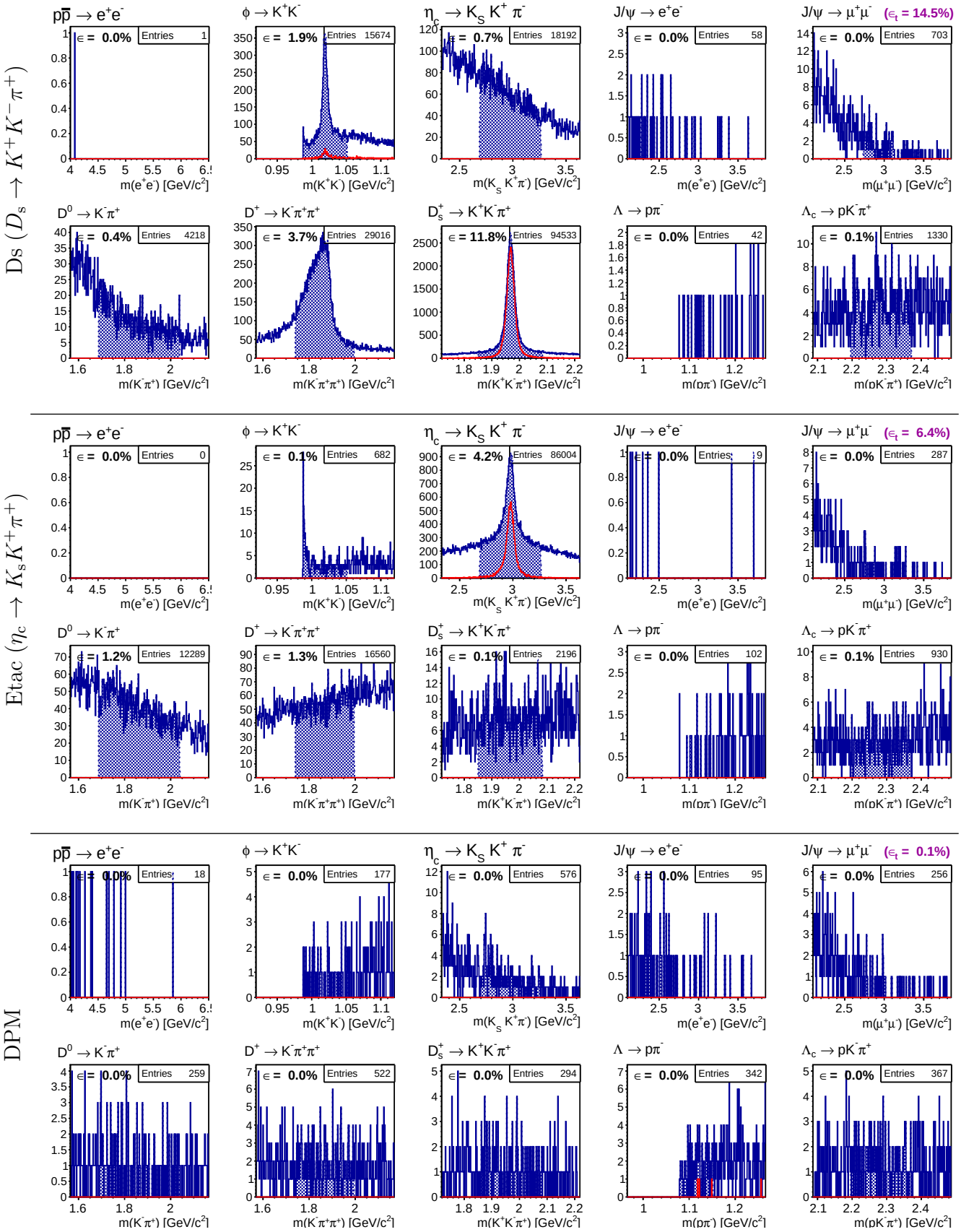

Figure 27: *FullMC – High suppression selection:* Illustration of simultaneous tagging for the two signal *dataset examples Ds (top)* and *Etac (centre)*, and the *DPM background dataset (bottom)* at $\sqrt{s}$= 5.5 GeV. The individual signal efficiencies ϵ for the different trigger lines are given on the corresponding plots, in addition the global efficiency ϵ_t for all channels applied simultaneously for triggering are given top/right for each set of 10 plots.

Table 24: *FullMC – High efficiency selection:* Complete summary of obtained tag fractions obtained with the trigger lines of the different data (set) modes (Efficiencies in %.).

mode	$\sqrt{s}$	e^+e^-	ϕ	η_c	J/ψ (1)	J/ψ (2)	D^0	$D^\pm$	D_s	Λ	Λ_c	ϵ_{tot}
ee	2.4	49.21	0.00	–	–	–	–	–	–	0.00	–	49.21
Phi	2.4	0.01	31.11	–	–	–	–	–	–	0.11	–	31.20
Lam	2.4	0.00	0.00	–	–	–	–	–	–	17.16	–	17.16
DPM	2.4	0.00	0.02	–	–	–	–	–	–	0.29	–	0.31
ee	3.77	37.45	0.00	0.00	40.82	0.00	0.00	0.00	–	0.00	–	41.67
Phi	3.77	0.00	29.01	0.78	0.00	0.00	11.88	5.81	–	0.11	–	36.44
Etac	3.77	0.00	0.08	7.02	0.00	0.00	0.75	17.60	–	0.22	–	21.41
J2e	3.77	27.52	0.00	0.00	39.13	0.00	0.00	0.00	–	0.02	–	39.27
J2mu	3.77	0.00	0.00	0.00	0.00	53.23	0.00	0.00	–	0.04	–	53.24
D0	3.77	0.01	0.66	1.14	0.00	0.00	35.67	10.11	–	0.11	–	40.64
Dch	3.77	0.00	0.15	0.43	0.00	0.00	1.39	26.90	–	0.11	–	27.66
Lam	3.77	0.00	0.00	0.00	0.00	0.00	0.00	0.00	–	17.84	–	17.84
DPM	3.77	0.01	0.01	0.02	0.00	0.00	0.02	0.28	–	0.45	–	0.76
ee	4.5	34.09	0.00	0.00	15.17	0.00	0.00	0.00	0.00	0.00	–	43.95
Phi	4.5	0.00	26.16	0.17	0.00	0.00	1.98	4.30	4.83	0.13	–	31.41
Etac	4.5	0.00	0.06	7.38	0.00	0.00	16.90	18.24	16.66	0.08	–	35.07
J2e	4.5	0.11	0.00	0.01	36.27	0.00	0.00	0.00	0.00	0.02	–	36.31
J2mu	4.5	0.00	0.00	0.00	0.00	50.06	0.00	0.00	0.00	0.02	–	50.07
D0	4.5	0.00	0.11	1.88	0.00	0.00	40.18	9.86	11.06	0.07	–	46.06
Dch	4.5	0.00	0.09	1.74	0.00	0.00	6.18	29.40	25.60	0.05	–	36.90
Ds	4.5	0.00	0.28	0.72	0.00	0.00	5.89	23.58	32.86	0.04	–	39.00
Lam	4.5	0.00	0.00	0.01	0.00	0.00	0.00	0.00	0.00	17.57	–	17.58
DPM	4.5	0.00	0.01	0.29	0.00	0.00	0.22	0.75	0.74	0.60	–	2.06
ee	5.5	26.77	0.00	0.00	5.55	0.00	0.00	0.00	0.00	0.48	0.00	32.54
Phi	5.5	0.00	25.39	0.44	0.01	0.02	4.20	3.99	5.40	1.36	1.30	32.85
Etac	5.5	0.00	0.07	7.48	0.00	0.01	25.61	15.44	14.63	0.28	2.68	38.91
J2e	5.5	0.01	0.00	0.00	32.13	0.00	0.00	0.00	0.00	0.18	0.23	32.43
J2mu	5.5	0.00	0.00	0.02	0.00	48.59	0.00	0.00	0.00	0.15	0.21	48.76
D0	5.5	0.00	0.19	1.52	0.01	0.02	42.06	9.06	10.35	0.26	1.69	47.68
Dch	5.5	0.00	0.23	2.51	0.01	0.03	10.95	29.31	25.52	0.32	2.89	39.18
Ds	5.5	0.00	2.54	1.94	0.01	0.02	12.62	26.01	32.93	0.25	2.98	43.81
Lam	5.5	0.00	0.00	0.03	0.00	0.00	0.01	0.01	0.01	17.74	1.13	18.40
Lamc	5.5	0.00	0.06	1.50	0.00	0.00	5.42	20.45	24.12	0.12	33.56	43.79
DPM	5.5	0.00	0.01	1.00	0.02	0.00	0.82	2.03	1.97	0.72	8.60	12.24

Table 25: *FullMC – High suppression selection:* Complete summary of obtained tag fractions obtained with the trigger lines of the different data (set) modes (Efficiencies in %.).

mode	$\sqrt{s}$	e^+e^-	ϕ	η_c	J/ψ (1)	J/ψ (2)	D^0	$D^\pm$	D_s	Λ	Λ_c	ϵ_{tot}
ee	2.4	49.21	0.00	–	–	–	–	–	–	0.00	–	49.21
Phi	2.4	0.01	30.45	–	–	–	–	–	–	0.03	–	30.48
Lam	2.4	0.00	0.00	–	–	–	–	–	–	12.27	–	12.27
DPM	2.4	0.00	0.01	–	–	–	–	–	–	0.08	–	0.10
ee	3.77	37.45	0.00	0.00	40.82	0.00	0.00	0.00	–	0.00	–	41.67
Phi	3.77	0.00	29.01	0.08	0.00	0.00	9.93	0.80	–	0.03	–	33.21
Etac	3.77	0.00	0.08	6.68	0.00	0.00	0.49	0.27	–	0.01	–	7.35
J2e	3.77	27.52	0.00	0.00	39.13	0.00	0.00	0.00	–	0.01	–	39.26
J2mu	3.77	0.00	0.00	0.00	0.00	53.23	0.00	0.00	–	0.01	–	53.23
D0	3.77	0.01	0.66	0.68	0.00	0.00	33.74	0.96	–	0.01	–	34.55
Dch	3.77	0.00	0.15	0.18	0.00	0.00	1.25	19.38	–	0.01	–	20.19
Lam	3.77	0.00	0.00	0.00	0.00	0.00	0.00	0.00	–	10.65	–	10.65
DPM	3.77	0.01	0.01	0.01	0.00	0.00	0.01	0.02	–	0.04	–	0.09
ee	4.5	34.09	0.00	0.00	15.17	0.00	0.00	0.00	0.00	0.00	–	43.95
Phi	4.5	0.00	25.32	0.15	0.00	0.00	0.11	0.13	0.22	0.04	–	25.80
Etac	4.5	0.00	0.03	4.88	0.00	0.00	2.26	1.52	0.16	0.01	–	8.10
J2e	4.5	0.11	0.00	0.00	36.27	0.00	0.00	0.00	0.00	0.01	–	36.30
J2mu	4.5	0.00	0.00	0.00	0.00	50.06	0.00	0.00	0.00	0.00	–	50.06
D0	4.5	0.00	0.04	1.23	0.00	0.00	23.75	1.05	0.78	0.01	–	25.27
Dch	4.5	0.00	0.03	1.11	0.00	0.00	0.78	14.04	1.44	0.00	–	16.04
Ds	4.5	0.00	0.08	0.48	0.00	0.00	0.47	1.13	13.44	0.00	–	14.88
Lam	4.5	0.00	0.00	0.00	0.00	0.00	0.00	0.00	0.00	9.72	–	9.73
DPM	4.5	0.00	0.01	0.01	0.00	0.00	0.01	0.02	0.02	0.02	–	0.09
ee	5.5	26.77	0.00	0.00	5.31	0.00	0.00	0.00	0.00	0.06	0.00	32.05
Phi	5.5	0.00	24.98	0.09	0.01	0.02	0.14	0.28	0.28	0.03	0.03	25.47
Etac	5.5	0.00	0.06	4.20	0.00	0.01	1.16	1.25	0.13	0.00	0.07	6.37
J2e	5.5	0.01	0.00	0.00	29.84	0.00	0.00	0.00	0.00	0.01	0.00	29.85
J2mu	5.5	0.00	0.00	0.00	0.00	48.59	0.00	0.00	0.00	0.01	0.00	48.59
D0	5.5	0.00	0.16	1.13	0.01	0.02	25.36	0.73	0.40	0.01	0.04	26.51
Dch	5.5	0.00	0.18	1.17	0.01	0.03	0.54	12.80	1.84	0.00	0.08	14.68
Ds	5.5	0.00	1.89	0.75	0.01	0.02	0.36	3.72	11.82	0.00	0.11	14.51
Lam	5.5	0.00	0.00	0.00	0.00	0.00	0.00	0.00	0.00	10.60	0.00	10.60
Lamc	5.5	0.00	0.04	0.27	0.00	0.00	0.12	0.24	0.15	0.00	10.25	10.81
DPM	5.5	0.00	0.01	0.01	0.01	0.00	0.01	0.02	0.01	0.01	0.02	0.10

Appendix – TMVA

Similar additional information as for the ToyMC and FullMC case are compiled in this section for the two TMVA approaches:

- Performance of different TMVA classifiers (Fig. 28, Fig. 29)
- Variables used for TMVA appr. 1 (Tab. 26)
- Tag fractions for TMVA appr. 1, high eff. (Tab. 27), high suppr. (Tab. 28)
- Tag fractions for TMVA appr. 2, high eff. (Tab. 29), high suppr. (Tab. 30)

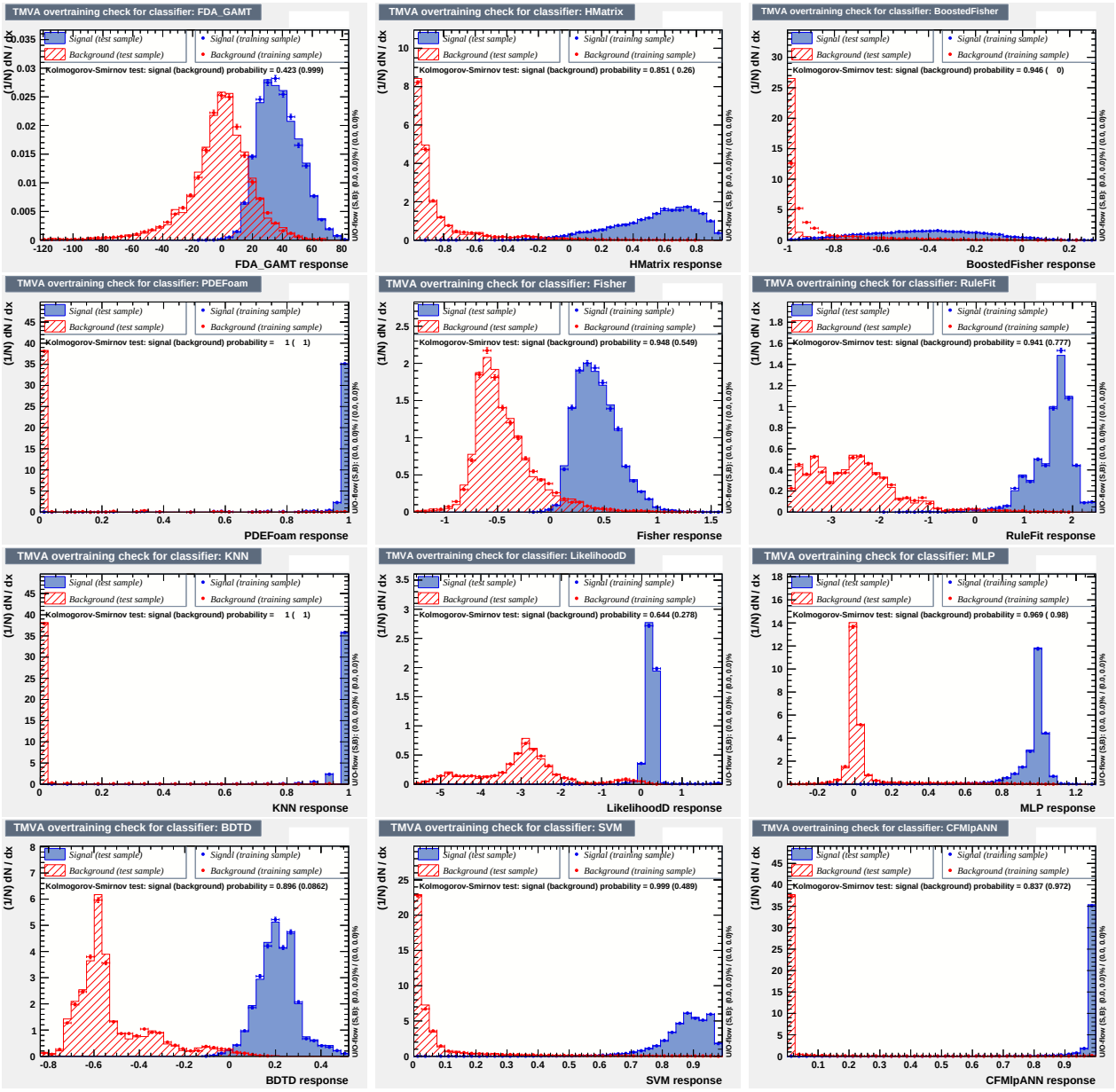

Figure 28: Classification results of 12 different $TMVA$ algorithms for the selection of $J/\psi \to \ell^+\ell^-$ in $\bar{p}p \to J/\psi\pi^+\pi^-$ reactions at $\sqrt{s} = 5.5$ GeV.

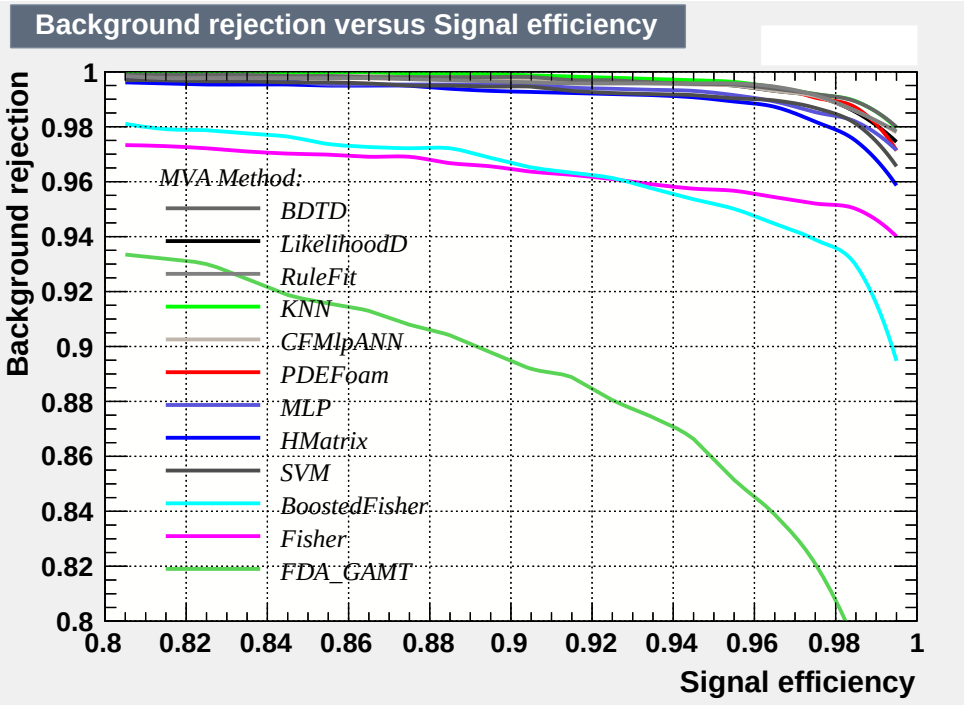

Figure 29: Relative operating characteristic (ROC) curve: Background rejection as a function of signal efficiency obtained by the 12 different algorithms for the selection of $J/\psi \to \ell^+\ell^-$ in $\bar{p}p \to J/\psi\pi^+\pi^-$ reactions at $\sqrt{s} = 5.5$ GeV. The closer a curve passes the point (1,1), the better the separation.

Table 26: List of trigger line specific training variables for each trigger and the corresponding data set (TMVA approach 1).

Trigger	Selection	# of var.
$p\bar{p} \to e^+e^-$	lnpide & detemcsum & eepcm	3
$\phi(K^+K^-)$	lnpidk & phipcm & phipt & thr	4
$\eta_c(K_SK^-\pi^+)$	lnpidk & lnpidpi & lnpide & mmiss & ptmax & npart sumptc & etacpcm & etacd1p & etacd1pt & etacd0pt & etacecm	12
$J/\psi(e^+e^-)$	lnpide & jpsipcm & detemcmax & jpsid1tht	4
$J/\psi(\mu^+\mu^-)$	lnpidmu & jpsipcm	2
$D^0(K^-\pi^+)$	lnpidk & d0pcm & d0p & d0tht & d0d0pt & d0d0pidk & d0d1p	7
$D^+(K^-\pi^+\pi^+)$	lnpidk & dpmp & dpmpcm & dpmpt & dpmd0pt & mmiss	6
$D_s^+(K^+K^-\pi^+)$	lnpidk & dspcm& dspt & dsp & dsthtcm	5
$\Lambda(p\pi^-)$	lnpidp & lampcm& lampt &lamp & thr apl & fw1 & sumpt & mmiss & lamd0pcm	10
$\Lambda_c(pK^-\pi^+)$	lnpidk & lnpidp & lamcp & lamcpt& lamcpcm	5

Table 27: *TMVA Approach 1 (FullMC, High efficiency selection)*: Complete summary of tag fractions obtained with the trigger lines on the different data (set) modes – After mass window cuts and TMVA approach 1 with high efficiency selection applied. Efficiencies are given in %.

mode	$\sqrt{s}$	e^+e^-	ϕ	η_c	J/ψ (1)	J/ψ (2)	D^0	$D^\pm$	D_s	Λ	Λ_c	ϵ_{tot}
ee	2.4	45.33	0.00	–	–	–	–	–	–	0.00	–	45.33
Phi	2.4	0.00	30.95	–	–	–	–	–	–	0.07	–	31.00
Lam	2.4	0.00	0.00	–	–	–	–	–	–	17.15	–	17.15
DPM	2.4	0.00	0.02	–	–	–	–	–	–	0.28	–	0.30
ee	3.77	33.71	0.00	0.00	40.38	0.00	0.00	0.00	–	0.00	–	41.24
Phi	3.77	0.00	28.82	0.75	0.00	0.00	14.06	5.80	–	0.14	–	37.00
Etac	3.77	0.00	0.08	6.80	0.00	0.00	1.35	17.51	–	0.10	–	21.51
J2e	3.77	17.48	0.00	0.00	35.41	0.00	0.00	0.02	–	0.02	–	36.25
J2mu	3.77	0.00	0.00	0.00	0.00	48.00	0.00	0.00	–	0.03	–	48.01
D0	3.77	0.00	0.76	0.95	0.00	0.00	35.66	10.11	–	0.05	–	40.53
Dch	3.77	0.00	0.50	0.29	0.00	0.00	1.44	27.32	–	0.04	–	28.17
Lam	3.77	0.00	0.00	0.00	0.00	0.00	0.00	0.00	–	17.85	–	17.85
DPM	3.77	0.00	0.01	0.01	0.00	0.00	0.02	0.59	–	0.23	–	0.84
ee	4.5	30.72	0.01	0.00	14.36	0.00	0.00	0.07	0.00	0.00	–	40.82
Phi	4.5	0.00	26.14	1.13	0.00	0.00	16.59	4.23	6.02	0.19	–	37.15
Etac	4.5	0.00	0.12	7.37	0.00	0.00	12.13	19.29	13.58	0.08	–	32.59
J2e	4.5	0.07	0.01	0.02	33.30	0.00	0.01	0.49	0.00	0.02	–	33.68
J2mu	4.5	0.00	0.04	0.00	0.00	45.25	0.01	1.07	0.00	0.02	–	45.74
D0	4.5	0.00	0.22	2.47	0.00	0.00	40.16	10.10	10.39	0.06	–	46.12
Dch	4.5	0.00	0.17	2.07	0.00	0.00	6.66	29.82	22.21	0.05	–	36.87
Ds	4.5	0.00	2.19	1.41	0.00	0.00	9.26	23.44	32.90	0.04	–	40.28
Lam	4.5	0.00	0.06	0.01	0.00	0.00	0.03	0.45	0.01	17.56	–	17.82
DPM	4.5	0.00	0.01	0.23	0.00	0.00	0.33	1.86	0.65	0.17	–	2.71
ee	5.5	24.14	0.01	0.00	7.49	0.00	0.00	0.04	0.00	0.13	0.22	31.78
Phi	5.5	0.00	25.36	0.69	0.01	0.02	10.16	3.96	5.60	1.14	4.44	35.43
Etac	5.5	0.00	0.11	7.49	0.00	0.01	15.27	16.34	13.59	0.14	11.78	34.47
J2e	5.5	0.01	0.02	0.01	32.10	0.00	0.01	0.53	0.00	0.05	0.83	33.12
J2mu	5.5	0.00	0.05	0.01	0.00	44.80	0.01	0.55	0.01	0.07	0.57	45.30
D0	5.5	0.00	0.22	2.28	0.01	0.02	41.99	9.22	9.55	0.11	8.41	48.64
Dch	5.5	0.00	0.23	3.34	0.01	0.03	10.46	29.72	25.33	0.12	18.73	41.01
Ds	5.5	0.00	2.66	3.01	0.01	0.02	17.07	25.92	33.43	0.12	22.18	46.72
Lam	5.5	0.00	0.06	0.01	0.00	0.00	0.03	0.34	0.02	17.72	1.05	18.42
Lamc	5.5	0.00	0.05	2.09	0.00	0.00	4.56	20.12	21.62	0.13	33.37	41.17
DPM	5.5	0.00	0.01	0.57	0.01	0.00	0.74	2.99	2.12	0.12	9.52	11.72

Table 28: *TMVA Approach 1 (FullMC, High suppression selection)*: Complete summary of tag fractions obtained with the trigger lines on the different data (set) modes – After mass window cuts and TMVA approach 1 with high suppression selection applied. Efficiencies are given in %.

mode	$\sqrt{s}$	e^+e^-	ϕ	η_c	J/ψ (1)	J/ψ (2)	D^0	$D^\pm$	D_s	Λ	Λ_c	ϵ_{tot}
ee	2.4	50.37	0.00	–	–	–	–	–	–	0.00	–	50.37
Phi	2.4	0.00	19.75	–	–	–	–	–	–	0.01	–	19.76
Lam	2.4	0.00	0.00	–	–	–	–	–	–	10.18	–	10.18
DPM	2.4	0.00	0.01	–	–	–	–	–	–	0.08	–	0.10
ee	3.77	37.43	0.00	0.00	41.45	0.00	0.00	0.00	–	0.00	–	42.27
Phi	3.77	0.00	26.65	0.78	0.00	0.00	12.23	0.60	–	0.05	–	31.92
Etac	3.77	0.00	0.06	7.07	0.00	0.00	0.76	0.20	–	0.02	–	7.88
J2e	3.77	27.51	0.00	0.00	39.08	0.00	0.00	0.00	–	0.01	–	39.21
J2mu	3.77	0.08	0.00	0.00	0.00	53.23	0.00	0.00	–	0.01	–	53.26
D0	3.77	0.00	0.65	1.13	0.00	0.00	31.34	0.86	–	0.02	–	32.23
Dch	3.77	0.00	0.47	0.42	0.00	0.00	1.20	11.92	–	0.02	–	13.33
Lam	3.77	0.00	0.00	0.01	0.00	0.00	0.00	0.00	–	2.90	–	2.91
DPM	3.77	0.01	0.01	0.02	0.00	0.00	0.01	0.01	–	0.03	–	0.09
ee	4.5	34.09	0.01	0.00	14.82	0.00	0.00	0.00	0.00	0.00	–	43.61
Phi	4.5	0.00	21.19	0.27	0.00	0.00	0.00	1.82	2.41	0.07	–	23.06
Etac	4.5	0.00	0.07	6.48	0.00	0.00	0.00	0.53	0.02	0.03	–	7.00
J2e	4.5	0.12	0.01	0.00	35.30	0.00	0.00	0.00	0.00	0.01	–	35.35
J2mu	4.5	0.00	0.03	0.00	0.00	50.02	0.00	0.00	0.00	0.01	–	50.05
D0	4.5	0.00	0.12	1.36	0.00	0.00	0.00	1.42	0.81	0.02	–	3.38
Dch	4.5	0.00	0.08	1.09	0.00	0.00	0.00	1.32	1.10	0.02	–	3.25
Ds	4.5	0.00	1.11	0.36	0.00	0.00	0.00	1.92	8.63	0.02	–	10.30
Lam	4.5	0.00	0.04	0.00	0.00	0.00	0.00	0.00	0.00	2.08	–	2.12
DPM	4.5	0.00	0.01	0.01	0.00	0.00	0.00	0.02	0.02	0.02	–	0.08
ee	5.5	26.76	0.01	0.00	7.33	0.00	0.00	0.00	0.00	0.00	0.00	33.99
Phi	5.5	0.00	21.17	0.07	0.01	0.02	0.00	1.41	1.63	0.11	0.13	22.50
Etac	5.5	0.00	0.07	5.57	0.00	0.01	0.00	0.37	0.01	0.05	0.07	6.04
J2e	5.5	0.02	0.01	0.00	30.51	0.00	0.00	0.00	0.00	0.02	0.00	30.54
J2mu	5.5	0.00	0.03	0.00	0.00	43.93	0.00	0.00	0.00	0.02	0.00	43.95
D0	5.5	0.00	0.14	0.90	0.01	0.02	0.00	0.61	0.22	0.03	0.09	1.88
Dch	5.5	0.00	0.11	1.14	0.01	0.03	0.00	2.59	0.46	0.04	0.17	4.18
Ds	5.5	0.00	1.37	0.36	0.01	0.02	0.00	1.57	4.32	0.04	0.30	6.49
Lam	5.5	0.00	0.05	0.00	0.00	0.00	0.00	0.00	0.00	0.04	0.00	0.09
Lamc	5.5	0.00	0.03	0.18	0.00	0.00	0.00	0.19	0.06	0.04	3.30	3.69
DPM	5.5	0.00	0.01	0.01	0.01	0.00	0.00	0.02	0.01	0.01	0.02	0.08

Table 29: *TMVA Approach 2 (FullMC, High efficiency selection)*: Complete summary of tag fractions obtained with the trigger lines on the different data (set) modes – After mass window cuts and TMVA approach 2 with high efficiency selection applied. Efficiencies are given in %.

mode	$\sqrt{s}$	e^+e^-	ϕ	η_c	J/ψ (1)	J/ψ (2)	D^0	$D^\pm$	D_s	Λ	Λ_c	ϵ_{tot}
ee	2.4	45.33	0.00	–	–	–	–	–	–	0.00	–	45.33
Phi	2.4	0.00	30.95	–	–	–	–	–	–	0.21	–	31.11
Lam	2.4	0.00	0.00	–	–	–	–	–	–	17.15	–	17.15
DPM	2.4	0.00	0.01	–	–	–	–	–	–	0.61	–	0.63
ee	3.77	33.71	0.00	0.00	41.42	0.00	0.00	0.00	–	0.00	–	42.18
Phi	3.77	0.00	28.82	0.76	0.00	0.00	13.74	4.17	–	0.01	–	36.50
Etac	3.77	0.00	0.06	6.80	0.00	0.00	2.25	17.41	–	0.02	–	21.96
J2e	3.77	1.89	0.00	0.00	35.41	0.00	0.00	0.00	–	0.01	–	35.43
J2mu	3.77	0.00	0.00	0.00	0.00	47.99	0.00	0.10	–	0.02	–	48.07
D0	3.77	0.00	0.51	0.97	0.00	0.00	35.67	9.88	–	0.01	–	40.30
Dch	3.77	0.00	0.10	0.28	0.00	0.00	1.49	27.34	–	0.01	–	28.04
Lam	3.77	0.00	0.00	0.00	0.00	0.00	0.00	0.00	–	17.84	–	17.85
DPM	3.77	0.00	0.00	0.01	0.00	0.00	0.02	0.43	–	0.15	–	0.60
ee	4.5	30.72	0.00	0.01	15.06	0.00	0.00	0.00	0.00	0.02	–	41.61
Phi	4.5	0.00	26.14	1.22	0.00	0.00	2.56	4.09	5.43	0.13	–	31.90
Etac	4.5	0.00	0.05	8.19	0.00	0.00	13.81	18.92	13.63	0.02	–	33.84
J2e	4.5	0.01	0.00	0.09	33.30	0.00	0.00	0.17	0.02	0.01	–	33.54
J2mu	4.5	0.00	0.00	0.04	0.00	45.25	0.12	0.23	0.01	0.09	–	45.54
D0	4.5	0.00	0.12	2.66	0.00	0.00	40.17	9.93	9.80	0.02	–	46.02
Dch	4.5	0.00	0.07	2.37	0.00	0.00	4.49	29.85	24.30	0.01	–	36.47
Ds	4.5	0.00	0.51	1.56	0.00	0.00	4.44	23.32	32.90	0.01	–	38.55
Lam	4.5	0.00	0.01	0.06	0.00	0.00	0.00	0.02	0.01	17.56	–	17.61
DPM	4.5	0.00	0.00	0.84	0.00	0.00	0.07	1.08	0.56	0.11	–	2.24
ee	5.5	24.14	0.01	0.00	7.60	0.00	0.23	0.34	0.00	0.09	0.56	32.38
Phi	5.5	0.00	25.36	0.49	0.00	0.00	5.43	4.15	5.23	1.42	4.54	34.74
Etac	5.5	0.00	0.03	7.39	0.00	0.00	23.03	20.19	11.09	0.10	13.32	42.47
J2e	5.5	0.00	0.01	0.02	32.10	0.00	2.89	2.04	0.02	0.05	1.71	36.14
J2mu	5.5	0.00	0.00	0.01	0.00	44.80	0.62	1.41	0.12	0.08	0.99	46.38
D0	5.5	0.00	0.11	2.17	0.00	0.01	42.00	10.46	8.13	0.09	9.05	49.78
Dch	5.5	0.00	0.08	3.10	0.00	0.01	9.55	33.02	23.33	0.09	20.26	43.80
Ds	5.5	0.00	1.02	2.27	0.00	0.00	11.49	27.06	31.85	0.07	22.74	46.43
Lam	5.5	0.00	0.00	0.00	0.00	0.00	0.05	1.09	0.03	17.72	1.39	18.84
Lamc	5.5	0.00	0.02	1.35	0.00	0.00	2.78	25.51	15.29	0.11	37.25	45.44
DPM	5.5	0.00	0.00	0.23	0.00	0.00	0.38	16.02	1.11	0.10	18.11	24.55

Table 30: *TMVA Approach 2 (FullMC, High suppression selection)*: Complete summary of tag fractions obtained with the trigger lines on the different data (set) modes – After mass window cuts and TMVA approach 2 with high suppression selection applied. Efficiencies are given in %.

mode	$\sqrt{s}$	e^+e^-	ϕ	η_c	J/ψ (1)	J/ψ (2)	D^0	$D^\pm$	D_s	Λ	Λ_c	ϵ_{tot}
ee	2.4	45.33	0.00	–	–	–	–	–	–	0.00	–	45.33
Phi	2.4	0.00	30.95	–	–	–	–	–	–	0.21	–	31.11
Lam	2.4	0.00	0.00	–	–	–	–	–	–	17.15	–	17.15
DPM	2.4	0.00	0.01	–	–	–	–	–	–	0.61	–	0.63
ee	3.77	33.71	0.00	0.00	41.42	0.00	0.00	0.00	–	0.00	–	42.18
Phi	3.77	0.00	28.82	0.76	0.00	0.00	13.74	4.17	–	0.01	–	36.50
Etac	3.77	0.00	0.06	6.80	0.00	0.00	2.25	17.41	–	0.02	–	21.96
J2e	3.77	1.89	0.00	0.00	35.41	0.00	0.00	0.00	–	0.01	–	35.43
J2mu	3.77	0.00	0.00	0.00	0.00	47.99	0.00	0.10	–	0.02	–	48.07
D0	3.77	0.00	0.51	0.97	0.00	0.00	35.67	9.88	–	0.01	–	40.30
Dch	3.77	0.00	0.10	0.28	0.00	0.00	1.49	27.34	–	0.01	–	28.04
Lam	3.77	0.00	0.00	0.00	0.00	0.00	0.00	0.00	–	17.84	–	17.85
DPM	3.77	0.00	0.00	0.01	0.00	0.00	0.02	0.43	–	0.15	–	0.60
ee	4.5	30.72	0.00	0.01	15.06	0.00	0.00	0.00	0.00	0.02	–	41.61
Phi	4.5	0.00	26.14	1.22	0.00	0.00	2.56	4.09	5.43	0.13	–	31.90
Etac	4.5	0.00	0.05	8.19	0.00	0.00	13.81	18.92	13.63	0.02	–	33.84
J2e	4.5	0.01	0.00	0.09	33.30	0.00	0.00	0.17	0.02	0.01	–	33.54
J2mu	4.5	0.00	0.00	0.04	0.00	45.25	0.12	0.23	0.01	0.09	–	45.54
D0	4.5	0.00	0.12	2.66	0.00	0.00	40.17	9.93	9.80	0.02	–	46.02
Dch	4.5	0.00	0.07	2.37	0.00	0.00	4.49	29.85	24.30	0.01	–	36.47
Ds	4.5	0.00	0.51	1.56	0.00	0.00	4.44	23.32	32.90	0.01	–	38.55
Lam	4.5	0.00	0.01	0.06	0.00	0.00	0.00	0.02	0.01	17.56	–	17.61
DPM	4.5	0.00	0.00	0.84	0.00	0.00	0.07	1.08	0.56	0.11	–	2.24
ee	5.5	24.14	0.01	0.00	7.60	0.00	0.23	0.34	0.00	0.09	0.56	32.38
Phi	5.5	0.00	25.36	0.49	0.00	0.00	5.43	4.15	5.23	1.42	4.54	34.74
Etac	5.5	0.00	0.03	7.39	0.00	0.00	23.03	20.19	11.09	0.10	13.32	42.47
J2e	5.5	0.00	0.01	0.02	32.10	0.00	2.89	2.04	0.02	0.05	1.71	36.14
J2mu	5.5	0.00	0.00	0.01	0.00	44.80	0.62	1.41	0.12	0.08	0.99	46.38
D0	5.5	0.00	0.11	2.17	0.00	0.01	42.00	10.46	8.13	0.09	9.05	49.78
Dch	5.5	0.00	0.08	3.10	0.00	0.01	9.55	33.02	23.33	0.09	20.26	43.80
Ds	5.5	0.00	1.02	2.27	0.00	0.00	11.49	27.06	31.85	0.07	22.74	46.43
Lam	5.5	0.00	0.00	0.00	0.00	0.00	0.05	1.09	0.03	17.72	1.39	18.84
Lamc	5.5	0.00	0.02	1.35	0.00	0.00	2.78	25.51	15.29	0.11	37.25	45.44
DPM	5.5	0.00	0.00	0.23	0.00	0.00	0.38	16.02	1.11	0.10	18.11	24.55

References

[1] *PANDA Collaboration*, Physics Performance Report for PANDA: Strong Interaction Studies with Antiprotons (2009); arXiv:0903.3905v1

[2] `https://panda-wiki.gsi.de/foswiki/bin/view/Computing/PandaRoot`

[3] GSI Grid Engine Wiki, `https://wiki.gsi.de/cgi-bin/view/Linux/GridEngine`

[4] *PANDA Collaboration*, Technical Design Report for the PANDA Straw Tube Tracker (2012); arXiv:1205.5441v2

[5] *D. Kang*, Talk given at PandRoot EVO meeting, 04.11.2013; *E. Atomssa*, Talk given at PANDA collaboration meeting, Computing session, 09.12.2013 (2013)

[6] *R. Aaij et al.*, The LHCb Trigger and its Performance in 2011 (2011); arXiv:1211.3055v2

[7] *The LHCb Collaboration*, The LHCb Detector at the LHC, JINST 3 (2008) S08005

[8] *The E835 Collaboration*, High precision charmonium spectroscopy in anti-p p annihilations, Nucl. Phys. A655 (1999) 29-34

[9] *W. Baldini et al.*, The charged trigger of the experiment E835 at Fermilab, NIM A 449 (2000) 331-343

[10] EvtGen, `http://evtgen.warwick.ac.uk/`

[11] *A. Capella et al.*, Dual Parton Model, Physics Reports, 236 (1994) 225-329

[12] *S. Mrenna*, Event Shapes, `http://home.fnal.gov/~mrenna/lutp0613man2/node233.html`

[13] *A. Hoecker et al.*, *T*MVA Toolkit for Multivariate Data Analysis with ROOT, `http://tmva.sourceforge.net/`

[14] `http://zeromq.org/`